Investigation of Dibenzo[*b*,*j*][1,10]phenanthroline and N-Propanoic Acid Spiropyrans and Spirooxazines for Use in Dye-Sensitized Solar Cells

A Thesis
Submitted to the Faculty
of
Drexel University
by
Noah Johnson
in partial fulfillment of the
requirements for the degree
of
Doctor of Philosophy in Chemistry

July 2016

© Copyright 2016
Noah Johnson. All Rights Reserved.

Dedication

This work is dedicated to my family, who have supported me in all that I do. Without them I would be nothing. With them, I can be anything.

Acknowledgements

I thank my committee members: my chair Dr. Aaron T. Fafarman, Dr. Reinhard Schweitzer-Stenner, Dr. Daniel King, Dr. Kenneth Lau, Dr. Massoud Soroush, and Dr. Michael Zdilla from Temple University. Thank you all for your advice and your guidance.

I thank my advisor, Dr. Frank Ji, for supporting me throughout the years, and guiding my work toward completion. Your incredible creativity has helped me overcome many obstacles, and provided me with a goal to aspire to in my future career. The variety of projects that I have been exposed to has broadened my knowledge base, and helped teach me how to work within the scientific community.

I thank my co-workers, collaborators, and colleagues here at Drexel University. Thank you to Tim Wade and Dr. Johnathan Soffer, for training me on equipment and helping me to design my experiments. Thank you to Dr. Kenneth Lau and Yuriy Smolin, for helping with the assembly and testing of the solar cell devices presented in this work. Thank you to my group members, past and present, especially: Dr. Arben Kojtari, Dr. Joshua Smith, Daniel Hagaman, and Dayne Swearer. You have all advised me, amused me, amazed me, and aided me, and I wouldn't be here without you. Thank you to Mohammad Nozari, for sharing with me your thoughts and ideas. Thank you as well to LT Dr. Christopher Castillo and Dr. Nicholas Paparoidamis, for advising me, and showing me the path through graduate school.

I thank my girlfriend, Charlotte Burns. You have been a constant rock throughout this process, and saved me from myself. Thank you for keeping me in balance, and helping me be better than I thought I could.

I thank my brothers, Luke, Nick, and Aaron. Thank you for pushing me to always be greater, while never letting me forget where I started.

I thank my parents, Jeff and Terri. Your constant sacrifice and shining example have made me who I am. Without you, I wouldn't be here.

Contents

1 Introduction 1

1.1 The Problem of Current Energy Use . . . 1

1.2 Solar Spectrum . . . 2

1.3 Theoretical Limitations . . . 3

1.4 Photon Absorption . . . 4

1.5 Charge Separation . . . 5

1.6 Charge Transfer . . . 6

1.7 Architecture of a Solar Cell . . . 6

1.8 Types of Solar Cell . . . 7

  1.8.1 Silicon Cells . . . 7

  1.8.2 Thin Film Cells . . . 9

  1.8.3 Organic Solar Cells . . . 10

  1.8.4 Dye-Sensitized Solar Cells (DSSCs) . . . 12

1.9 Organization of the Thesis . . . 17

1.10 References . . . 18

2 Color-Changing Solar Cells 24

2.1 Abstract . . . 24

2.2 Overview . . . 24

2.3 Photochromism . . . 25

2.4 UV-VIS Analysis . . . 28

  2.4.1 Spiropyrans . . . 28

  2.4.2 Spirooxazines . . . 30

2.5 The Effect of Solvent . . . 32

  2.5.1 Spiropyrans . . . 32

  2.5.2 Spirooxazines . . . 35

2.6 The Effect of pH . . . 36

2.7 The Effect of COOH . . . 38

2.8 Coordination to TiO_2 . . . 41

2.9 Solar Cell Characteristics . . . 46

2.10 Future Work . . . 47

  2.10.1 Binding Mechanism . . . 47

  2.10.2 Color-Changing Solar Cells . . . 48

2.11 Conclusions . . . 49

2.12 Experimental . . . 50

  2.12.1 UV-Vis . . . 50

  2.12.2 Infrared . . . 50

  2.12.3 Solar cell assembly and testing . . . 51

  2.12.4 Synthesis . . . 51

2.13 References . . . 54

3 Dibenzo[*b*,*j*][1,10]Phenanthrolines 58

3.1 Abstract . . . 58

3.2 Overview . . . 58

  3.2.1 Aromaticity . . . 60

3.3 Predictions . . . 63

  3.3.1 Analogous Compounds . . . 63

  3.3.2 Density Functional Theory . . . 65

3.4 Synthesis . . . 65

3.5 Chemistry . . . 68

  3.5.1 Friedländer . . . 68

  3.5.2 Palladium-catalyzed dehydrogenation . . . 68

  3.5.3 Oxidation . . . 70

3.5.4 Bromination 71
3.5.5 Reduction 71
3.5.6 Ullmann-Goldberg 73
3.5.7 Buchwald-Hartwig 75
3.5.8 Ring closing 77
3.5.9 Complexation 78
3.6 Solar Cell Characteristics 79
3.7 Future Work 81
3.7.1 Aromaticity 81
3.7.2 Derivatives 81
3.8 Conclusions 82
3.9 Experimental 83
3.9.1 Density Functional Theory 83
3.9.2 Solar Cell Assembly and Testing 83
3.9.3 Synthesis 83
3.10 References 94

Appendix **98**

Vita **138**

List of Figures

1.1 Global energy consumption over time by source, in million tonnes of oil equivalent. 1

1.2 Solar irradiance spectrum for different atmosphere interferences. . . 3

1.3 Diagram of the most efficient solar cells in recent history, separated by class and conditions. 8

1.4 Global production of photovoltaic modules. 8

1.5 (Left) Schematic representation of a CdTe solar cell. (Right) Schematic representation of a CIGS solar cell. 10

1.6 (a) Finely mixed donor and acceptor (b) bilayer arrangement (c) ideal "finger" orientation (d) typic bulk heterogenuous processing. . 11

1.7 Molecular structure of the common "N3" dye. 12

1.8 Plot of improvement in photon conversion efficiency (PCE) over time for different classes of DSSC sensitizing dyes. 14

1.9 Schematic diagram of various electron transfer processes in a dye-sensitized solar cell 16

2.1 General structure of the spiro compounds. CH = spiropyrans, N = spirooxazines. 26

2.2 Mechanism of photochromic behavior in spiropyrans and spirooxazines 26

2.3 Diagrams of the studied compounds 27

2.4 UV-VIS Absorbance of Sp_1 in Acetonitrile Before and After Irradiation with UV light 29

2.5 UV-VIS Absorbance of Sp_2 in Acetonitrile Before and After Irradiation with UV light . . . 29
2.6 Comparison of UV-VIS Absorbance of Sp_1 and Sp_2 in Acetonitrile After Irradiation with UV light . . . 30
2.7 UV-VIS Absorbance of Ox_1 in Hexane Before and After Irradiation with UV light . . . 31
2.8 UV-VIS Absorbance of Ox_2 in Acetonitrile Before and After Irradiation with UV light . . . 31
2.9 Comparison of UV-VIS Absorbance of Sp_1 in Various Solvents After Irradiation with UV light . . . 32
2.10 Comparison of UV-VIS Absorbance of Sp_1 in THF and Hexane . . . 33
2.11 Comparison of solvochromatic effect using different polarity indices 34
2.12 Comparison of UV-VIS Absorbance of Sp_2 in Various Solvents After Irradiation with UV light . . . 35
2.13 (Left) 0.5 mM Sp2 in MeOH (Right) 0.5 mM Sp2 in MeOH upon addition of 100 µL of pyridine. . . . 36
2.14 UV Spectrum of Sp_2 in CH_3CN, being titrated with Et_3N . . . 37
2.15 Comparison of a) λ_{max} and b) ring-closing rate for Sp_{1M} and Sp_{2M} vs. solvent polarity . . . 38
2.16 Decay of λ_{max} for Sp_{1M} over time . . . 40
2.17 Comparison of a) λ_{max} and b) ring-closing rate of Ox_{1M} and Ox_{2M} vs. solvent polarity . . . 41
2.18 a) Appearance and b) UV-VIS spectrum of Sp_2 absorbed onto TiO_2 compared to N-719 . . . 42
2.19 Comparison of UV-VIS Absorbance of a) Sp_{1M} and b) Sp_{2M} in THF 43
2.20 a) Appearance and b) behavior of Sp_2 and Ox_2 adsorbed onto TiO_2 in toluene . . . 44
2.21 Infrared spectra of Sp_2 in the merocyanine form, and Sp_2 bound to TiO_2 . . . 45

2.22 Proposed surface binding of of Sp_2 on TiO_2 46
2.23 Power and JV curves of a DSSC loaded with Sp_2 in a a) polar and b) nonpolar solvent 47
2.24 Power and JV curves of a DSSC loaded with Ox_2 in toluene 48
2.25 Second attempt at a high-efficiency color-changing DSSC 49
2.26 Future attempts for a high-efficiency color-changing DSSC 49

3.1 UV-Vis absorption spectra of Ru dyes absorbed on TiO_2, acetonitrile and ethanol 59
3.2 5,8-dimethyl-dibenzo[*b,j*][1,10]phenanthroline 60
3.3 Some exceptions to Hückel's rule 61
3.4 Predictions under Clar's rule 62
3.6 The Clar structures of **1** and potential analogous compounds 63
3.7 The Clar structures of **1** and potential analogous compounds 64
3.8 The Clar structure of acridine after oxidation 64
3.9 The Clar structure of **1** following oxidation, presuming reactivity similar to (left) phenanthroline and (right) acridine 65
3.10 The calculated HOMO/LUMO of **1** 66
3.11 The calculated HOMO/LUMO of **2** 67
3.12 Mechanism for a metal-catalyzed condensation using palladium (A), and copper (B). 74
3.13 Ligands for the Buchwald-Hartwig amination of 1,2-dibromobenzene with 2'-aminoacetophenone 76
3.14 Power and JV curves of a DSSC loaded with **3** in a nonpolar solvent 80
3.15 Library for comparing the effect of planarity 82

List of Schemes

3.1 Proposed reaction mechanisms for Friedländer condensation 69

3.2 Friedlander condensation 69

3.3 An oxidation of **2** with selenium dioxide 71

3.4 An oxidation of **2** with Jones' reagent 71

3.5 Mechanism for the bromination/dehydrobromination of **2** with NBS 72

3.6 Bromination/dehydrobromination of **2** with NBS 72

3.7 Reduction of **9** with $NaBH_4$ 73

3.8 Ullmann condensation of 1,2-diiodobenzene with 2'-aminoacetophenone 75

3.9 Buchwald-Hartwig amination 77

3.10 6-exo-trig ring closing reaction of **10** 78

3.11 Coordination of **1** to ruthenium 79

3.12 Coordination of **1** to ruthenium 80

3.13 Horner-Wadsworth-Emmons reaction of **4** 82

Abstract

Investigation of Dibenzo[*b,j*][*1,10*]phenanthroline and N-Propanoic Acid
Spiropyrans and Spirooxazines for Use in Dye-Sensitized Solar Cells
Noah Johnson

Finding alternative energy sources is one of the great problems of science today. One potential solution, the dye-sensitized solar cell (DSSC) has been studied thoroughly since its discovery in 1991. They are composed of a sensitizing dye adsorbed on to the surface of a semiconducting metal oxide. Much research has been done trying to improve the DSSC efficiency, mainly by creating new derivatives of the sensitizing dye. However, despite the large number of derivatives made, most have utilized the same strategy of extending conjugation to increase overall efficiency. In this work, I investigated a different class of compounds, the dibenzo[*b,j*][1,10]phenanthrolines, which highlight the effect of extended aromaticity on the properties of ruthenium-based DSSCs. First, I developed a synthetic scheme which improves upon those used before, opening up the possibility of creating a library of compounds to be used for future investigations. Second, the chemistry of these compounds was investigated, which was shown to be different from the [1,10]phenanthrolines. Specifically, they were shown to be more sensitive to oxidative, reductive, and alkaline conditions, along with being more resistant to formation via the Pd- catalyzed dehydrogenation. Finally, these compounds were evaluated for their ability to form a DSSC, showing low conversion efficiencies, but with promise for better results in the future. This lays the groundwork for the creation of a library of DSSCs based on this backbone. As well, we report the creation of color-changing dye-sensitized solar cells (DSSCs) using N-propanoic acid-functionalized spiropyrans and spirooxazines. We investigated the photophysical properties of these compounds in various solvents and pH conditions using UV-Vis spectroscopy, and their behavior on a TiO_2 surface using a combination of UV-Vis and FT-IR. Their performance as sensitizing dyes for DSSCs was analyzed. This study reveals a number of properties for this class of compounds that affect their performance as both photochromic compounds and DSSC sensitizers, which allow for future creation of an efficient photochromic DSSC.

(This page is intentionally left blank)

Chapter 1: Introduction

1.1 The Problem of Current Energy Use

The energy needs of the human population has been consistently climbing for a long time. While renewable energy sources are growing rapidly,[1] they are still greatly outpaced by consumption of hydrocarbons such as coal, oil, and natural gas (Figure 1.1).

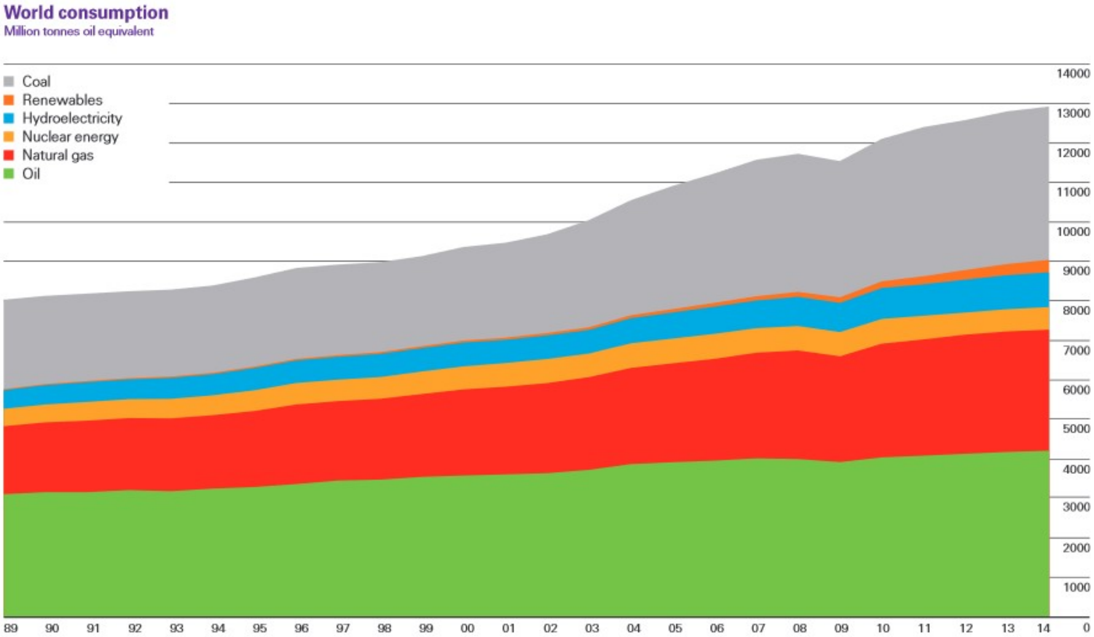

Figure 1.1. Global energy consumption over time by source, in million tonnes of oil equivalent.[2]

This, combined with other human activities, has led to a drastic change in the overall world climate through ocean acidification, ozone layer depletion, and increase in temperature through greenhouse gas concentration.[3–5] The solution to this would be to substitute hydrocarbon fuel sources with renewable energy, but consumption has, thus far, outpaced renewable sources. One major reason for this is the current low cost to extract energy from hydrocarbon sources compared to the relatively higher cost of renewable energy. While some have managed to match the cost of coal, such as wind and hydroelectric, renewable energy still needs a great deal of development to replace hydrocarbon in the growing energy market.[6] As the main driving force behind all energy production on earth, directly capturing the energy of the sun is an attractive and elegant solution to the planet's energy needs. However, it is currently much more expensive to produce, as well as less consistent, being highly subject to weather and axial tilt throughout the year, as well as light/dark cycles throughout the day. For this reason, solar energy is currently most useful as a supplemental, distributed energy source that is mainly used during favorable conditions and in remote locations, while a constant supply of energy from consistent sources such as nuclear and coal provide a steady energy grid. Therefore, research into solar energy will be most beneficial when it can be used as an inconsistent supplement.

1.2 Solar Spectrum

The sun emits light mostly as a black body with a temperature of 5800 K.[7,8] However, once this light reaches our planet, it interacts with the atmosphere through a combination of absorption, Rayleigh,[9] and Mie[10] scattering. Therefore, depending on the path length of this light, which is related to latitudinal position on the surface, the spectrum will vary widely. This change is represented by the air-mass coefficient, where AM 1.0 is a perpendicular path to the planet's surface.[11] As most major population centers are a considerable distance from the equator, AM 1.5 has become the international standard for solar cell measurements (Figure 1.2).

This emission profile outputs the most energy in the visible region, with more than 40% of all irradiance generated between 400 and 700 nm.

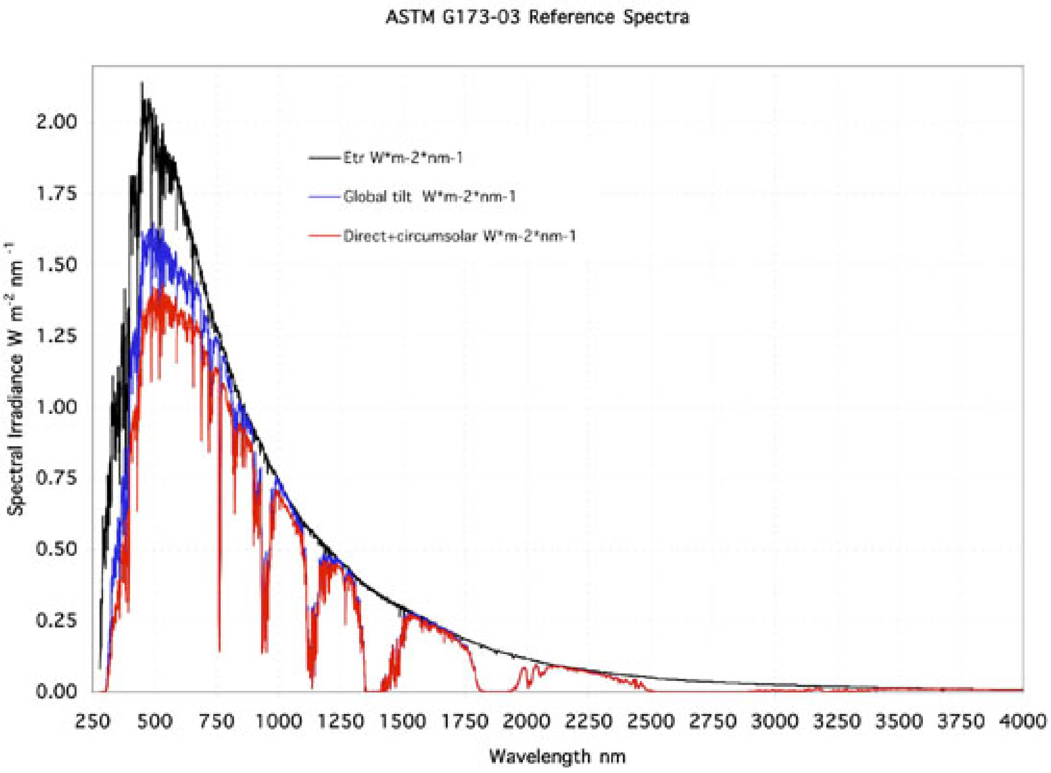

Figure 1.2. Solar irradiance spectrum for different atmosphere interferences.[12]

1.3 Theoretical Limitations

The basic process of energy capture involves taking a photon and converting its energy into a usable form, normally an electron capable of doing work. By taking into account various thermodynamic principles, it is possible to calculate the theoretical limitation of any solar cell. A single bandgap cell is going to have a thermodynamic maximum conversion efficiency of 33.7%. This conclusion was reached by Shockley and Queisser in 1961.[13] While this theory is modified on a regular basis,[14] the value of 33.7% is still the most commonly cited. This was calculated by taking into account the major sources of loss in an ideal solar cell, with the following assumptions:

1. Only one bandgap
2. Only one exciton generated per absorbed photon

3. Any excess energy is lost to thermal relaxation
4. Solar cell reaches equilibrium at 300 K.
5. Illumination occurs under unconcentrated light

The majority of the energy lost is due to the single bandgap. Any photon below the bandgap will be completely lost, and any above the bandgap will have part of its energy wasted. Therefore, a bandgap was chosen that captures the most energy. By using the irradiance spectrum (Figure 1.2) Queisser and Shockley calculated a bandgap of 1.34 eV to convert the most energy possible. Even so, this ends up being the largest contributor to energy loss, bringing conversion efficiency down to around 48% without accounting for any other losses. Any solar cell is going to lose energy from its own blackbody radiation, which is going to be dependent on the temperature of the cell. Even maintaining a temperature of 20°C will cause a loss of around 7% of incoming energy, and solar cells normally reach thermal equilibrium at much higher temperatures. Finally, even an ideal cell will experience losses from recombination of hole-electron pairs. While impurities and defects will greatly increase the contribution of this loss, a perfect cell will still experience losses from the principle of detailed balance. Knowing these assumptions allow for increasing the efficiency of solar cells above the Shockley-Queisser limit, by using multiple bandgaps, concentrating light, capturing multiple electrons per photon, etc.

1.4 Photon Absorption

A photon carries energy according to Plank's equation, which states that the energy of a photon will be directly proportional to the frequency of the electromagnetic wave that it composes. This energy can be directly transferred to an electron in a material, causing it to be excited to a higher energy state. This creates both an excited electron, and an empty position in the energy field below it, known as a "hole." This electron/hole pair is commonly referred to as an exciton, and is a formally neutral species. These excitons are unstable, and will quickly decay unless the electron and hole are separated. All materials will interact with photons differently, in both magnitude and frequency. The frequency of the light is going to drastically change how many excitons can be produced for any given color of light, and some frequencies are more valuable than others (Figure 1.2). The magnitude of the interaction strength will determine the number of photons absorbed for a given thickness of material. While the material can be made thicker to improve the number of photons collected, this will have negative repercussions in other aspects of the solar cell.

1.5 Charge Separation

In a pure semiconductor such as silicon, charge separation is a nearly spontaneous matter at room temperature, as the binding strength of the exciton is so small (14-15 meV).[15,16] However, organic molecules have exciton binding energies more than an order of magnitude greater than this, and so require a neighboring electron or hole acceptor to force charge separation. The diffusion length of the exciton then determines the thickness of the light-absorbing layer in a solar cell, as the exciton must travel to the interface in order to prevent dissociation. The diffusion is generally thermal in nature, as the neutral exciton is mostly unaffected by the electric field in the solar cell, especially in thicker cells.[17] This diffusion length is determined both by the nature and purity/order of the material, but is generally on the order of 10 nm for organic materials. Once the exciton reaches the donor/acceptor interface, a difference in the energy levels of the two will drive the separation of the exciton. The excited electron can relax into the slightly lower excited energy state of the electron acceptor material (or vice versa for the hole). Once the charges are separated, they are subject to the electric field of the solar cell, and so quickly move toward the electrodes.

1.6 Charge Transfer

There are two main regimes for charge movement through a material: band and hopping. In the band regime, the different units throughout the material are strongly coupled electronically. This allows the charge to be delocalized across the entire surface. This is the standard model for traditional semiconductors, and generally offers higher charge mobility. By contrast, the hopping regime has the charge moving between adjacent units by coupling to phonons in the material, inducing polarization and geometrical relaxation as it moves. In a given material, any combination of these may occur: for example, there might be delocalization across one segment of a semiconductor, followed by hopping over a grain boundary. The charge may also become trapped by impurities in the material, or recombine with an opposing charge. As such, charge mobilities are somewhat dependent upon the material used, but will also depend on its purity and preparation.

1.7 Architecture of a Solar Cell

In order to function properly, a solar cell needs to perform a number of tasks: it needs to absorb photons and use the energy to create an electron/hole pair; it needs to separate the charge carriers; and it needs to move those charges to the working circuit. All solar cells need a component that will absorb photons and turn them into excitons (Section 1.4). This can range from a perfect crystal of silicon to a polymer matrix. The main requirement for these materials is that they need to have an excited state that can be easily reached by the absorption of a photon, but can be improved by also increasing charge separation and transfer. This is also the greatest determining factor in overall solar conversion efficiency, as well as the largest contributor to the overall cost of the system. As such, when discussing solar cells, they tend to be defined by this material. Solar cells also require a donor/acceptor interface to separate the two charges that compose the exciton (Section 1.5). This can involve doping a material to create an electronic junction, chemically binding a compound to an interface,[18] designing a single molecule with acceptor/donor moieties,[19] or physically connecting differing materials.[20] The nature of the interface will not only influence the efficiency of charge separation; it will also determine how the solar cell is designed. The interface must always be within the diffusion distance of the exciton, and this can sometimes be a significant limitation, or necessitate a great deal of engineering. Finally, solar cells need to efficiently transfer the separated charge carriers to the working circuit. Charge mobility is the main limitation that some solar cells have in this regard. Too high of a charge mobility will increase the chance of recombination destroying the energy stored in the charge pair, but too low of a charge mobility will negatively influence charge separation and lead to more charge trapping. A mismatch of charge mobility can also occur, which can cause charge buildup in the solar cell, also decreasing efficiency. Charge mobility can be increased (and recombination minimized) by using high purity materials and strongly ordering the material during production. This allows for an optimal path for charges to diffuse to the electrodes.

1.8 Types of Solar Cell

1.8.1 Silicon Cells

While Becquerel first observed the photoelectric effect in silver chloride solutions in 1839,[22] it wasn't until 1954 that the first practical solar cells were created by Bell Labs from silicon transistors.[23] Ever since, they have been the gold standard and are still the most widely distributed type, making up over 80% of the photovoltaic market (Figure 1.4). They come in multiple varieties, from pure single crystal cells to polycrystalline and purely amorphous.

Silicon solar cells all have a similar mechanism of action. While pure silicon has an inherent bandgap of 1.12 eV, it is commonly "doped" with a small amount of material that is designed to slightly increase or decrease the electron density

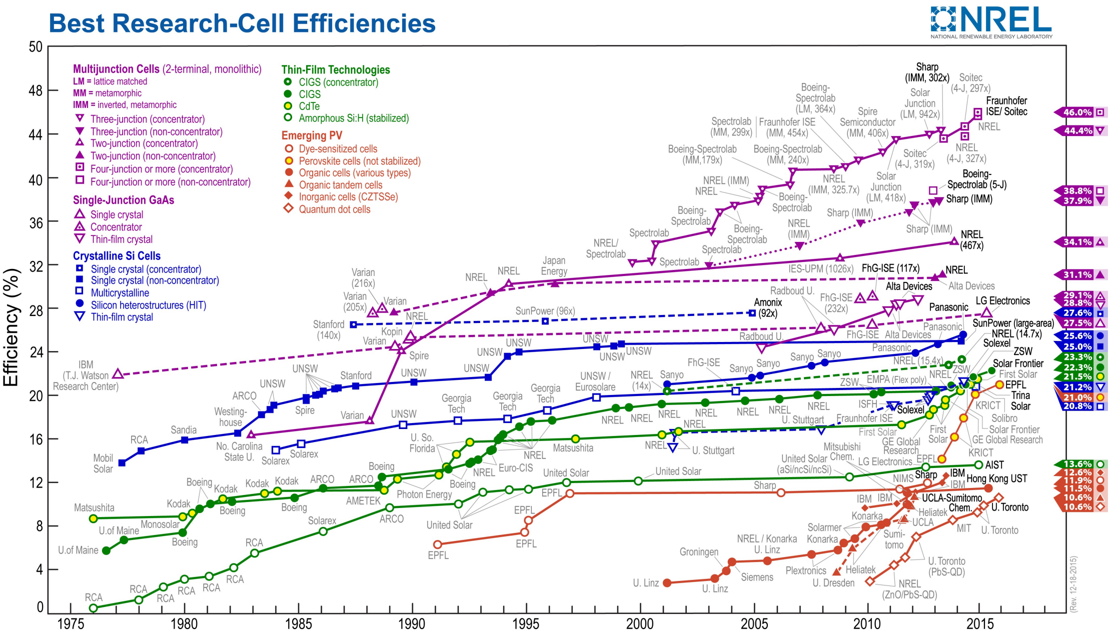

Figure 1.3. Diagram of the most efficient solar cells in recent history, separated by class and conditions.[21]

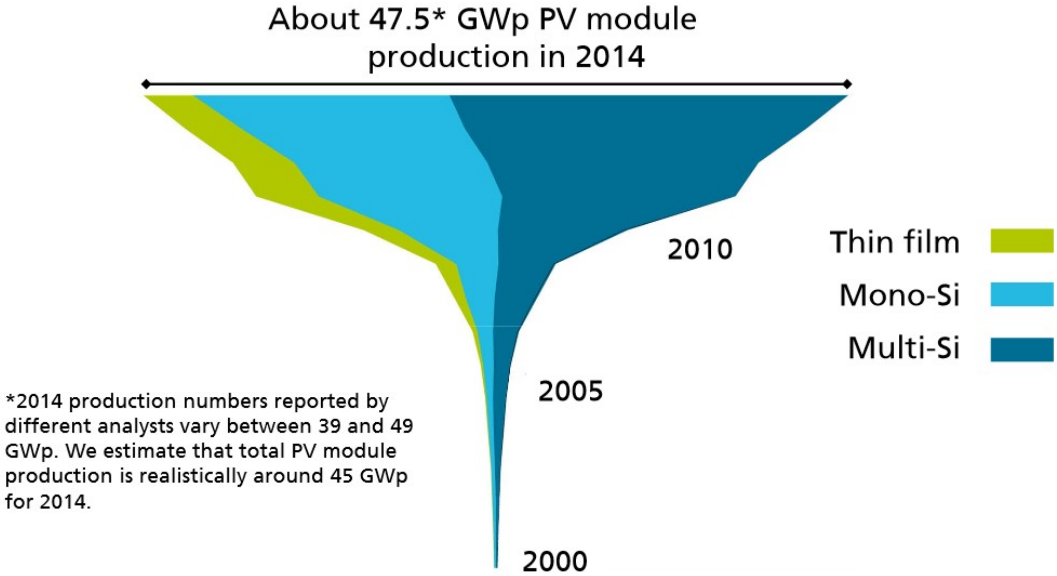

Figure 1.4. Global production of photovoltaic modules.[24]

inside of different halves of the silicon crystal.[25] By doing so, the average energy levels can be shifted in different sections of the crystal. When these sections are connected, it creates a region with an intrinsic electric field at room temperature. In this way, when a photon strikes the material, the exciton can be rapidly split into the electron and hole, with each traveling along different paths to the external circuit. The conversion efficiencies for crystalline and multicrystalline silicon cells have nearly reached the theoretical limit, with recent production of 25.6% and 20.4% efficient solar cells, respectively.[26,27] They also benefit from the massive demand for silicon for transistor applications in most electronics. However, they have a number of drawbacks that limit their distribution. The most prevalent problem is the prohibitive cost, as crystalline silicon requires a very high purity and very careful preparation to insure a highly crystalline material. This combined with the weak absorption of an indirect band gap semiconductor, means that a great deal of very expensive material is necessary.[28] This can account for nearly half the cost of the final product.[29] Along with this, the cells are brittle, and therefore their use cases are limited to those that minimize impacts, and require a maximum amount of power output regardless of cost. For this reason, they are especially prevalent for rooftop panels and solar farms. While amorphous silicon cells do mitigate the problems of crystalline cells, they do so at a large efficiency cost, only achieving 10.1% in a laboratory setting,[30] and as such are only used for low-power applications such as calculators.

1.8.2 Thin Film Cells

While “thin film” solar cell is a broad classification, it is normally used to refer to the second generation of solar cells. These are made out of materials that have a very high absorption coefficient, and so require less material than the traditional silicon. This decreases the price, however the materials used are generally rare and toxic heavy metals that are vapor-deposited on the surface in a low-output process. The three major technologies are cadmium telluride (CdTe), copper indium gallium selenide (CIGS), and gallium arsenide (GaAs) (Figure 1.5).

Cadmium telluride cells are the most popular thin film technology, taking around 5% of the global PV market. They have reached an efficiency of 21%, bringing them close to the performance of crystalline silicon cells.[32] They are also cheaper per kilowatt hour than silicon,[33] as well as having a smaller environmental

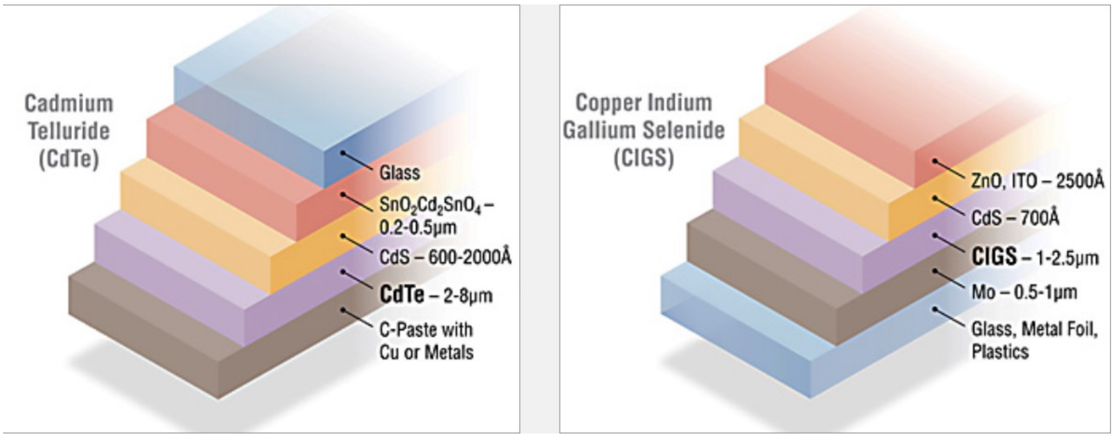
Cadmium Telluride (CdTe)
Glass
SnO₂Cd₂SnO₄ – 0.2-0.5μm
CdS – 600-2000Å
CdTe – 2-8μm
C-Paste with Cu or Metals
Copper Indium Gallium Selenide (CIGS)
ZnO, ITO – 2500Å
CdS – 700Å
CIGS – 1-2.5μm
Mo – 0.5-1μm
Glass, Metal Foil, Plastics

Figure 1.5. (Left) Schematic representation of a CdTe solar cell. (Right) Schematic representation of a CIGS solar cell.[31]

footprint and a shorter energy payback time.[34] However, they require the use of cadmium, a toxic heavy metal, and tellurium, a rare compound. The cadmium limits development by negatively impacting public perception, and the tellurium limits production by its rarity and cost.[35] CIGS cells are a complex heterojunction, direct-band gap material. They have a variable amount of indium and gallium, with a bandgap that can be anywhere between 1.0 eV and 1.7 eV.[36] Generally, a 0.3 ratio of Ga/(Ga+In) is used to get a bandgap between 1.1 and 1.2 eV, similar to silicon.[37] CIGS cells have managed to reach an efficiency of 21.0%,[38] However, their manufacturing process is quite complex, which makes large-scale production quite difficult. GaAs cells are the most expensive of the thin film technologies, but also have the highest efficiencies (27.6%).[39] Combined with a wide bandgap (1.424 eV), suitable for absorbing infrared radiation, this is a solar cell technology well fitted for space applications.

1.8.3 Organic Solar Cells

Organic solar cells are where the semiconductor region is made entirely of organic, generally polymeric, compounds. This drastically decreases the price when compared to other varieties of solar cells, as source materials are not a limiting factor. However, this comes with a similarly drastic decrease in overall solar conversion

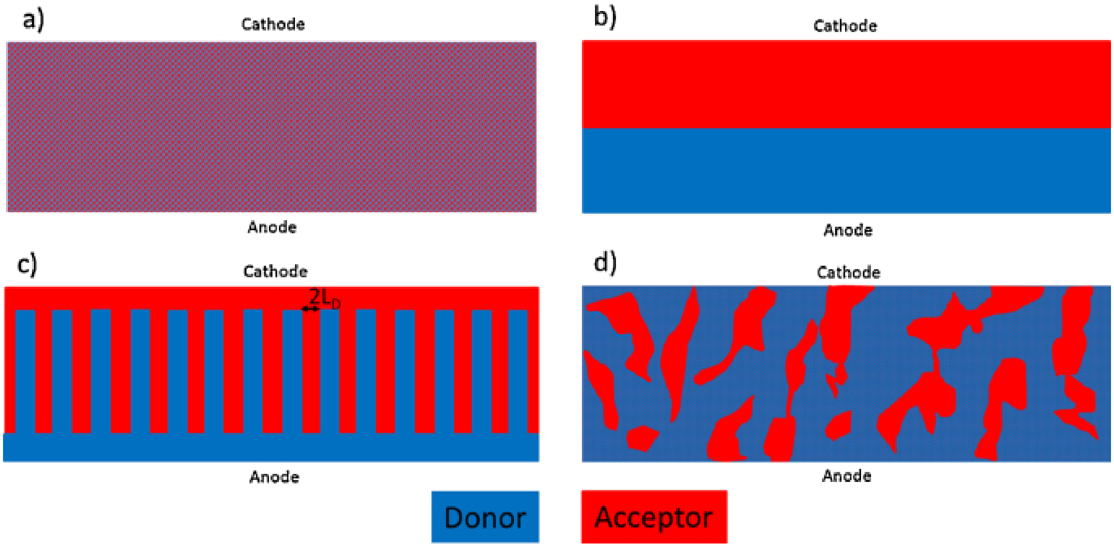

Figure 1.6. (a) Finely mixed donor and acceptor (b) bilayer arrangement (c) ideal "finger" orientation (d) typic bulk heterogenuous processing.[40]

efficiency, as organic cells have only reached 10.7%.[41] There are many reasons for this: the overall photon absorption is decreased due to a decrease in light absorption over the entire solar spectrum when compared to silicon solar cells, the recombination rate is increased due to a drastic drop in exciton diffusion length, and the fill factor and power conversion efficiency are decreased due to an imbalance in charge mobilities. The combination of these factors necessitates a great deal of engineering to find a usable architecture. The p and n junctions of the semiconductor need to be in intimate contact to allow for charge separation to occur efficiently, but the organic region needs to be thick to compensate for the low extinction coefficient. The architecture normally chosen is heterogeneous for exactly this reason (Figure 1.6).

Despite their low cost, ease of processing, and potential applications, the low efficiency and stability of organic cells have so far proven insurmountable challenges, and they have not yet been widely deployed.

1.8.4 Dye-Sensitized Solar Cells (DSSCs)

The first report of a photoelectric effect from a sensitized oxide layer occurred in 1968.[42] After this, DSSCs were mainly used to study photon mechanisms. This involved using chlorophyll to study photosynthesis,[43] and studying excitation mechanisms of ZnO[44] and SnO_2.[45] However, in 1991 the first efficient dye-sensitized solar cell was made by Michael Gratzel and Brian O'Regan,[46] using cis-bis(isothiocyanato)bis(2,2'-bipyridyl-4,4'-dicarboxylato ruthenium(II) as the sensitizing dye. This dye later became known simply as N3 and is still frequently used as a standard for testing solar cell efficiencies (Figure 1.7).

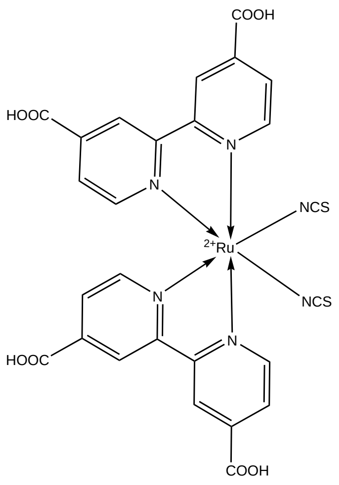

N3

Figure 1.7. Molecular structure of the common "N3" dye.

It had an overall conversion efficiency of 7% in full sunlight, but it was especially noted to have a 12% efficiency in diffuse light, which was something that other solar cells had struggled with at the time. Since then, a great deal of research has gone into addressing the various weaknesses of the DSSC. This has involved expanding the absorption range, stabilizing the dye, replacing the electrolyte, as well as many tricks to improve the solar cells in minor ways. However, most research still uses the basic design published by Gratzel. This design involves using a high surface area semiconductor with a thin layer of a strongly absorbing dye chemisorbed to the surface.

As the light-absorbing portion of most solar cells tends to be the cost-limiting factor, this greatly reduces the cost of the solar cell by decreasing the amount of sensitizing material necessary. While the most efficient DSSCs tend to have an organometallic sensitizing dye, completely organic dyes are also used (Figure 1.8). Like most thin cells, they also have the advantage over silicon cells in flexibility of deployment, as they can be placed in many locales that a crystalline silicon cell could not. However, they have a unique advantage in their excitation mechanism, which injects the excited electron into the semiconductor layer of the solar cell. The electron-withdrawing groups that tend to "anchor" the dye to the semiconductor layer also serve to localize the lowest unoccupied molecular orbital (LUMO) of the molecule near the surface. This brings the excited electron near the semiconductor layer both electronically and spatially, allowing for a very efficient injection mechanism. This drastically reduces the rate of recombination for the solar cell, which can be especially problematic for other solar cell varieties in low-light conditions.

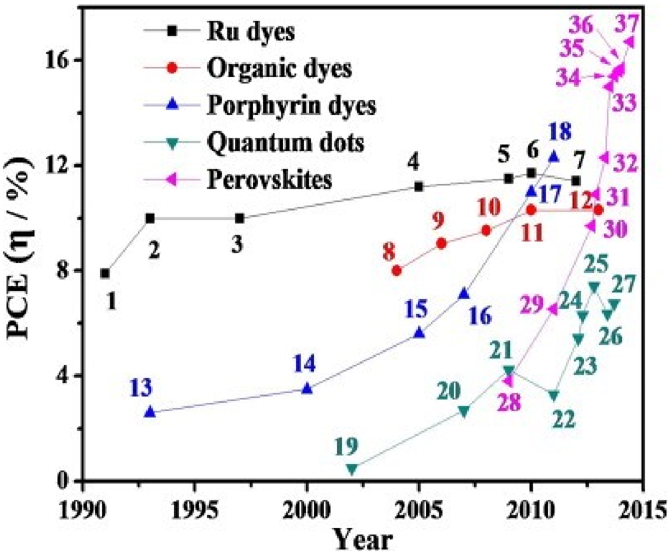

Figure 1.8. Plot of improvement in photon conversion efficiency (PCE) over time for different classes of DSSC sensitizing dyes.[47]

Because of this setup, dye-sensitized solar cells tend to have very high quantum efficiencies, regularly converting more than 80% of incident photons into an electron, with electron injection efficiencies near unity.[48–51] This is a strong contrast to silicon solar cells, which are generally below 50%.[52] As the majority of photons are converted to electrons, the major limiting factor is the overall absorption of the dye. As such, most of the research into improving the overall efficiency of DSSCs is increasing or redshifting the absorption of the dyes.

Improving the absorption spectrum or other properties of the sensitizing dye has given rise to development in a number of classes. The original and still the most common, ruthenium (II) polypyridyl complexes have the advantage of a great deal of optimization and study. This can be as small as changing the cationic counterion,[53] or increasing the dentation,[54] but most of the improvements involve adding conjugated π-systems (to redshift the maximum absorption)[55,56] or conjugated electron donors.[57] These generally lead to improvements, but no significant change has been made in the class for a decade. This could be due to reaching the potential for the class, or it could be due to a lack of fundamental understanding in the field, as many seemingly-promising dyes fail due to unforeseen interactions.

Along with ruthenium dyes, there have been pushes in a number of other categories, some more promising than others. Organic solar cells have the potential to be much less expensive, as they eschew the rare metal components of ruthenium.[19,58] However, their efficiencies have never been particularly promising, and as such, widespread distribution would only be seen if they have some unique property. Likewise, quantum dot DSSCs[59,60] have the potential to improve efficiencies above the Queisser-Shockley limit, as they can generate multiple excitons for each photon. However, they are plagued by recombination problems, and lose much of the generated charge before it can create a usable electron, which inhibits their open-circuit voltage and fill factor. Porphyrin-based solar cells were the first to beat ruthenium dyes in 2011 with an efficiency of 12%,[61] but haven't improved much since.[62] This might be due to the challenge of absorbing the infrared range without co-sensitizing the surface, which greatly complicates cell design. Finally, there are the perovskites, which have generated a great deal of interest since the first was created in 2009[63] The first had an efficiency of 3.81%, but the class rapidly overtook all others, becoming the most efficient class of DSSC in 2013, and still hold that record at 16.7%.[64] This advancement occurred so rapidly due to the cheap and easy nature of the perovskite sensitizers, which allowed optimization by improving each detail of the cell to match the dye, such as the hole-conductor.[65] However, these cells have seen no widespread deployment, as the perovskites are highly water-sensitive, undergoing hydrolysis in the presence of any moisture.

While the focus of most research is the dye,[66] every piece of a dye-sensitized solar cell plays into the overall efficiency, as well as the practicality (Figure 1.9). Just as in most solar cells, the bandgap of the light-sensitive portion is going to strongly influence the overall efficiency, as per the calculations of Shockley and Queisser (Section 1.3). However, dye-sensitized solar cells have additional limitations imposed by the need to move the separated charges through different intermediaries before reaching the electrodes. As such, the conduction band of the semiconductor oxide needs to be lower than the LUMO of the chemisorbed dye

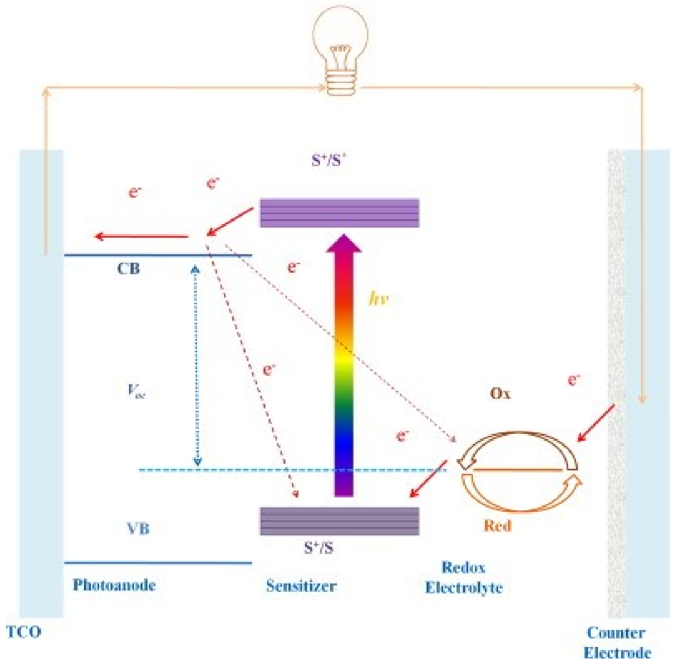

Figure 1.9. Schematic diagram of various electron transfer processes in a dye-sensitized solar cell[47]

to insure efficient electron injection, and the highest occupied molecular orbital (HOMO) of the molecule needs to be lower in energy than the electrolyte to pass the hole toward the cathode. This means that, unlike in silicon solar cells, the open-circuit voltage is necessarily less than the bandgap of the sensitizing dye, and will in fact be determined by the energy difference between the conduction band of the semiconductor and the electrolyte. This also means that there are a lot more points of interaction, and many more functional pieces to study in order to improve the overall cell efficiency.

An example of this is the electrolyte solution. Moving an electron through a high-surface area oxide in contact with an electrolyte would normally be a cause for great concern. Indeed, when using one-electron electrolytes - such as the standard ferrocene/ferrocenium redox couple - most produced electrons recombine with the electrolyte, and so choosing an electrolyte is often a matter of trial and error.[67] However, iodine/triiodide has a very slow recombination rate with electrons coming from the conduction band of most oxide semiconductors, specifically TiO_2, with recombination times on the order of 100 ns, and so is generally the electrolyte of choice.[18] This behavior is generally attributed to the complex kinetics of the iodide/triiodide redox couple.[68] However, other electrolytes have been proven to work to great effect, including radical redox initiators[69] and cobalt[70,71] electrolytes, which were used to create a (then)record-breaking cell.[61] A broader range of electrolytes can also be used (or current ones improved) by using additives such as 4-tertbutylpyridine and guanidium thiocyanate, which serve to passivate the surface and can increase recombination times up to 1 ms.[72,73]

1.9 Organization of the Thesis

This work is focused on investigating fundamental properties of two classes of compounds as they pertain to the creation of advanced dye-sensitized solar cells. Those two classes of compounds are carboxylic acid-functionalized spiropyrans/spirooxazines and dibenzo[*b,j*][1,10]phenanthrolines.

Chapter 2 details the work done on the spiropyrans and spirooxazines. These compounds have unique color-changing properties that could be very useful in the production of solar cells, but also have acid-base sensitivities that haven't been fully explored. As sensitizing dyes are generally anchored using acid-base chemistry with the surface, the effect of such functionalities on the spiran chemistry and effectiveness is explored in this chapter.

Chapter 3 describes the work done on the dibenzo[*b,j*][1,10]phenanthrolines. These compounds are polycyclic heteroaromatic hydrocarbons, which can redshift UV-Vis absorption, in a way that's different from the standard conjugated aromatic systems normally seen in DSSCs. However, using a different backbone is also going to bring a different chemistry from that seen in the common bipyridine-based ligands. For that reason, the chemistry of these compounds is thoroughly explored in this chapter, as well as their potential for use in DSSCs.

1.10 References

(1) Massin, G.; Latour, M.; Rekinger, M.; Theologitis, I.-T.; Papoutsi, M. *Global Market Outlook for Photovoltaics*; 2013.

(2) BP-PLC *Statistical Review of World Energy*; British Petroleum, 2009.

(3) Gillett, N. P.; Arora, V. K.; Flato, G. M.; Scinocca, J. F.; Von Salzen, K. *Geophys. Res. Lett.* **2012**, *39*, 1–5.

(4) Lean, J. L.; Rind, D. H. *Geophys. Res. Lett.* **2008**, *35*, L18701.

(5) Huber, M.; Knutti, R. *Nat. Geosci.* **2011**, *5*, 31–36.

(6) NREL *OpenEI Transparent Cost Database*; 2015.

(7) Iqbal, M., *An Introduction to Solar Radiation*; Academic Press: 1983.

(8) Williams, D. R.

(9) Strutt, J. *Philos. Mag.* **1899**, *47*, 375–394.

(10) Stratton, J., *Electromagnetic Theory*; McGraw-Hill: New York, 1941.

(11) Wurfel, P., *The Physics of Solar Cells*; Wiley-VCH: Weinheim, 2005.

(12) ASTM G173-03 *Standard Tables for Reference Solar Spectral Irradiances: Direct Normal and Hemispherical on 37° Tilted Surface*; West Conshohocken, PA: ASTM International, 2012.

(13) Shockley, W.; Queisser, H. J. *J. Appl. Phys.* **Mar. 1, 1961**, *32*, 510–519.

(14) Richter, A.; Hermle, M.; Glunz, S. W. *IEEE J. Photovolt.* **Oct. 2013**, *3*, 1184–1191.

(15) Shaklee, K. L.; Nahory, R. E. *Phys. Rev. Lett.* **Apr. 1970**, *24*, 942–945.

(16) Green, M. A. *AIP Adv.* **Nov. 2013**, *3*, 112104.

(17) Carlson, D., *Topics in Applied Physics: Amorphous Semiconductors: Amorphous silicon solar cells*, 1985.

(18) Haque, S. A.; Tachibana, Y.; Klug, D. R.; Durrant, J. R. *J. Phys. Chem. B* **1998**, *102*, 1745–1749.

(19) Feng, J.; Jiao, Y.; Meng, S. *J. Phys. Chem. C* **2013**.

(20) Yang, L.-G.; Chen, F.; Xu, H.; Wang, M.; Chen, H.-Z. *J. Appl. Phys.* **2009**, *106*, 073701.

(21) NREL *Best Research-Cell Efficiencies*; NREL, 2013, p 1.

(22) Becquerel, M. E. *Comptes Rendus* **1839**, *9*, 561–567.

(23) Chapin, D. M.; Fuller, C. S.; Pearson, G. L. *J. Appl. Phys.* **1954**, *25*, 676–677.

(24) Burger, B.; Kiefer, K.; Kost, C.; Nold, S.; Philipps, S.; Preu, R.; Schindler, R.; Schlegl, T.; Stryi-Hipp, G.; Willeke, G.; Wirth, H.; Brucker, I.; Häberle, A.; Schacht, V.; Warmuth, W. *Photovoltaics Report*; Fraunhofer Institute for Solar Energy Systems, 2013, p 39.

(25) A. Green, M. *Sol. Energy* **2004**, *76*, 3–8.

(26) *Panasonic HIT Solar Cell Achieves World ' s Highest Energy Conversion Efficiency of 25.6% at Research Level*; Panasonic Corporation, 2014, pp 41–43.

(27) Schultz, O.; Glunz, S. W.; Willeke, G. P. *Prog. Photovolt. Res. Appl.* **2004**, *12*, 553–558.

(28) Hegedus, S. S.; Luque, A. In *Handbook of Photovoltaic Science and Engineering*, Luque, A., Hegedus, S., Eds.; John Wiley & Sons, Ltd: 2003, pp 1–43.

(29) Campbell, S. A., *The Science and Engineering of Microelectronic Fabrication*, 2001; Vol. 476; 688 pp.

(30) Benagli, S.; Borrelo, D.; Vallat-Sauvain, E.; Meier, J.; Kroll, U.; Hoetzel, J.; Bailat, J.; Steinhauser, J.; Marmelo, M.; Monteduro, G.; Castens, L. In *24th EUPVSEC, Hamburg, Germany*, 2009, pp 21–25.

(31) NREL.

(32) Solar, F.; Solar, F.; Solar, A. F. **2015**, –1.

(33) Biello, D. *Sci. Am.* **2008**.

(34) De Wild-Scholten, M. J. *Sol. Energy Mater. Sol. Cells* **2013**, *119*, 296–305.

(35) Woodhouse, M.; Goodrich, A.; Margolis, R.; James, T.; Dhere, R.; Gessert, T.; Barnes, T.; Eggert, R.; Albin, D. *Sol. Energy Mater. Sol. Cells* **2012**, *115*, 199–212.

(36) Tinoco, T.; Rincón, C.; Quintero, M.; Pérez, G. S. *Phys. Status Solidi A* **1991**, *124*, 427–434.

(37) Kemell, M.; Ritala, M.; Leskelä, M. *Crit. Rev. Solid State Mater. Sci.* **2005**, *30*, 1–31.

(38) Osborne, M.

(39) Kayes, B. M.; Nie, H.; Twist, R.; Spruytte, S. G.; Reinhardt, F.; Kizilyalli, I. C.; Higashi, G. S. In *Conference Record of the IEEE Photovoltaic Specialists Conference*, 2011, pp 000004–000008.

(40) Scharber, M. C.; Sariciftci, N. S. *Prog. Polym. Sci.* **Dec. 2013**, *38*, 1929–1940.

(41) Service, R. F. *Science* **2011**, *332*, 293–293.

(42) Gerischer, H.; Michel-Beyerle, M.; Rebentrost, E.; Tributsch, H. *Electrochem. Acta* **1968**, *13*, 1509–1515.

(43) Tributsch, H. *Photochem. Photobiol.* **1972**, *16*, 261–269.

(44) Pettinger, B.; Schöppel, H.-R.; Gerischer, H. *Berichte Bunsenges. Für Phys. Chem.* **Oct. 1973**, *77*, 960–966.

(45) Memming, R.; Schröppel, F. *Chem. Phys. Lett.* **Apr. 1979**, *62*, 207–210.

(46) O'Regan, B.; Grätzel, M. *Nature* **Oct. 1991**, *353*, 737–740.

(47) Ye, M.; Wen, X.; Wang, M.; Iocozzia, J.; Zhang, N.; Lin, C.; Lin, Z. *Mater. Today* **Apr. 2015**, *18*, 155–162.

(48) Nazeeruddin, M. K.; Kay, A.; Rodicio, I.; Humphry-Baker, R.; Mueller, E.; Liska, P.; Vlachopoulos, N.; Graetzel, M. *J. Am. Chem. Soc.* **1993**, *115*, 6382–6390.

(49) Nazeeruddin, K. **1997**, *1*, 1705–1706.

(50) Ito, S.; Murakami, T.; Comte, P.; Liska, P.; Gratzel, C.; Nazeeruddin, M.; Gratzel, M. *Thin Solid Films* **May 2008**, *516*, 4613–4619.

(51) Chen, X.; Liu, L.; Yu, P. Y.; Mao, S. S. *Science* **Feb. 2011**, *331*, 746–50.

(52) Jiao, K.; Zhang, D.; Chen, Y. *RSC Adv* **Oct. 2014**, *4*, 55300–55304.

(53) Nazeeruddin, M. K.; De Angelis, F.; Fantacci, S.; Selloni, A.; Viscardi, G.; Liska, P.; Ito, S.; Takeru, B.; Grätzel, M. *J Am Chem Soc* **2005**, *127*, 16835–16847.

(54) Han, L.; Islam, A.; Chen, H.; Malapaka, C.; Chiranjeevi, B.; Zhang, S.; Yang, X.; Yanagida, M. *Energy Environ. Sci.* **2012**, *5*, 6057.

(55) Mishra, A.; Pootrakulchote, N.; Fischer, M. K. R.; Klein, C.; Nazeeruddin, M. K.; Zakeeruddin, S. M.; Bäuerle, P.; Grätzel, M. *Chem. Commun. Camb. Engl.* **Dec. 2009**, 7146–8.

(56) Mishra, A.; Pootrakulchote, N.; Wang, M.; Moon, S.-J.; Zakeeruddin, S. M.; Grätzel, M.; Bäuerle, P. *Adv. Funct. Mater.* **Mar. 2011**, *21*, 963–970.

(57) Yum, J.-H.; Jung, I.; Baik, C.; Ko, J.; Nazeeruddin, M. K.; Grätzel, M. *Energy Environ. Sci.* **Dec. 2009**, *2*, 100.

(58) Horiuchi, T.; Miura, H.; Sumioka, K.; Uchida, S. **2004**, *126*, 12218–12219.

(59) Plass, R.; Pelet, S.; Krueger, J.; Gra, M. *J. Phys. Chem.* **2002**, *106*, 7578–7580.

(60) Pan, Z.; Zhao, K.; Wang, J.; Zhang, H.; Feng, Y.; Zhong, X. *ACS Nano* **2013**, *7*, 5215–5222.

(61) Yella, A.; Lee, H.-W.; Tsao, H. N.; Yi, C.; Chandiran, A. K.; Nazeeruddin, M. K.; Diau, E. W.-G.; Yeh, C.-Y.; Zakeeruddin, S. M.; Grätzel, M. *Science* **Nov. 2011**, *334*, 629–34.

(62) Mathew, S.; Yella, A.; Gao, P.; Humphry-Baker, R.; Curchod, B. F. E.; Ashari-Astani, N.; Tavernelli, I.; Rothlisberger, U.; Nazeeruddin, M. K.; Grätzel, M. *Nat. Chem.* **2014**, *6*, 242–7.

(63) Kojima, A.; Teshima, K.; Shirai, Y.; Miyasaka, T. *J. Am. Chem. Soc.* **2009**, *131*, 6050–1.

(64) Jeon, N. J.; Lee, H. G.; Kim, Y. C.; Seo, J.; Noh, J. H.; Lee, J.; Seok, S. I. *J. Am. Chem. Soc.* **2014**, *136*, 7837–40.

(65) Kim, H.-S.; Lee, C.-R.; Im, J.-H.; Lee, K.-B.; Moehl, T.; Marchioro, A.; Moon, S.-J.; Humphry-Baker, R.; Yum, J.-H.; Moser, J. E.; Grätzel, M.; Park, N.-G. *Sci. Rep.* **2012**, *2*, 591.

(66) Yin, J.-F.; Velayudham, M.; Bhattacharya, D.; Lin, H.-C.; Lu, K.-L. *Coord. Chem. Rev.* **Dec. 2012**, *256*, 3008–3035.

(67) A. Gregg, B.; Pichot, F.; Ferrere, S.; Fields, C. L. *J. Phys. Chem. B* **2001**, *105*, 1422–1429.

(68) Boschloo, G.; Hagfeldt, A. *Acc. Chem. Res.* **2009**, *42*, 1819–1826.

(69) Zhang, Z.; Chen, P.; Murakami, T. N.; Zakeeruddin, S. M.; Graetzel, M. *Adv. Funct. Mater.* **2008**, *18*, 341–346.

(70) Nusbaumer, H.; Moser, J. E.; Zakeeruddin, S. M.; Nazeeruddin, M. K.; Grätzel, M. *J. Phys. Chem. B* **2001**, *105*, 10461–10464.

(71) Hattori, S.; Wada, Y.; Yanagida, S.; Fukuzumi, S. *J. Am. Chem. Soc.* **2005**, *127*, 9648–9654.

(72) Boschloo, G.; Häggman, L.; Hagfeldt, A. *J. Phys. Chem. B* **July 1, 2006**, *110*, 13144–13150.

(73) Kopidakis, N.; Neale, N. R.; Frank, A. J. *J. Phys. Chem. B* **2006**, *110*, 12485–12489.

.

Chapter 2: Color-Changing Solar Cells

2.1 Abstract

In this chapter, I investigate the potential use of acid-functionalized spiropyrans and spirooxazines in the creation of color-changing dye-sensitized solar cells (DSSCs). To this end, their photophysical and photochromic properties were investigated in various solvents and pH conditions using UV-Vis spectroscopy. Their surface interactions with TiO_2 were investigated using IR spectroscopy. Finally, their performance as sensitizing dyes in DSSCs were investigated. I discovered that the acid functionalization encouraged aggregation, which inhibited efficiency of the solar cells without careful solvent control. Along with this, other functional groups interacted with the TiO_2 in unexpected ways to inhibit photochromism. I was successful in making both effective and photochromic DSSCs using these compounds, and with the knowledge gained from investigating their fundamental properties, a DSSC that is both effective and photochromic could be made.

2.2 Overview

As stated in Section 1.8.4, dye-sensitized solar cells (DSSCs) are separated into multiple independent components, which allows for manipulating the properties of each individual piece. This means that DSSCs can be given properties that might not be possible in other solar cells, as there is no need to optimize for photon absorption, injection efficiency, exciton separation, electron transfer, etc. Using the above reasoning, we may therefore propose giving a DSSC another desirable property, which would give it niche applications outside of what is possible for other systems that could compensate for the unchanging low efficiencies.[1]

The property chosen was photochromism. By creating a DSSC that could change color upon light exposure, the hope was to create a system that could serve a purpose similar to transition sunglasses, while generating a usable current. In order to do this, a photochromic compound was necessary that could bind to the semiconductor surface, which is generally accomplished with acidic functionalities.

The most common photochromic compounds are the spiropyrans and spirooxazines, however their interaction with acidic functionalities and conditions is not well-studied, and their performance as a sensitizing dye is unknown. Therefore, I had the following goals:

1. Synthesize a set of spiropyrans and spirooxazines that are capable of binding to a metal-oxide semiconductor
2. Study the photochromic behavior of this new set of compounds in solution, in varying pH conditions, and on a TiO_2 surface
3. Create a DSSC sensitized with these dyes, and evaluate its performance
4. Using the above information, attempt to create a photochromic DSSC

The basic information obtained from the photochromic studies would provide an expansion of our knowledge for the behavior of these compounds. Their incorporation into a DSSC would provide the first known example of their use as a sensitizing dye and would open an entirely new class of compounds for further exploration. Finally, if successful, the creation of a photochromic DSSC would create new possibilities for this class of solar cells, and allow for further experimentation beyond simply attempting to increase efficiency.

2.3 Photochromism

Photochromism is a coloration in response to light exposure. From a purely chemical standpoint, this indicates the presence of a bond on the molecule that is sen-

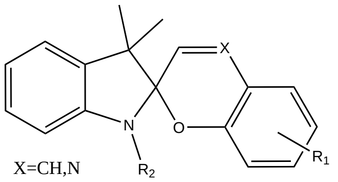

Figure 2.1. General structure of the spiro compounds. CH = spiropyrans, N = spirooxazines.

sitive to the incoming changing dipole of a sufficiently high-energy photon. The fracture (or formation) of this bond then leads to a conjugated π-system which allows for absorption of longer wave electromagnetic radiation. This allows for a large number of applications, including optical storage,[2] color-changing glass or lenses,[3] shape changing polymers, and many other types of photonic devices.[4] The chemical classes most commonly used for these devices are azas,[5] diarylethenes,[2,6] and spiropyrans and spirooxazines.[7–11]

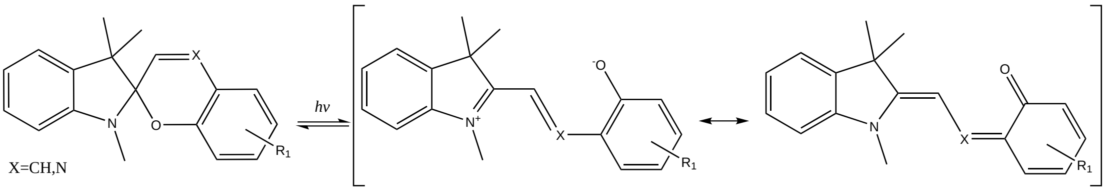

Figure 2.2. Mechanism of photochromic behavior in spiropyrans and spirooxazines

Discovered in 1952, spiropyrans were one of the earliest compounds found with photochromic behavior.[12] Since then, they have become one of the most studied compounds in this class, along with their derivatives, the spirooxazines (Figure 2.1). They were chosen for this project due to their long history and well known chemistry, as well as for their strong absorption in the visible range, which has the largest solar output (Figure 1.2). I will refer to the two combined in this chapter as simply “spirans.”

In these spirans, the C-O bond from the spiro carbon is weakened from the donation of the nitrogen's loan pair into the empty σ^*orbital, lengthening the C-O bond from 1.41 Å for a standard C_{sp_3}-O bond to 1.460 Å for a relatively neutral spiran.[13] This bond can then be further weakened by irradiation with >300 nm light. This excitation causes an intramolecular charge transfer, leading to a positive charge on the oxygen.[14] The increased positive charge causes further lengthening of the C-O bond, followed by fracture. The electrons from the C-O bond can then electronically connect the two separate π systems, allowing for the absorption of visible light.

There are two main resonance forms to this structure - one involves a zwitterionic charge separation between the indoline nitrogen and the phenoxide, and the other involves a less polar quinoidal form (Figure 2.2). Excitation of this merocyanine-like structure leads to the formation of a structure intermediate in polarity between these two resonance forms. Depending on which is predominant in the merocyanine form, excitation can either lead to an increase or a decrease in polarity. Many of the studied properties rely on this polarity difference, and as such, we will designate the merocyanine form separately from the spiran form. For example: Sp_1 and Sp_{1M}.

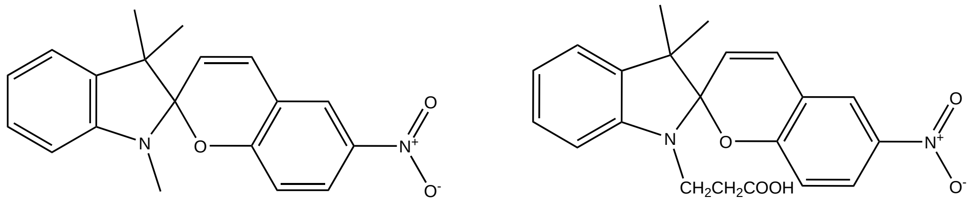

(a) 1',3',3'-trimethyl-6-nitrospiro[chromene-2,2'-indoline] **(Sp_1)**

(b) 3-(3',3'-dimethyl-6-nitrospiro[chromene-2,2'-indolin]-1'-yl)propanoic acid **(Sp_2)**

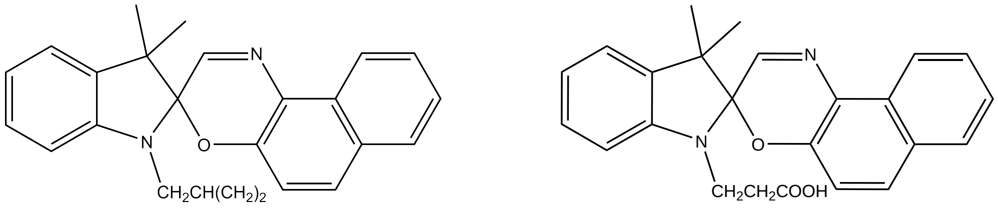

(c) 1-isobutyl-3,3-dimethylspiro[indoline-2,3'-naphtho[2,1-b][1,4]oxazine]**(Ox_1)**

(d) 3-(3,3-dimethylspiro[indoline-2,3'-naphtho[2,1-b][1,4]oxazin]-1-yl)propanoic acid **(Ox_2)**

Figure 2.3. Diagrams of the studied compounds

Anchoring to the TiO_2 commonly used in DSSCs generally requires the use of an acidic moiety,[15] and spiran compounds are well known for their sensitivity to acidic conditions.[16–18] In this work, we took common, neutral examples of photochromic spirans, and synthesized a propanoic-acid functionalized derivative. This would allow us to study the effect of the added acidic group along with the general spiran functionality (Figure 2.3). Two main classes of compound were compared: the nitrospiropyrans Sp_1 and Sp_2 (Figures 2.3a and 2.3b) and the naphthospirooxazines Ox_1 and Ox_2 (Figures 2.3c and 2.3d). The nitrospiropyrans are the more reactive of the two derivatives, but the naphthospirooxazines are the more stable. Depending on their behavior on the TiO_2 surface, each of these properties could be desirable in different situations. For example, more reactivity would be desired if the compounds were resistant to color change, but more stability would be desirable if they were easily switchable. The merocyanine structure of Sp_1, Sp_2, Ox_1, and Ox_2 are designated Sp_{1M}, Sp_{2M}, Ox_{1M}, and Ox_{2M}, respectively. It should be noted that as the spiran forms of these compounds are colorless, the strongly colored MC forms will be the strongest contributors to solar cell efficiency (Figure 2.2)

2.4 UV-VIS Analysis

2.4.1 Spiropyrans

The spiran compounds are composed of two separate π systems, each with a heteroatom. These π systems are perpendicular to one another, and only electronically interact under rare circumstances. Therefore, each π system should behave relatively independently from each other, and the absorption spectrum in the UV-visible range should be dominated by π-π* and n-π* transitions, especially in higher energy ranges.

And indeed, this is exactly what we see for our spiropyran compounds. Compound Sp_1 has two π-π* transitions that occur closely together at 247 and 270

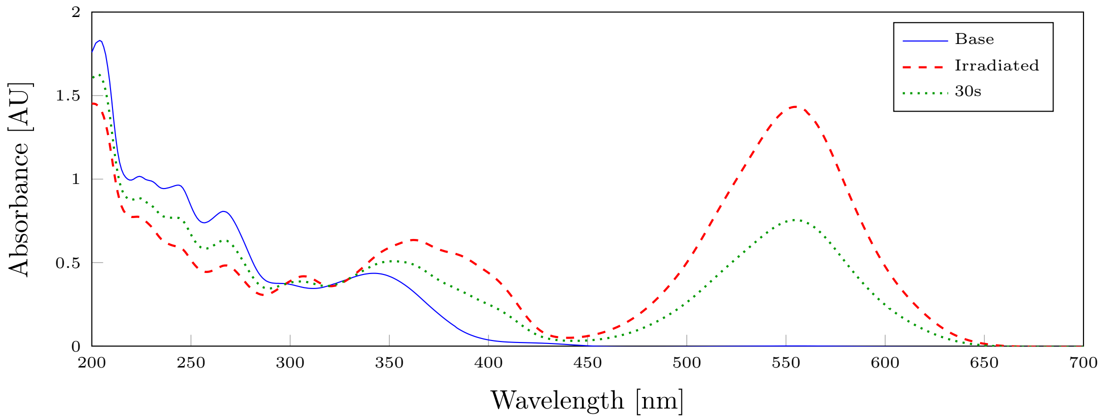

Figure 2.4. UV-VIS Absorbance of Sp_1 in Acetonitrile Before and After Irradiation with UV light

nm in CH_3CN, whereas a combined n-π* and π-π* transition occurs at 342 nm (Figure 2.4) in CH_3CN.[19] Compound Sp_2 is very similar, with the π-π* transitions occurring at 245 and 267 nm, and the n-π* transition at 342 nm (Figure 2.5) in CH_3CN.[20]

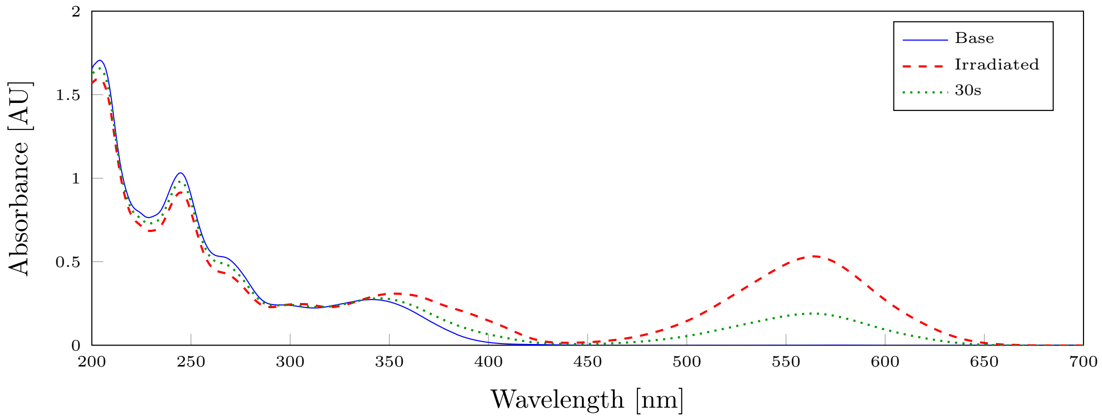

Figure 2.5. UV-VIS Absorbance of Sp_2 in Acetonitrile Before and After Irradiation with UV light

However, the most important feature for each of these compounds is the growth of a new π-π* transition in the visible portion of the UV-Vis spectrum when irradiated with UV light. This is the mode associated with the new open merocyanine form, which is going to contain a single conjugated π-system, rather than two smaller separate ones. This conjugation lowers the energy of the transition, bringing it far into the visible range, and is a convenient target for spectroscopic studies.

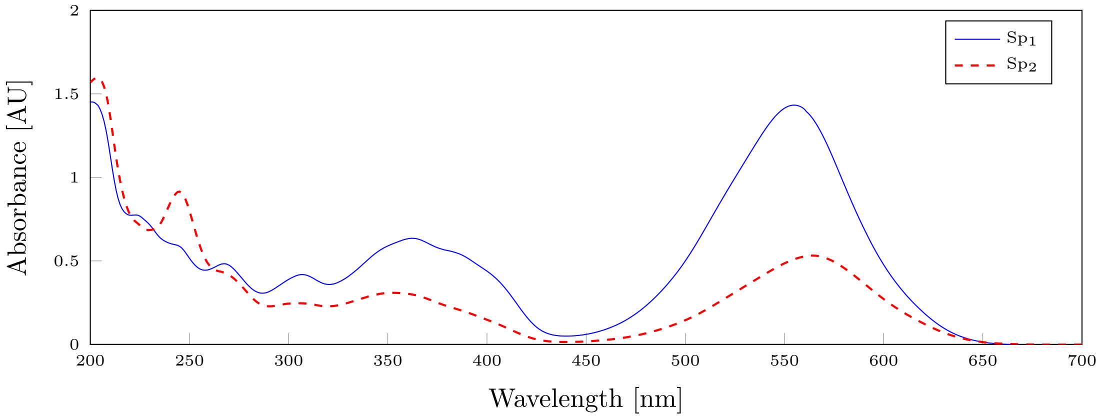

Figure 2.6. Comparison of UV-VIS Absorbance of Sp_1 and Sp_2 in Acetonitrile After Irradiation with UV light

A direct comparison between Sp_{1M} and Sp_{2M} (Figure 2.6) shows a strong similarity between their spectra, as would be expected when the relevant systems have been changed so little. There are two major differences between the two compounds: the π-π* transition is quite visibly modified, with compound Sp_{2M} showing a more distinct absorption at 245 nm than Sp_{1M}. The second major difference is the overall colourizability. While each are treated under identical conditions, the ratio between the initial spiran π-π* transitions and the newly created merocyanine π-π* transition is much greater for Sp_1, which indicates a more stable Sp_{1M}.

2.4.2 Spirooxazines

The same analysis can be done for the spirooxazines, with similar results. Ox_1 has a very clear set of π-π* transitions at 239 nm, which are all overlapped (Figure 2.7).

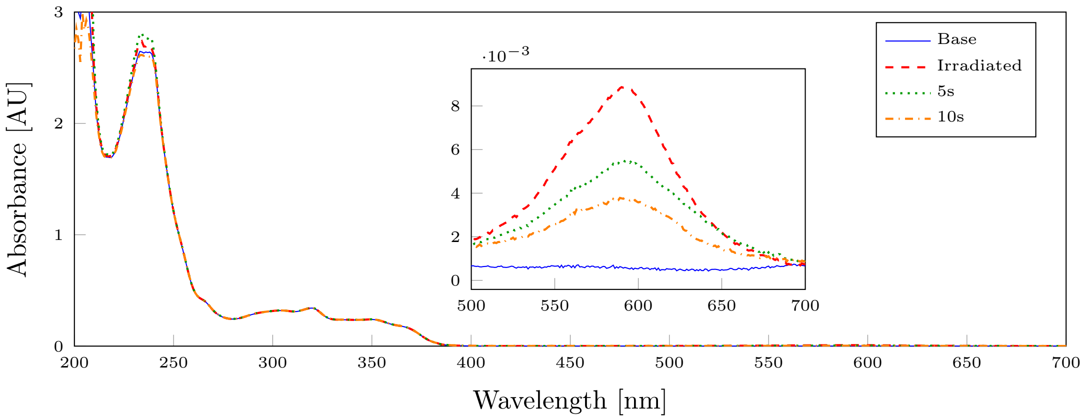

Figure 2.7. UV-VIS Absorbance of Ox_1 in Hexane Before and After Irradiation with UV light

It also has a complex collection of n-π* transitions between 275 and 375 nm, which is to be expected from the addition of another heteroatom into the compound. Ox_2 has a nearly identical pattern (Figure 2.8).

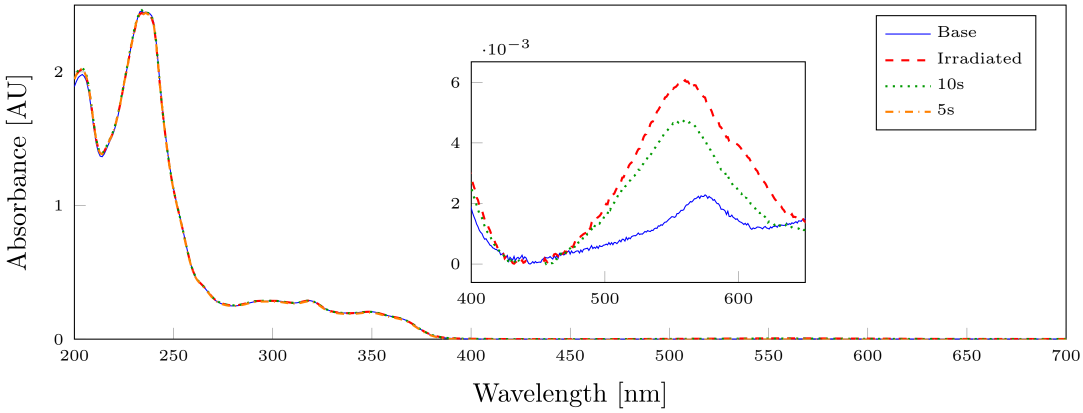

Figure 2.8. UV-VIS Absorbance of Ox_2 in Acetonitrile Before and After Irradiation with UV light

However, one clear point of departure from the spiropyrans Sp_{1M} and Sp_{2M} is the drastic difference in stability of Ox_{2M}. While the merocyanine structure for the spiropyrans was highly evident in the UV-Vis, it is nearly absent here. The reason is not necessarily a weaker absorption, but more likely can be attributed to a lower concentration of the merocyanine. The naphthooxazine creates a much less stable extended structure, which causes a great deal to decay to the spiran before it is measured. This is likely due to a drastic difference in the final structure of the merocyanine. In the naphtooxazines, the additional annulation will stabilize a quinoidal resonance structure of the final merocyanine, rather than a zwitterionic one (Figure 2.2). This non-aromatic structure is less stable than the aromatic zwitterion, and will rapidly decay back to the spiran.

2.5 The Effect of Solvent

As was stated earlier, solvent is going to have a very strong effect on the properties of these compounds. Stabilization/destabilization of the extended merocyanine, the closed spiran, or any intermediate is going to affect the rate of closing/opening, energy levels, and overall behavior.

2.5.1 Spiropyrans

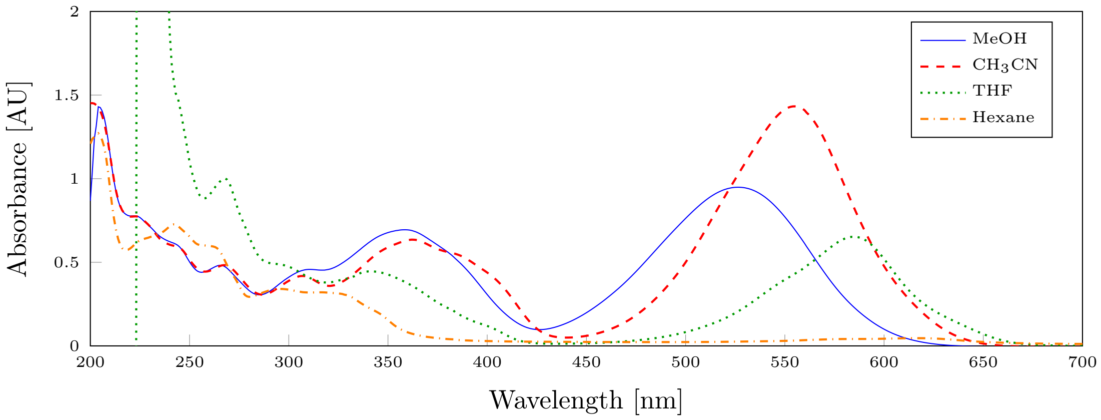

Figure 2.9. Comparison of UV-VIS Absorbance of Sp_1 in Various Solvents After Irradiation with UV light

The nitrospiropyrans are traditionally used for studying the effects of photochromism, as they tend to have a very stable merocyanine structure that is very easily studied. This is also the case here, with Sp_1 displaying visible photochromism in all the studied solvent systems (Figure 2.9). Compound Sp_{1M} has a very clear redshift of the π-π* transition with decreasing polarity, while the π-π* and n-π* transitions of the spiran form are nearly identical throughout the various solvent systems. The main difference between the solvents seem to be, again, colourizability. The THF, by a clear margin, has a much higher concentration of merocyanine with the same irradiation, which can be presumed to be related to the decreased ring closing or the increased ring opening rate.

Another worthwhile feature is the appearance of a shoulder on the THF spectrum, occurring at 540 nm. This is likely due to aggregation in the solution. While this is visibly present in the THF, this could be due either to the polarity of the solvent, or the higher concentration of merocyanine in solution. However, there are two main points of evidence against concentration being the cause. First, the shoulder remains despite decreasing concentration of merocyanine in THF, and second, this shoulder is far more pronounced in hexane (Figure 2.10), which indicates that the aggregate formation is a function of solvent polarity, with lower polarity leading to more aggregation.

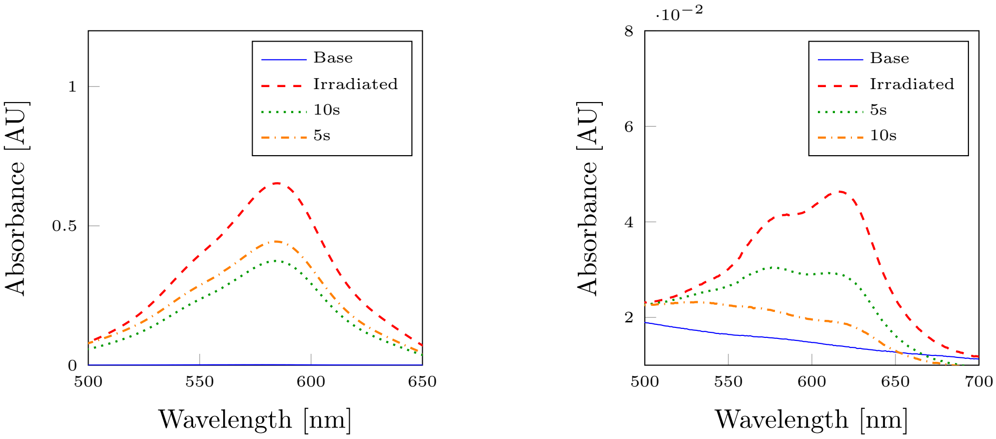

(a) THF

(b) Hexane

Figure 2.10. Comparison of UV-VIS Absorbance of Sp_1 in THF and Hexane

Along with the change in general features of the UV-Vis spectra in each solvent, there is a general trend in the solvents with changing polarity. The Dimroth-Reichardt polarity scale (Et) was used to compare the solvents.[21] The polarities were normalized from 0-1, where zero corresponds to tetramethylsilane, and one corresponds to water. This choice of polarity scale is quite important. When using the more common Snyder polarity index, the linear relationship is lost. As the Dimroth-Reichardt scale is derived from the solvatochromic behavior of a zwiterionic dye, it is quite appropriate for measuring the behavior of this system.

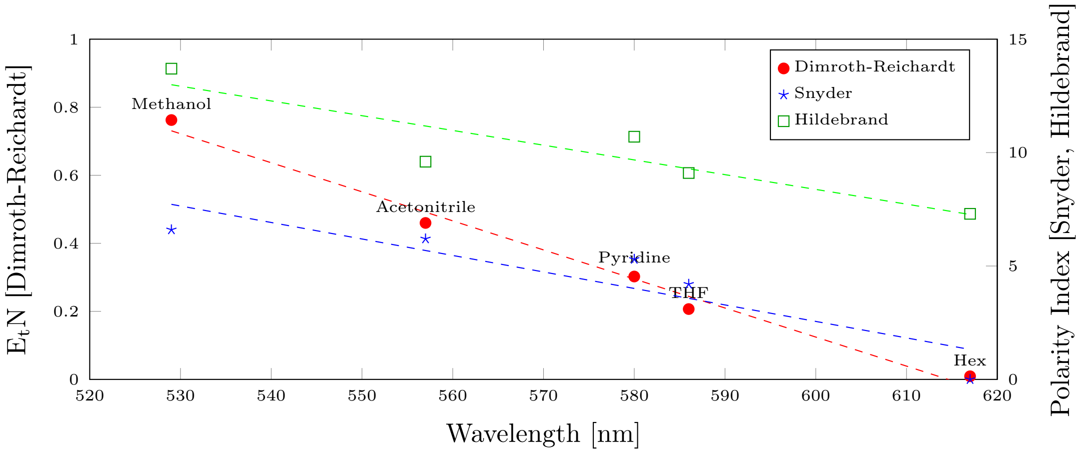

Figure 2.11. Comparison of solvochromatic effect using different polarity indices

Plotting λ_{max} vs E_t yields a very clear picture of the overall shift in λ_{max}, and a clearer picture of the excited state for the compound (Figure 2.11). In this graph, increased polarities are blueshifting the wavelength, which would indicate an increased difference in energy between the excited state and the ground state, which could either be a stabilization of the ground state, or a destabilization of the excited state. Considering that the merocyanine ground state was described as zwitterionic in character, this trend is not surprising. This same reasoning explains the slight redshift in the 350 nm λ_{max} of Sp_1, as the intramolecular charge transfer transition will have the polarized state stabilized by the increasingly polar solvent.

Compound Sp_2 follows a very similar trend as Sp_1 (Figure 2.12).

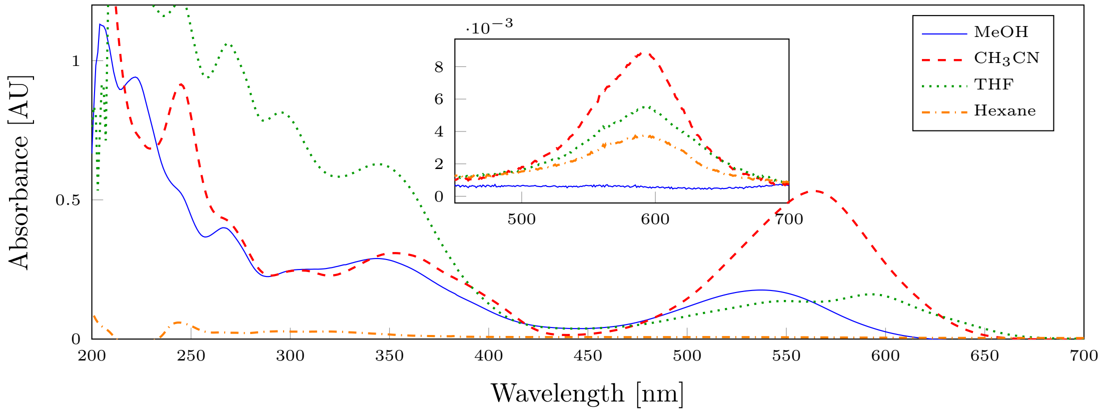

Figure 2.12. Comparison of UV-VIS Absorbance of Sp_2 in Various Solvents After Irradiation with UV light

The appearance of aggregates in solution still occurs in THF for Sp_{2M}, with the rest of the spectrum mostly unchanged. This effect is also more pronounced, with the aggregate peak being much stronger in THF than for Sp_{1M}. This is very likely due to the polar propanoic acid moiety, which would increasingly interact with neighboring molecules in nonpolar solvent. Along with this, there is the appearance of a new transition at 298 nm in THF, which was not present before. This is potentially due to π-stacking in the aggregates creating a new π-π* transition.

2.5.2 Spirooxazines

The spirooxazines are much more difficult to study. As was seen earlier, the concentration of merocyanine form is much lower by the time measurements can be made. This can generally be attributed to a rapid ring closing rate due to the less favorable quinoidal resonance structure being dominant in the napthooxazines. As an example, compound Ox_{1M} has the only measurable decay rate in the standard solvents at a log(k) of -1.451 in hexane. This is significantly faster than all those measured for compound Sp_{1M}.

2.6 The Effect of pH

Coordination with the metal oxide semiconductors commonly found in DSSCs is generally done with acidic functionalities, such as carboxylic acids, sulfonic acids, phosphoric acids, etc.[15] These can then undergo an acid/base reaction with the surface to form a strong bond that enables efficient electron transfer from the dyes into the surface. While acid-functionalized derivatives of the spiran compounds have been made,[22,23] they are normally synthesized as an intermediate to create other derivatives, with their photochromic properties being left unstudied.[24–26] Research on the effect of pH on these spirans is also rare, with most of the research focusing on the protonation of the basic phenoxide in acidic conditions. This protonation has been found to quench the visible π-π* transition of the MC forms. This form is known as the protonated merocyanine (MCH^+).[16,18] Comparatively, very little research has been done on the effect of alkaline conditions,[10] which would be especially relevant with an acid-functionalized compound.

Our study on the acid-functionalized spirans showed that the addition of pyridine to a solution of Sp_2 in methanol caused an immediate conversion of the compound to a colored form, without the input of any ultraviolet light (Figure 2.13). This effect was independent of the base used, as it was also seen with added triethylamine, piperidine, and K_2CO_3. This same effect was seen in acetonitrile, but was not apparent in THF or hexane. Added base also had no visible effect on Sp_1, or either spirooxazine.

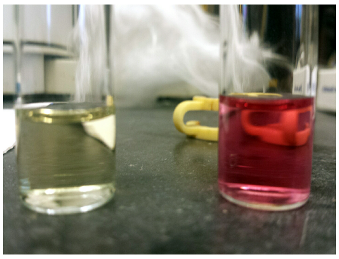

Figure 2.13. (Left) 0.5 mM Sp2 in MeOH (Right) 0.5 mM Sp2 in MeOH upon addition of 100 µL of pyridine.

As this color change is only seen in highly polar solvents, it likely is an effect that requires stabilization of the merocyanine. One hypothesis was that the propanoic acid moiety was protonating the spiran to form the MCH^+. These compounds are mostly colorless, and would rapidly convert to the colored merocyanine upon addition of base. This was tested by titrating an acidic solution of Sp_2 with triethylamine (Figure 2.14). Indeed, there is very little difference between Sp_2 in neutral and acidic conditions, indicating that the propanoic acid functionality could be protonating Sp_{2M} under neutral conditions. This was seen to reverse upon addition of the base, with the formation of the visible transition occurring as the acid was neutralized. This supports the idea of the observed color change being caused by MCH^+ being neutralized to the colored MC form.

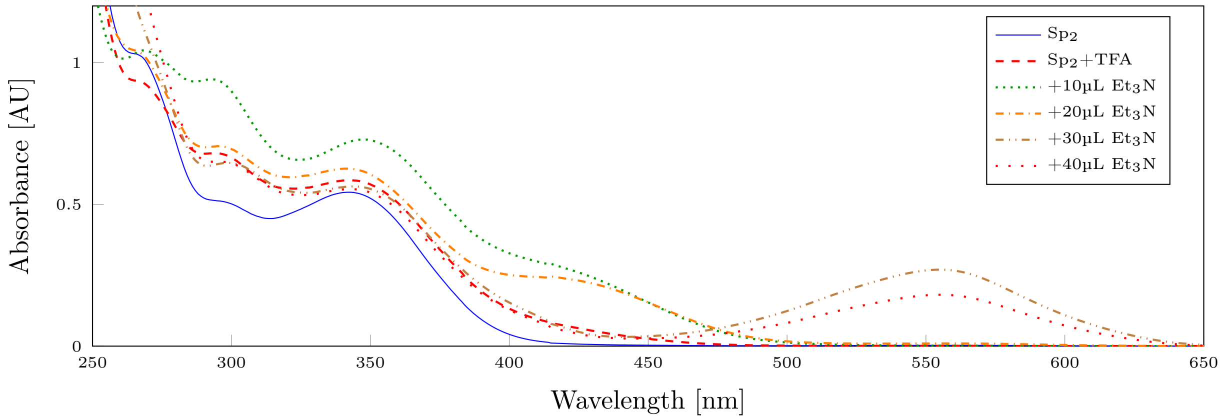

Figure 2.14. UV Spectrum of Sp_2 in CH_3CN, being titrated with Et_3N

We also investigated the effect of basic solvents on the photophysical properties of spirans. As such, the same spectroscopic tests as before were undertaken in pure triethylamine, piperidine, and pyridine. Results here, however, were different than with added base. Rather than causing interconversion in the spiropyrans, the basic solvents alone simply stabilized the zwiterrionic MC form, following the polarity trend predicted by the Dimroth and Reichardt scale.[21] The basic solvents alone also had no appreciable effect on the rate of the ring-closing reaction in spiropyrans

(Figure 2.15b).

2.7 The Effect of COOH

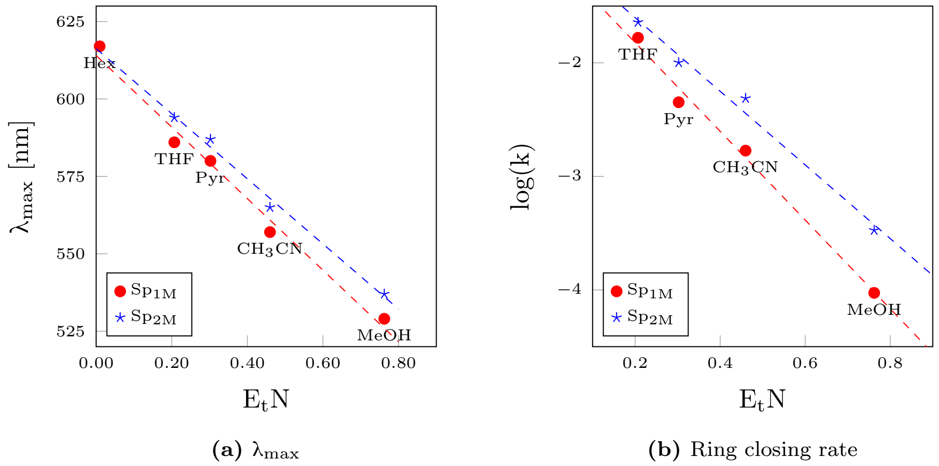

(a) λ_{max} **(b)** Ring closing rate

Figure 2.15. Comparison of a) λ_{max} and b) ring-closing rate for Sp_{1M} and Sp_{2M} vs. solvent polarity

There has been a lot of study on how the structure of spiropyrans and their derivatives affect their properties. One of the earliest breakthroughs was that the addition of electron withdrawing groups to the benzopyran portion of the molecules can drastically extend the lifetime of the extended merocyanine form.[27] These electron withdrawing groups serve the dual purpose of weakening the C-O bond, lengthening it to 1.497 Å for nitro-substituted compounds,[13] while stabilizing the zwitterionic resonance structure of the merocyanine form.

This allowed for much more extensive research than was previously possible, and the research since has supported the conclusion that substituents on the benzopyran moiety strongly affect the photochromic properties of the molecule, while substituents elsewhere have little effect.[13] However, little effect does not mean none. N-substitution of spiropyrans has been shown to have an influence on the ring opening and closing reaction, due to both sterics and electronics.[13] It has also been shown that the ring closing rate, as well as the $\lambda_{\max}$ of the merocyanine, are affected by mildly electron-withdrawing groups attached to the indoline nitrogen.[23] This effect can be clearly seen when comparing the $\lambda_{\max}$ of Sp_1 and Sp_2. Throughout the range of solvents, $\mathrm{Sp}_{2\mathrm{M}}$ is clearly redshifted with respect to $\mathrm{Sp}_{1\mathrm{M}}$, indicating a destabilized ground state. As the electron-withdrawing carboxylic acid moiety is connected to a positively-charged nitrogen in the zwitterionic state, this is not a surprising conclusion. Sp_2 also has a weaker sensitivity to solvent polarity, which is somewhat unusual. This could be due to intramolecular hydrogen bonding compensating for the lack of stabilization by the solvent, or inherently lower response due to the decreased polarity of the merocyanine.

Data can also be obtained for the rate of ring closure. After fully irradiating the compound, the absorbance can be measured at the $\lambda_{\max}$, watching the peak decay over time (Figure 2.16). This has been shown to have a first order decay rate, which can then be converted to find the rate constant in various solvents. As this decay is going to be strongly related to the relative stability of the closed spiran and the open merocyanine, this decay rate can be used to draw conclusions about the nature of the various compounds.

Using this information, a nearly identical trend is seen with the rate of the ring-closing reaction, and is likely due to the same phenomenon (Figure 2.15b).

The naphthospirooxazines, however, have a much more interesting response to the addition of the propanoic acid moiety. What we observed was a different trend in $\lambda_{\max}$, where solvent polarity red-shifts the maximum absorbance (Figure 2.17a), rather than the blue-shift seen for the spiropyrans (Figure 2.15a). This is likely due to the less polar nature of their MC form, which will change how the solvent interacts with the compound.

As the blueshift from the spiropyrans with increasing solvent polarity can be explained by the zwiterrionic structure of the MC form, this $\lambda_{\max}$ redshift of $\mathrm{Ox}_{1\mathrm{M}}$ and $\mathrm{Ox}_{2\mathrm{M}}$ can be explained by a more polar excited MC state, which would be stabilized by the increased polarity. However, the sensitivity to the solvent polarity

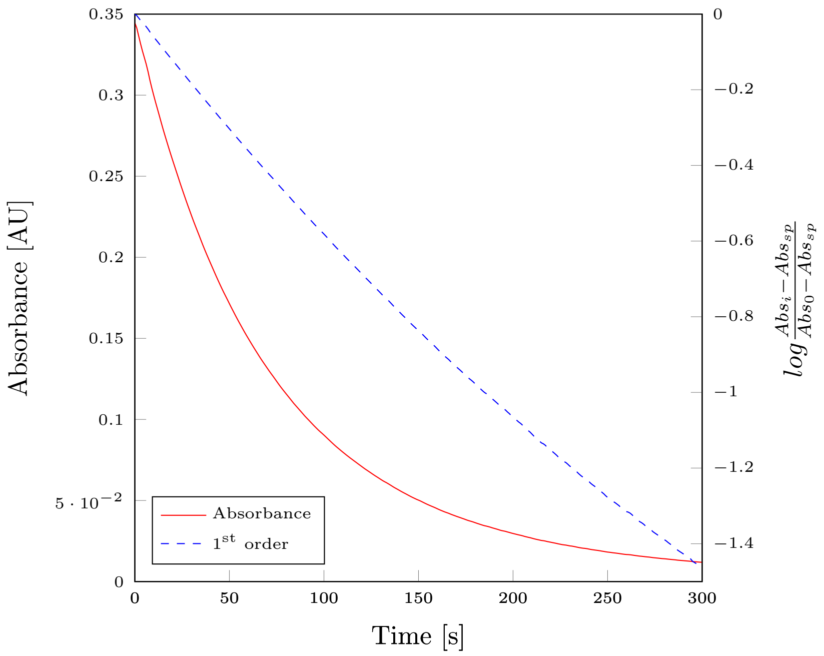

Figure 2.16. Decay of λ_{max} for Sp_{1M} over time

is different between these two compounds.

Figure 2.17b shows a different trend in decay rate for Ox_{1M} and Ox_{2M}. The increase in decay rate for Ox_{1M} with solvent polarity matches our trend for λ_{max}. However, Ox_{2M} shows the opposite trend. The previous explanation for Figure 2.17a would predict the opposite, so the hypothesis of compensating intramolecular forces that we used for Sp_{2M} becomes more feasible. A hypothetical intramolecular interaction with the propanoic acid moiety would become less pronounced in more polar solvents, causing a competing trend that decreases the ring-closing rate.

The increase in decay rate for Ox_{1M} with solvent polarity matches our trend for λ_{max}, which gives generally no problems. However, Ox_{2M} shows the opposite trend, which doesn't match the story that the electronics gave us. As this isn't driven by the electronics of the compound, the hypothesis of the effect of intermolecular forces becomes more feasible. A hypothetical intermolecular interaction between the propanoic acid moiety would become less pronounced in more polar solvents, causing a competing trend that decreased the reaction rate.

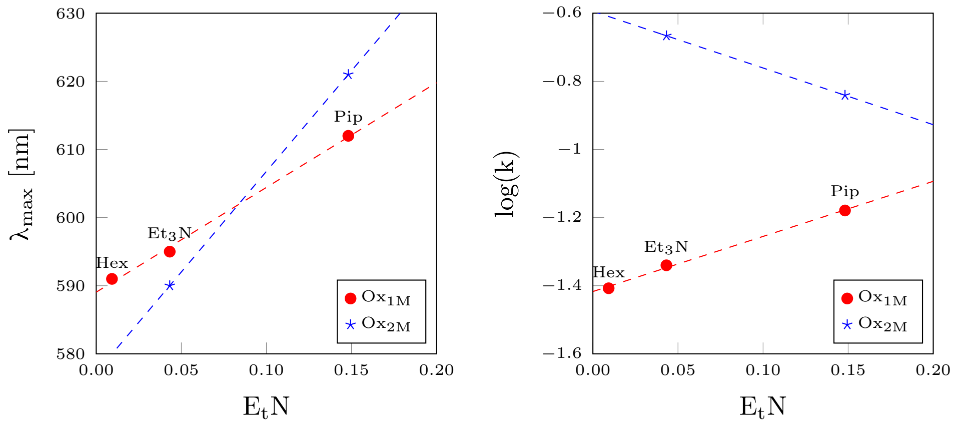

(a) λ_{max} **(b)** Ring-closing rate

Figure 2.17. Comparison of a) λ_{max} and b) ring-closing rate of Ox_{1M} and Ox_{2M} vs. solvent polarity

2.8 Coordination to TiO$_2$

As one of the most common metal oxide semiconductor used in DSSCs, we decided to use TiO$_2$ as the substrate of choice. As such, studies were necessary to determine optimal binding conditions. The standard procedure for coordination of a chosen compound to TiO$_2$ is to soak the prepared electrode in a solution of around 0.5 mM for 24-72 hours. Solvents such as acetonitrile and t-butanol are generally used for this binding,[28] but any solvent or cosolvent system that is unreactive and solvates the chosen compound is suitable. As such, methanol was initially chosen for this coordination (the compound was unstable in acetonitrile). The electrodes were prepared according to the procedure described previously.[28] A titanium dioxide paste was purchased from Solaronix (Ti-Nanoxide T/SP). The paste was then doctor bladed onto FTO glass (Hartford Glass, 7 $\Omega/\square$) and sintered at 500°C for 1 h and cooled to 80°C, at which point it was immersed in the respective dye solutions (0.5 mM in methanol) for 48h. These electrodes were a faint yellow color, as opposed to the N-719 standard (Figure 2.18a).

This could be attributed to two factors: a very low dye loading or a very weak visible absorption (or both). The TiO$_2$ surface was not responsive to UV light, which supports the conclusion of low dye loading, or it could indicate inhibited molecules. The UV-Vis spectrum, however, was more instructive (Figure 2.18b).

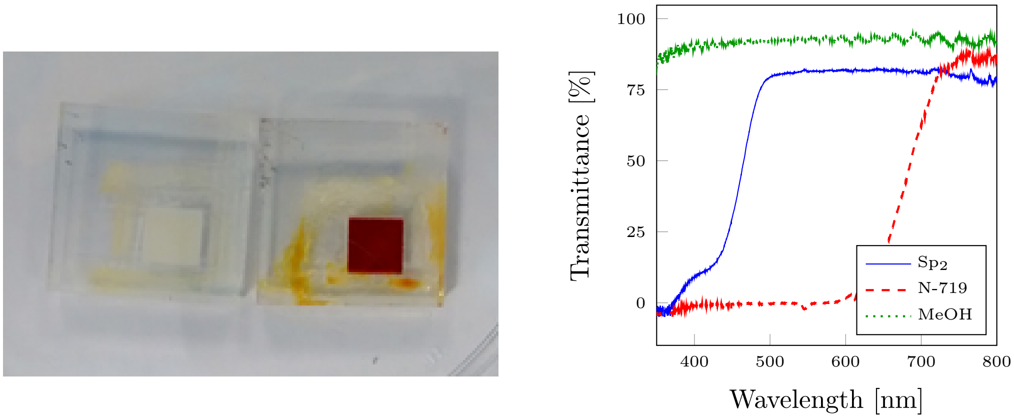

(a) Assembled DSSCs with (left) Sp_2 and (right) N-719

(b) UV-Vis transmittance spectrum of N-719, Sp_2, and methanol over a TiO_2 surface

Figure 2.18. a) Appearance and b) UV-VIS spectrum of Sp_2 absorbed onto TiO_2 compared to N-719

The dye loading of Sp_2 appears to be quite sufficient, as the transmittance quickly drops to 0% below 500 nm. This would indicate that rather than having too few dye molecules, Sp_2 is simply not absorbing in the visible range. As it has been shown that spiran complexes are still photoswitchable when immobilized on surfaces,[29,30] it must be presumed that the compound forms aggregates that inhibit photochromic behavior. This is possibly due to the stabilizing nature of the polar solvent, which will support the formation of merocyanine during the coordination process, forcing head-to-tail aggregation of molecules as they bind to the surface. By contrast, a nonpolar solvent should maintain the spiran form during binding to the TiO_2. After binding, the compound could then be free to open to the merocyanine structure.

One piece of evidence supporting the hypothesis of intramolecular interaction is aggregation in solution. The MC form is known to aggregate under the right conditions, a fact which has been used to assist the supramolecular interaction.[31] These MC structures align in a head-to-tail conformation, driven by the separated charges on the zwitterionic MC.[8] While Sp_{1M} can be seen to undergo some aggregation in less polar solvents like THF (Figure 2.19a), as evidenced by the appearance of a shoulder peak at 562 nm,[32] the J-aggregate peak of Sp_{2M} at 542 nm is far more pronounced (Figure 2.19b). This would indicate that the propanoic acid moiety is aiding in stabilizing aggregation in nonpolar solvents through intermolecular interactions, and could similarly be stabilizing individual molecules through intramolecular interactions.

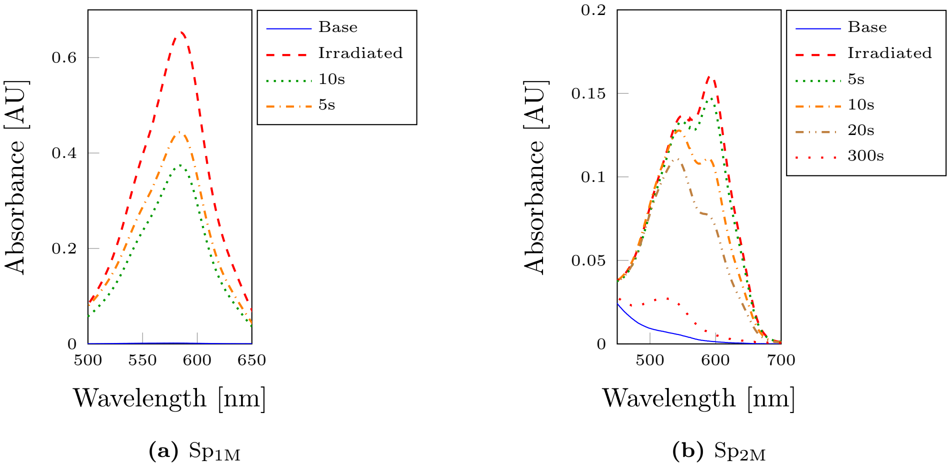

(a) Sp_{1M}

(b) Sp_{2M}

Figure 2.19. Comparison of UV-VIS Absorbance of a) Sp_{1M} and b) Sp_{2M} in THF

And, indeed, this is exactly what was found. When toluene was used as the solvent, a strongly colored surface was created, indicating a high loading of a visibly colored compound (Figure 2.20a). This corresponds to well-separated merocyanine, which would indicate that the spirans were coordinated to the surface independently. Their properties diverged from here, however. Sp_2 stayed the same color of red, and was unresponsive to UV light, visible light, and heat. After being left in darkness for one week, it still had not visibly lost any color, indicating a very stable merocyanine structure on the TiO_2 surface. By contrast, Ox_2 lost its color under ambient conditions over the course of 5 minutes, decaying to the plain white of undoped TiO_2. However, it maintained its photochromic properties while on the surface, responding to UV light to change back to the light green it was before. This was easily illustrated by using a UV LED to irradiate a small part of the surface, which caused the irradiated section to color green, as opposed to the surroundings (Figure 2.20b).

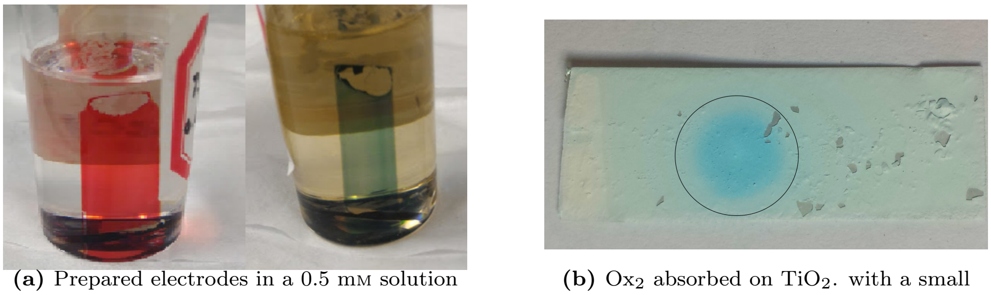

(a) Prepared electrodes in a 0.5 mM solution of (left) Sp_2 and (right) Ox_2 in toluene

(b) Ox_2 absorbed on TiO_2. with a small patch shown after irradiation by a UV LED

Figure 2.20. a) Appearance and b) behavior of Sp_2 and Ox_2 adsorbed onto TiO_2 in toluene

While Ox_2 does have a less stable merocyanine form than Sp_2, as has been illustrated previously, this behavior is nonetheless surprising, as that merocyanine is normally stabilized by the polar solvent, and still only had a lifetime on the order of minutes under the best conditions, not days as is seen here. Thus, it can be supposed that the TiO_2 is interacting with the merocyanine form of Sp_2 to stabilize it, in a way that it is not for Ox_2. The major difference between these two compounds is the different substitution on the benzopyran ring. Nitro groups, under very rare circumstances,[33] have been shown to be capable of anchoring to TiO_2, and that might be the case here. Anchoring the nitro in the open form could prevent the decay back to the closed spiran, giving rise to the effects seen here. The IR spectrum of the merocyanine form of Sp_2 was therefore compared to the IR spectrum of the compound anchored to TiO_2 (Figure 2.21).

There are three main possible binding modes for a carboxylic acid to TiO_2: monodentate, bidentate chelating, and bidentate bridging. These modes can be distinguished by the frequency separation of the carboxylate stretching bands.[34,35]

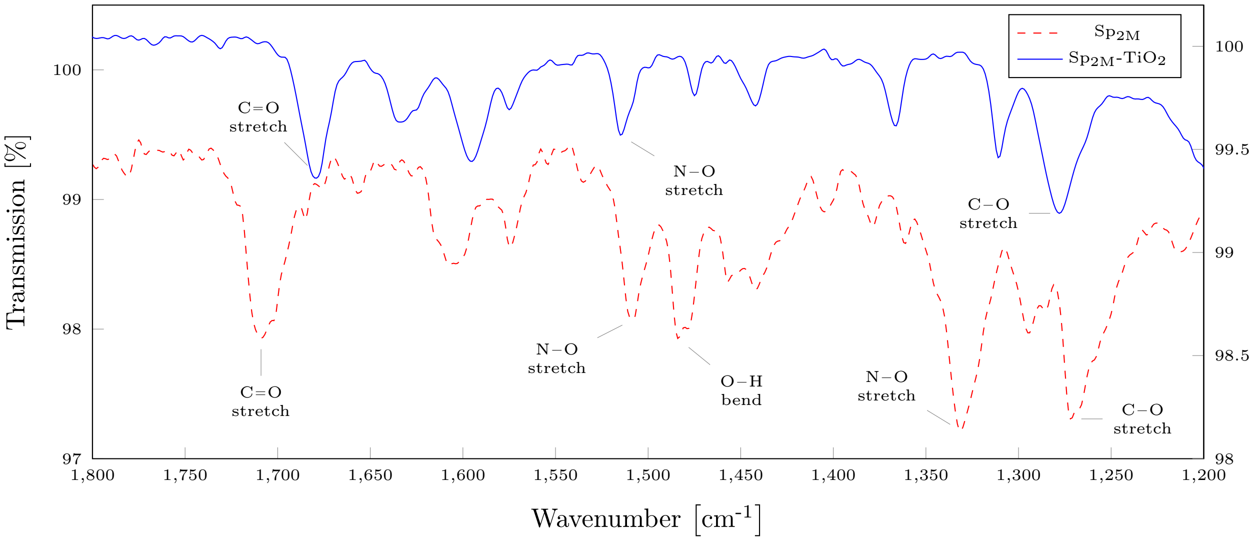

Figure 2.21. Infrared spectra of Sp_2 in the merocyanine form, and Sp_2 bound to TiO_2

In our case, ν(C=O) was shifted from the open value of 1708 to 1681 cm^{-1}, while ν(C-O) shifted from 1272 to 1279 cm^{-1}. This $\Delta\nu$ of 402 cm^{-1} is consistent with a monodentate binding mode, similar to an ester linkage. The binding of the carboxylate is also seen in the complete disappearance of the O-H bending mode. However, what is most interesting is the disappearance of one of the N-O stretching modes upon binding to TiO_2. This was seen in the previous case of -NO_2 binding to TiO_2,[33] but that only bound after the addition of significant current. This would seem to indicate that this is the first example of room-temperature binding of an -NO_2 to TiO_2, although further investigation of the binding mechanism is ongoing.

These results would explain the decreased ring closing rate of the spiropyran. If the $-NO_2$ functionality is coordinating secondarily to the surface, this would allow stabilization by holding the merocyanine structure in the open form (Figure 2.22). These results could be verified with specific surface analysis techniques, such as Raman analysis.

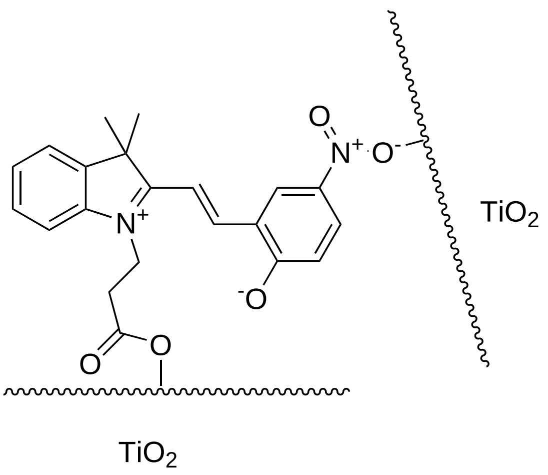

Figure 2.22. Proposed surface binding of of Sp_2 on TiO_2

2.9 Solar Cell Characteristics

Finally, the compounds were tested as the sensitizing dyes in a DSSC. Solar cells sensitized with Sp_2 in methanol had a conversion efficiency of 0.028% compared to a 1.9% efficiency for the reference N-719 cell (Figure 2.23a).[36] As was mentioned above, these cells appeared to either have a low dye loading or a great deal of aggregation, based on their UV-Vis spectra. Because of this, we experimented with a nonpolar solvent system for the binding process, an approach used in systems with similar compounds.[37] When toluene was used as the solvent, the color not only improved drastically (Figure 2.20a), but the overall efficiency did as well, rising by an order of magnitude to a conversion efficiency of 0.26% for Sp_2 (Figure 2.23b). This was mainly driven by an improved J_{sc} (from 0.1 mA cm^{-2} to 1.58 mA cm^{-2}).[36] As J_{sc} is the number of electrons passing through the system without a potential bias, it can be influenced by a number of factors. While the number of electrons excited is one of these factors, another is the number of electrons successfully injected. The -COOH group that is normally responsible for binding is separated from the main chromophore by two sp_3-hybridized carbons, so injection efficiency would be expected to be low through this path.

If the $-NO_2$ is coordinated to the TiO_2 surface, this would serve as a very

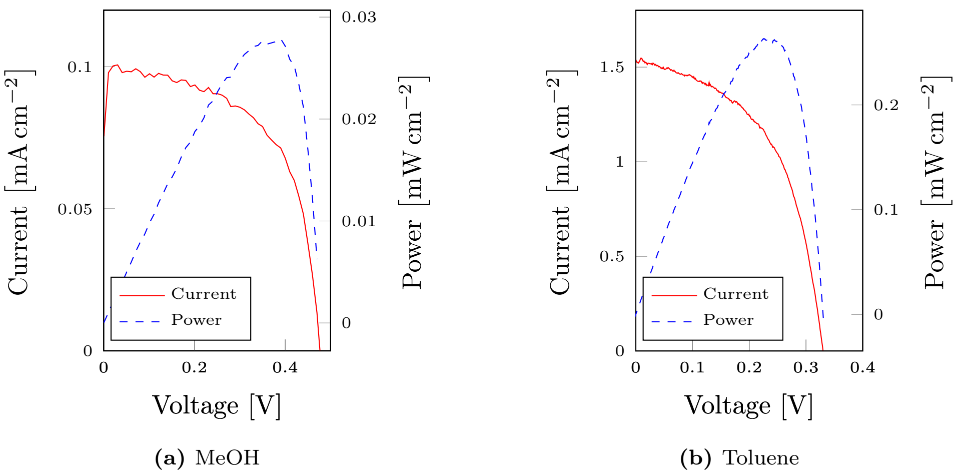

(a) MeOH **(b)** Toluene

Figure 2.23. Power and JV curves of a DSSC loaded with Sp_2 in a a) polar and b) nonpolar solvent

efficient electron injection pathway. This would also match well with the natural charge separation of the compound. However, the V_{oc} of 0.33 V is a significant drop from the original cell. This is a measurement of the potential difference between the electrolyte solution and the LUMO of the sensitizing dye, along with interfacial resistance and other factors. A simple explanation would be a drop in the LUMO of the sensitizing dye due to conjugation of the aromatic systems, but modeling would verify this.

While Sp_2 had a good efficiency, the nature of its dual binding sites to TiO_2 prevented it from relaxing back to its spiran form. By contrast, Ox_2 retains its photochromic properties on TiO_2 as it binds only from the flexible propanoic acid moiety (Section 2.8). However, this very property also decreases its solar conversion efficiency to 0.002%, as it lacks an efficient electron injection pathway (Figure 2.24).

2.10 Future Work

2.10.1 Binding Mechanism

The potential for room-temperature binding of an $-NO_2$ is very interesting. As of now, the only evidence for this is the long lifetime of the excited merocyanine

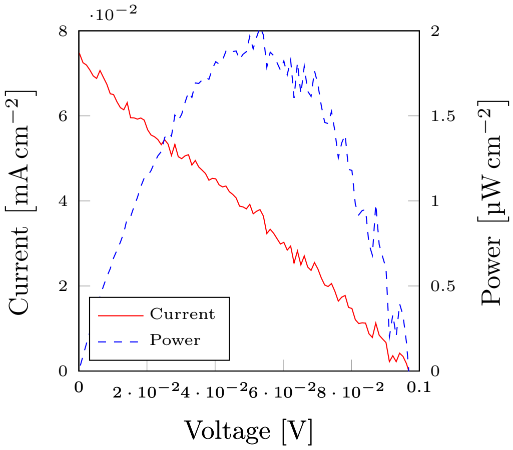

Figure 2.24. Power and JV curves of a DSSC loaded with Ox_2 in toluene

structure, and the IR shift of the bound vs the free $-NO_2$. Future work, involving Raman and XPS, could determine this more precisely.

If the $-NO_2$ is determined to be the binding group, there is a possibility for forcing binding of unique functionalities to metal oxide surfaces using chelating molecules.

2.10.2 Color-Changing Solar Cells

The work presented in this chapter provides the insight necessary to design a new class of compounds, with better efficiency than seen here. By using our knowledge of spiropyran chemistry, combined with their behavior in DSSCs, we can design compounds that sync better with a D-π-A framework.

In order to stabilize the open position, an electron-withdrawing group is needed on the benzopyran half of the compound.[27] As a $-COOH$, or other acidic group, is necessary to anchor to the TiO_2 substrate, this can serve both purposes simultaneously (Figure 2.25).

Assuming this is successful, further adjustment can increase the D-π-A nature of the compound. The addition of another electron-withdrawing functionality to the benzopyran would help localize the LUMO of the compound at that position. As well, adding electron-donating groups to the indoline would localize the HOMO

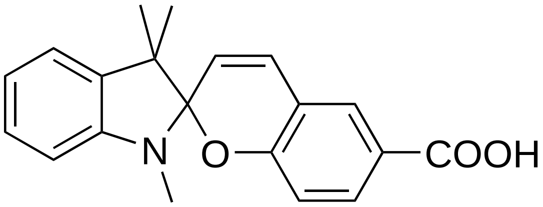

Figure 2.25. Second attempt at a high-efficiency color-changing DSSC

on the other side of the molecule. Any problems with aggregation could be mitigated by the addition of ether functionalities to physically separate neighboring molecules (Figure 2.26).

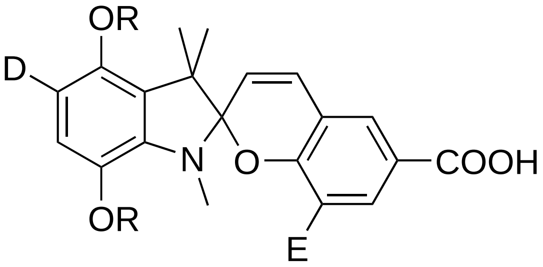

Figure 2.26. Future attempts for a high-efficiency color-changing DSSC

2.11 Conclusions

In this chapter, I have detailed the analysis of a set of nitrospiropyrans and naphthospirooxazines. Their unique chemistry was explored, specifically their behavior in different solvents, various pH conditions, and on surfaces. This behavior was then correlated to their photochromic activity, and investigated in the context of making a color-changing dye-sensitized solar cell. The data gave a few unique results:

1. The room-temperature binding of an aryl nitro to TiO_2
2. pH sensitive color changing properties

3. Solvent-dependent surface binding
4. The stabilization of a zwitterionic structure by a metal oxide surface

While the solar cell efficiency never rose to a level that would be considered usable, this information allows us to optimize this system in the future.

2.12 Experimental

2.12.1 UV-Vis

All UV-Vis spectra were taken on a Perkin-Elmer LAMBDA 35 Spectrophotometer. Acetone, methanol, acetonitrile, and hexane were spectroscopic grade and used as received. Pyridine, piperidine, and triethylamine were dried and distilled prior to use. All UV-Vis analysis was done at a concentration of 0.05 mM.

Initial spectra were taken by inserting the sample into the spectrophotometer and waiting for 5 minutes to allow the sample to come to equilibrium. The samples were then irradiated with a BLANK for 2 minutes, and immediately inserted into the spectrophotomer and measured. If the sample equilibrated too rapidly, it was irradiated in the spectrophotometer using a BLANK UV LED, and subsequently measured.

Ring closing rates were obtained by measuring the decay of the λ_{max} in the visible region after irradiation as previously described. The absorbance was converted into a first-order logarithmic decay, and the slope used to obtain the reaction rate.

2.12.2 Infrared

The merocyanine thin film was made by dropping a 0.5 mM toluene solution of Sp_2 onto glass, and then evaporating it under constant UV irradiation with a BLANK lamp at BLANK nm.

The $TiO_2 \cdot Sp_{2M}$ sample was made by soaking half of a doctor-bladed film of TiO_2 on glass in a 0.5 mM solution of Sp_2 in toluene overnight. The IR spectrum was then taken using the undoped side as a reference.

Infrared spectra were taken on a BLANK.

2.12.3 Solar cell assembly and testing

The solar cells were prepared according to the procedure described previously[28]. A titanium dioxide paste was purchased from Solaronix (Ti-Nanoxide T/SP). The paste was then doctor bladed onto FTO glass (Hartford Glass, 7 Ω/□) and sintered at 500 °C for 1 h and cooled to 80 °C, at which point it was immersed in the respective dye solutions (0.5 mM in methanol or toluene) for 48 h. Next, the photoanode was rinsed with ethanol and dried. The cell was completed by sandwiching an electrolyte solution consisting of 0.5 M lithium iodide (Aldrich 99.9%) and 0.05 M iodine (Aldrich 99%) in acetonitrile together with the photoanode and a counter electrode. The cathode was prepared by spin coating 50 µL of a 5 mM solution consisting of chloroplatinic acid hydrate (Aldrich, 99.9%) in 2-propanol (Aldrich, 99%) onto FTO glass (Hartford Glass, 15 Ω/□) and annealing at 400 °C for 40 min. The cells were assembled using standard published procedures[38].

The photoanode thickness, as determined by SEM, was 13 µm.

The solar cells were tested with a Gamry Reference 600 potentiostat, using a 300 W Xe lamp and 0.25 cm^2 mask, filtered to 1.5 AM (100 mW/cm^2).

2.12.4 Synthesis

1',3',3'-trimethyl-6-nitrospiro[chromene-2,2'-indoline] (Sp$_1$) and 1-isobutyl-3,3-dimethylspiro[indoline-2,3'-naphtho[2,1-b][1,4]oxazine] (Ox$_1$) were purchased from TCI Chemicals and Vivimed Labs Ltd, respectively, and used without further purification.

3-(3',3'-dimethyl-6-nitrospiro[chromene-2,2'-indolin]-1'-yl)propanoic acid (Sp$_2$) and 3-(3,3-dimethylspiro[indoline-2,3'-naphtho[2,1-b][1,4]oxazin]-1-yl)propanoic acid (Ox$_2$) were synthesized based on a modification of literature procedures.[29]

1-(2-carboxyethyl)-2,3,3-trimethyl-3H-indol-1-ium iodide

2,3,3-trimethylindolenine (1.0 g, 6.28 mmol) was dissolved in 1 mL methyl ethyl ketone (MEK). After addition of 3-iodopropionic acid (1.3 g, 6.50 mmol) the reaction mixture was refluxed and stirred overnight. After cooling to room temperature, the precipitated material was isolated and washed with cold hexane followed by diethyl ether to obtain 1-(2-carboxyethyl)-2,3,3-trimethyl-3H-indol-1-ium iodide (2.03 g, 90%) as a light-brown salt. ^{1}H-NMR (500 MHz, d6-DMSO) δ: 7.99 (m, 1H), 7.84 (m, 1H), 7.62 (m, 2H), 4.65 (t, J = 7.0 Hz,2H), 2.98 (t, J = 7.0 Hz, 2H,), 2.86 (s, 3H, C2-Me), 1.53(s, 6H, C3-Me2). HRMS-APCI (m/z): [M-I] + calc. for C 14 H 18 NO 2 232.1; found 232.2

3-(3',3'-dimethyl-6-nitrospiro[chromene-2,2'-indolin]-1'-yl)propanoic acid (**$\mathbf{Sp_2}$**)

A dry r.b. flask was wrapped in aluminum foil and then charged with 1-(2-carboxyethyl)-2,3,3-trimethyl-3H-indol-1-ium iodide (0.6 g, 1.67 mmol) and 3 mL MEK. Piperidine (.174 mL, 1.75 mmol) and 5-nitrosalicylaldehyde (0.28 g, 1.68 mmol) were added in one portion. The reaction mixture refluxed for 3 h. Then the reaction mixture was cooled to room temperature and stored overnight in a fridge (4 °C). The precipitated material was isolated and washed with cold MEK followed by methanol to obtain the product (0.37 g, 58%) as a yellow-green powder.^{1}H-NMR (500 MHz, d6-DMSO) δ: 12.75 (s, 1H, COOH), 8.22 (d, J = 2.92 Hz, 1H), 8.00 (dd, J= 2.92, 9.18 Hz, 1H,), 7.21 (d, J = 10.2 Hz, 1H), 7.13 (m, 2H), 6.87 (d, J = 9.25 Hz, 1H), 6.80 (t, J = 7.3, Hz, 1H), 6.66 (d, J = 7.79 Hz, 1H), 6.00 (d, J = 10.7 Hz, 1H), 3.52 – 3.34 (m, 2H, HA), 2.61 – 2.41 (m, 2H, HB), 1.18(s, 3H, C3-Me1), 1.07 (s, 3H, C3-Me2). HRMS-APCI (m/z): [MH]- calc. for C 21 H 21 N 2 O 5 380.1; found 380.3

3-(3,3-dimethyl-1,3-dihydrospiro[indole-2,3'-naphtho[1,2-e][1,3]oxazine]-1-yl)propanoic acid. (**Ox_2**)

1-nitroso-2-naphthol (150 mg) was dissolved in 1 mL ethanol. The mixture was heated to 78°C and a premixed solution of 1-(2-carboxyethyl)-2,3,3-trimethyl-3H-indol-1-ium iodide (310 mg) and triethylamine (0.2 mL) in 2 mL EtOH was added drop-wise. After refluxing for 2 h, the solvent was removed. The reaction mixture was purified using flash chromatography ($CHCl_3$:MeOH, 97:3). The product was isolated as tan crystals (120 mg, 40% yield). ^{1}H-NMR (500 MHz, CDCl 3) δ: 8.52 (d, J = 8.06 Hz, 1H), 7.75 (s, 1H), 7.72 (d, J = 8.06 Hz, 1H), 7.64 (d, J = 8.79 Hz, 1H), 7.55 (t, J = 7.32 Hz, 1H), 7.37 (t, J = 8.06 Hz, 1H), 7.20 (t, J = 8.79, 1H), 7.07 (d, J = 7.32 Hz, 1H), 6.96 (d, J = 8.79, 1H), 6.90 (t, J = 7.32 Hz, 1H), 6.61 (d, J = 8.06 Hz, 1H), 3.60 (m, 2H), 2.65 (m, 2H), 1.30 (s, 3H, C3-Me1), 1.29 (s, 3H, C3-Me2). HRMS-APCI (m/z): [MH] – calc. for C 24 H 23 N 2 O 3 387.44, found 387.17

2.13 References

(1) Ye, M.; Wen, X.; Wang, M.; Iocozzia, J.; Zhang, N.; Lin, C.; Lin, Z. *Mater. Today* **Apr. 2015**, *18*, 155–162.

(2) Yun, C.; You, J.; Kim, J.; Huh, J.; Kim, E. *J. Photochem. Photobiol. C Photochem. Rev.* **Sept. 2009**, *10*, 111–129.

(3) Levy, D.; Einhorn, S.; Avnir, D. *J. Non-Cryst. Solids* **Dec. 1989**, *113*, 137–145.

(4) Irie, M. *Pure Appl. Chem.* **1996**, *68*, 1367–1371.

(5) Bandara, H. M. D.; Burdette, S. C. *Chem. Soc. Rev.* **2012**, *41*, 1809.

(6) Pu, S.; Fan, C.; Miao, W.; Liu, G. *Tetrahedron* **Sept. 2008**, *64*, 9464–9470.

(7) Keum, S.-R.; Hur, M.-S.; Kazmaier, P. M.; Buncel, E. *Can. J. Chem.* **Dec. 1991**, *69*, 1940–1947.

(8) Klajn, R. *Chem. Soc. Rev.* **2014**, *43*, 148–84.

(9) Samanta, S.; Locklin, J. *Langmuir ACS J. Surf. Colloids* **Sept. 2008**, *24*, 9558–65.

(10) Wan, S.; Zheng, Y.; Shen, J.; Yang, W.; Yin, M. *ACS Appl. Mater. Interfaces* **Nov. 2014**, *6*, 19515–9.

(11) Xiaoliu, L.; Yongmei, W.; Teruo, M.; Jiben, M. *Heterocycles* **1999**, *51*, 2639–2651.

(12) Fischer, E.; Hirshberg, Y. *J. Chem. Soc.* **1952**, *11*, 4522–4524.

(13) Aldoshin, S. M. *Russ. Chem. Rev.* **1990**, *59*, 663–685.

(14) Kholmanskii, A. S.; Dyumaev, K. M. *Russ. Chem. Rev.* **1987**, *56*, 136–151.

(15) Zhang, L.; Cole, J. M. *Acs Appl. Mater. Interfaces* **Feb. 2015**, *7*, 3427–55.

(16) Hammarson, M.; Nilsson, J. R.; Li, S.; Beke-Somfai, T.; Andréasson, J. *J. Phys. Chem. B* **Oct. 2013**, *117*, 13561–71.

(17) Wojtyk, J. T. C.; Wasey, A.; Xiao, N.-N.; Kazmaier, P. M.; Hoz, S.; Yu, C.; Lemieux, R. P.; Buncel, E. *J. Phys. Chem. A* **Apr. 2007**, *111*, 2511–2516.

(18) Zhang, Y. Q.; Wang, J. X.; Shang, Y. L.; Song, Y. L.; Jiang, L. *Appl. Phys. A* **Nov. 2010**, *102*, 531–536.

(19) Tyer, N. W.; Becker, R. S. *J. Am. Chem. Soc.* **1970**, *92*, 1289–1294.

(20) Wilkinson, F.; Reeves, D. *J Chem Soc Faraday Trans 2* **1973**, *69*, 1381–1390.

(21) Reichardt, C.; Harbusch-Görnert, E. *Liebigs Ann. Chem.* **May 16, 1983**, 721–743.

(22) Namba, K.; Suzuki, S. *Bull. Chem. Soc. Jpn.* **1975**, *48*, 1323–1324.

(23) Wojtyk, J. T. C.; Wasey, A.; Kazmaier, P. M.; Hoz, S.; Buncel, E. *J. Phys. Chem. A* **Oct. 2000**, *104*, 9046–9055.

(24) Keum, S. R.; Ahn, S. M.; Roh, S. J.; Ma, S. Y. *Dyes Pigments* **2010**, *86*, 74–80.

(25) Saad, A.; Oms, O.; Marrot, J.; Dolbecq, A.; Hakouk, K.; El Bekkachi, H.; Jobic, S.; Deniard, P.; Dessapt, R.; Garrot, D.; Boukheddaden, K.; Liu, R.; Zhang, G.; Keita, B.; Mialane, P. *J. Mater. Chem. C* **2014**, *2*, 4748.

(26) Zhang, P.; Meng, J.; Li, X.; Wang, Y.; Matsuura, T. *J. Heterocycl. Chem.* **2002**, *39*, 179–184.

(27) Berman, E.; Fox, R. E.; Thomson, F. D. *J. Am. Chem. Soc.* **1959**, *81*, 5605–5608.

(28) Ito, S.; Murakami, T.; Comte, P.; Liska, P.; Gratzel, C.; Nazeeruddin, M.; Gratzel, M. *Thin Solid Films* **May 2008**, *516*, 4613–4619.

(29) Baumann, L.; Schöller, K.; de Courten, D.; Marti, D.; Frenz, M.; Wolf, M.; Rossi, R. M.; Scherer, L. J. *RSC Adv.* **Oct. 2013**, *3*, 23317.

(30) Evans, R. A.; Hanley, T. L.; Skidmore, M. A.; Davis, T. P.; Such, G. K.; Yee, L. H.; Ball, G. E.; Lewis, D. A. *Nat. Mater.* **Mar. 2005**, *4*, 249–53.

(31) Wismontski-Knittel, T.; Krongauz, V. *Macromolecules* **Nov. 1, 1985**, *18*, 2124–2126.

(32) Arsenov, V. D.; Parshutkin, A. A.; Marevtsev, V. S.; Cherkashin, M. I. *Russ Chem Bull* **Sept. 1984**, *33*, 1799–1806.

(33) Cong, J.; Yang, X.; Liu, J.; Zhao, J.; Hao, Y.; Wang, Y.; Sun, L. *Chem. Comm.* **July 2012**, *48*, 6663–5.

(34) Dobson, K.; McQuillan, A. *Spectrochim. Acta Part A* **1999**, *55*, 1395–1405.

(35) Dobson, K. D.; McQuillan, A. J. *Spectrochim. Acta - Part Mol. Biomol. Spectrosc.* **2000**, *56*, 557–565.

(36) Johnson, N. M.; Smolin, Y. Y.; Shindler, C.; Hagaman, D.; Soroush, M.; K. S. Lau, K.; Ji, H.-F. *AIMS Mater. Sci.* **2015**, *2*, 503–509.

(37) Ma, S.; Ting, H.; Ma, Y.; Zheng, L.; Zhang, M.; Xiao, L.; Chen, Z. *AIP Adv.* **May 2015**, *5*, 057154.

(38) Smestad, G. P. *J. Chem. Educ.* **June 1998**, *75*, 752–756.

.

Chapter 3: Dibenzo[*b,j*][1,10]Phenanthrolines

3.1 Abstract

In this chapter, I investigate the properties and potential use of dibenzo[*b,j*][1,10]phenanthrolines as ligands for a sensitizing dye in a dye-sensitized solar cell (DSSC). They were found to have unusual reactivity, both oxidizing and reducing far more easily than would be expected. Because of this unusual reactivity, a new synthetic method needed to be developed. As such, I created a new synthetic method compatible with both the sensitive aromatic functionalities and oxidation-sensitive functionalities such as aryl methyls. This was then used to create a ruthenium DSSC using a dibenzo[*b,j*][1,10]phenanthroline as an ancillary ligand. Performance of the DSSC was poor, most likely due to poor electronic overlap with the conducting band of the TiO_2. This, however, could be improved with future modification.

3.2 Overview

As stated in Section 1.8.4: Dye-Sensitized Solar Cells (DSSCs), one main benefit of DSSCs are their extremely high electron injection efficiency, which regularly approaches one. As nearly all absorbed photons generate an electron, the easiest way to improve the efficiency of DSSCs is to increase the number of absorbed photons. However, the absorption spectrum for most of the commonly used dyes is rather weak through the visible and infrared region (Figure 3.1).

However, the solar spectrum flux is the greatest in this region (Figure 1.2). Therefore, a great deal of research has been focused on increasing the overall absorption, with a specific emphasis on an overall redshift. This can usually be

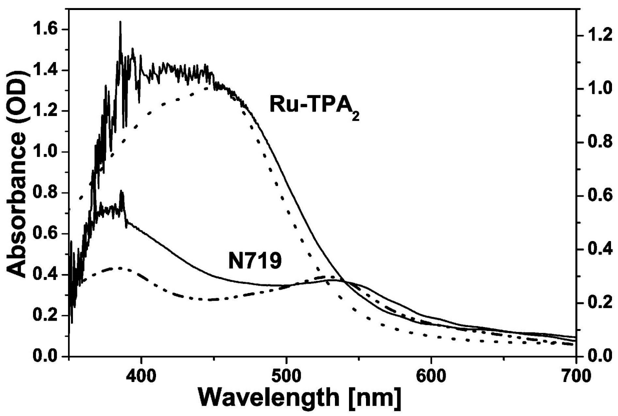

Figure 3.1. UV-Vis absorption spectra of Ru dyes absorbed on TiO_2 (–), acetonitrile (– · ·) and ethanol(– – –)[1]

accomplished by creating an extended π-system, which often serves both purposes simultaneously. However, while there have been many, many publications on extending the π-system through conjugation of aromatic systems,[2] there have been relatively few that work by expanding the aromatic system.[3] Those few attempts have shown very promising results in the shift in the absorption spectrum, however, the overall efficiency was quite low. The authors ascribed this to a low injection efficiency from the lower-level π-π* transitions due to being slightly lower in energy (0.1 eV) than the TiO_2 conduction band edge. Indeed, electron injection efficiency was improved when SnO_2 was used instead, but the overall cell efficiency was still drastically low (0.29%) compared to similar compounds. This likely means that the low electron injection efficiency was not purely due to a low-lying energy level, but could also be due to the homoleptic orientation, which would lead to inefficient charge separation on the compound. This is indicated by the low short-circuit current, which was 1.36 $\mathrm{mA\,cm^{-2}}$, compared to 18.2 $\mathrm{mA\,cm^{-2}}$ for N3. While this did increase to 2.12 $\mathrm{mA\,cm^{-2}}$ when the semiconductor was changed to one with a lower lying conduction band (SnO_2), this trend didn't continue with other similar semiconductors, such as In_2O_3.

As the case for an expanded aromatic system for a DSSC is not hopeless, I had the following goals:

1. Design an efficient synthesis for a polycylic heteroaromatic ligand
2. Incorporate the ligand into a sensitizing dye for a DSSC
3. Create a DSSC sensitized with the dye, and evaluate its performance
4. Using the obtained information, optimize the DSSC

With this goal in mind, we attempted to create a new ligand for Ru-based DSSCs, using an extended aromatic system with a backbone of dibenzo[*b,j*][1,10]phenanthroline (Figure 3.2).

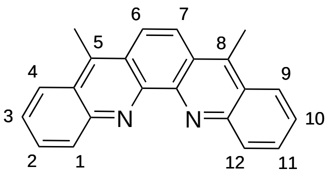

TMP1

Figure 3.2. 5,8-dimethyl-dibenzo[*b,j*][1,10]phenanthroline

3.2.1 Aromaticity

The simplest way to define aromaticity is a circular, coplanar, delocalized π-system that causes an additional stabilization of the molecule. However, these electrons can behave differently depending on their number and orientation. For example, the commonly used Hückel's rule[4] states that if the number of electrons in the π-system is equal to 4n+2, where n is a non-negative integer, then the system will be aromatic. If the number of electrons is 4n, then the system will be anti-aromatic, and be destabilized relative to the alkene. However, this rule ceases to apply in complex systems, and has only been definitively shown to be true for monocyclic systems.[5]

A common class of compounds that isn't well described by Hückel's rule is the polycyclic aromatic hydrocarbons (PAHs). These are compounds generally composed of fused six-membered ring systems, all made of sp_2-hybridized atoms. As the name suggests, they all show stabilization over the corresponding alkene, but this would not necessarily be predicted by Hückel's rule.

Common examples of this are pyrene and coronene, which have 16 and 24 π electrons, respectively (Figure 3.3a). Both show net stabilization over the corresponding alkene, but neither would be aromatic under Hückel's model. Another point of failure are the linear and bent PAHs. While these may have the same number of π electrons, they differ drastically in terms of stability (Figure 3.3b). Anthracene easily photodimerizes, while phenanthrene is quite stable under normal conditions. Therefore, a new model is needed that accounts for not only the number of π electrons, but the overall orientation of the molecule.

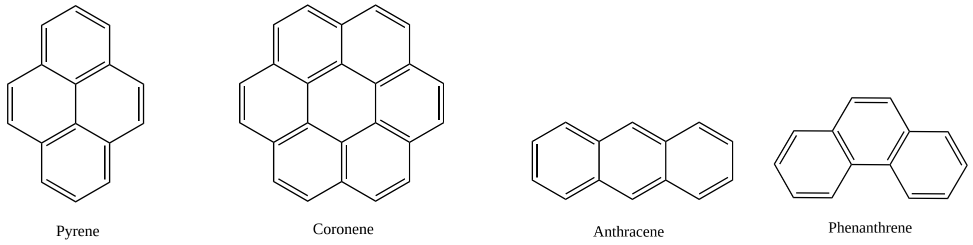

(a) Pyrene and Coronene **(b)** Anthracene and Phenanthrene

Figure 3.3. Some exceptions to Hückel's rule

One such model is Clar's rule.[6] Clar's rule states that aromaticity in the PAHs can be localized to those six-membered rings that contain a complete π sextet. Whichever resonance structure contains the most of these complete π sextets is known as the Clar structure, and will determine the properties of the molecule. Using this framework, we can go back and predict the aromatic properties of the PAHs mentioned earlier. It can be seen that both pyrene and coronene contain aromatic moieties, and so will have some properties of aromatics (Figure 3.4a). Similarly, we can compare the linear and bent PAHs anthracene and phenanthrene, respectively. We can see that while anthracene has a single π sextet in every resonance form, phenanthrene can contain either one or two (Figure 3.4b). This would predict that phenanthrene has more aromatic character than anthracene, and would therefore be more stable, which is consistent with observations.

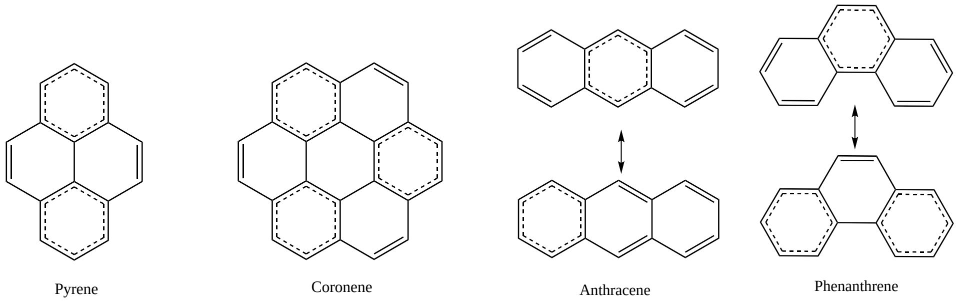

(a) Pyrene and Coronene **(b)** Anthracene and Pyrene

Figure 3.4. Predictions under Clar's rule

However, more information can be extracted from Clar structures than the average aromaticity in a given PAH. What the Clar structure also predicts is where the π electrons are stabilized in an aromatic structure, and where they are more olefinic. An example of this is the compound kekulene, a complex, circular PAH (Figure 3.5a). Based on this Clar structure, we would predict that there would be a total of six aromatic rings, and six double bonds. And, indeed, NMR analysis shows that there are three different types of protons in kekulene: outer aromatic, inner aromatic, and olefinic, at an integration ratio of 1:1:2.[7]

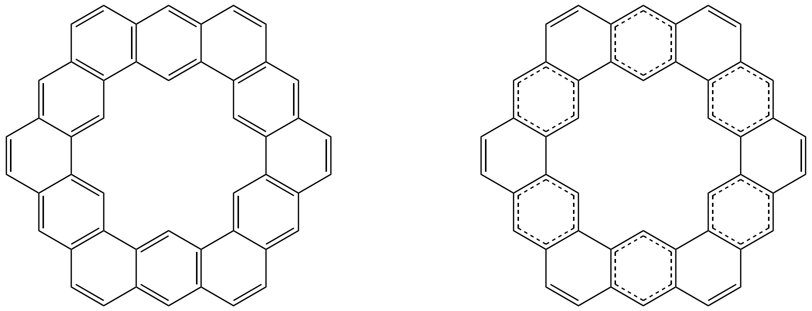

(a) Kekulene **(b)** The Clar structure of Kekulene

3.3 Predictions

3.3.1 Analogous Compounds

As the target compound (**1**) is not very well known, it would be worthwhile to use some predictions to guess as to its reactivity. One potential set of compounds is phenanthrene/phenanthroline. These two share the bent configuration of **1**, and so would share a similar Clar structure (Section 3.3.1).

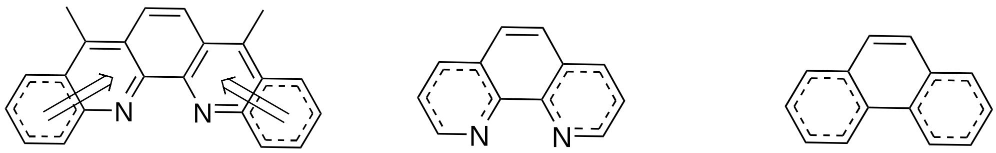

(a) **1** **(b)** Phenanthroline **(c)** Phenanthrene

Figure 3.6. The Clar structures of **1** and potential analogous compounds

Looking at the Clar structure for all three compounds, the central π bond should behave in reactions as an olefin, as it lacks the aromatic character of the other π bonds. And this is generally what is seen: phenanthrene is sensitive to standard olefin reaction conditions, including oxidation,[8] halogenation,[9] reduction,[10] and ozonolysis.[11]

On the contrary, phenanthroline is generally resistant to nucleophilic and oxidative conditions due to a π deficient system caused by the electron-withdrawing nitrogens. Oxidation is only possible using sulfuric acid, nitric acid, and potassium bromide at elevated temperatures.[12] Bromination addition doesn't occur, and substitution is only possible with fuming sulfuric acid and bromine over multiple days.[13]

Another possibility is that **1** will behave more like acridine or anthracene (Section 3.3.1). This is supported by the fact that pentaphene reacts similarily to two connected anthracenes under oxidative and Diels-Alder conditions.[14] If this is the

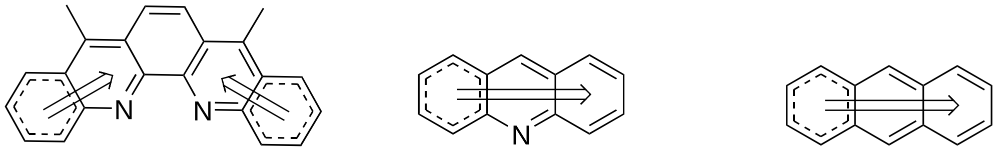

(a) 1 **(b)** Acridine **(c)** Anthracene

Figure 3.7. The Clar structures of **1** and potential analogous compounds

case, we would expect reactivity similar to acridine. Acridine both reduces and oxidizes at the heteroaromatic ring,[15,16] which is reasonable, as it creates a more stable Clar's structure (Figure 3.8)

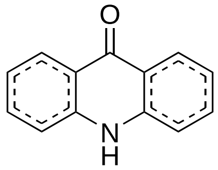

Figure 3.8. The Clar structure of acridine after oxidation

Therefore, using analogous compounds to predict the reactivity of our target leads to two different conclusions. One predicts that **1** would be most reactive at the C6-C7 double bond at the center of the compound, while the other predicts a higher reactivity at the heteroaromatic rings. Using Clar's rule as our guiding principle, we would predict higher olefinic reactivity at the heteroaromatic rings, as this would split the compound into three separate π sextets. As an example, we can look at a sample oxidation reaction, and compare and contrast the two major products using each assumption (Figure 3.9).

As we can see, Clar's rule would predict a similar reactivity to acridine, as it creates a Clar structure containing three separate aromatic systems, while reacting similarly to phenanthroline would create two delocalized aromatic systems.

Therefore, we would expect an analogous reaction to pentaphene, while being resistant to oxidative conditions due to the π deficiency.

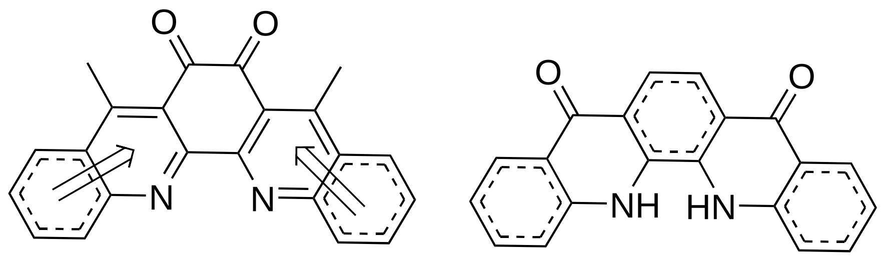

Figure 3.9. The Clar structure of **1** following oxidation, presuming reactivity similar to (left) phenanthroline and (right) acridine

3.3.2 Density Functional Theory

Rudimentary density functional theory (DFT) analysis was undertaken to further predict the properties of **1**

Our DFT calculations somewhat bear up the predictions from analogous compounds (Figure 3.10). In the HOMO, there is a general lack of electron density in the system, except for at the nitrogen atoms, which would support a generally π deficient system. The lack of electron density in the HOMO at the central double bond is also supportive of our prediction using analagous compounds, which would predict that reactivity would be centered at the heteroaromatic ring. However, the LUMO strongly localizes electron density at the central bond, which would give reactivity more similar to phenanthrene and phenanthroline.

Also of note is how strongly stabilized this system is from the central double bond. The HOMO is depressed by 2.5 eV compared to the C6-C7 dihydro derivative (Figure 3.11). This would indicate that the central double bond is contributing strongly to the aromaticity of the system, in contrast to our predictions from analogous compounds.

3.4 Synthesis

Many routes were tested for the synthesis of the target ligand, and will be detailed in a separate section. However, the final successful route was a two step synthesis, beginning from o-dibromobenzene and o-aminoacetophenone.

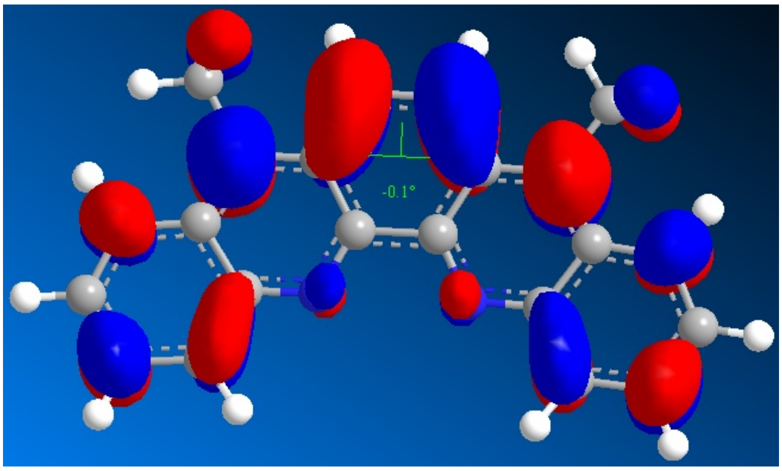

(a) LUMO (-5.289 eV)

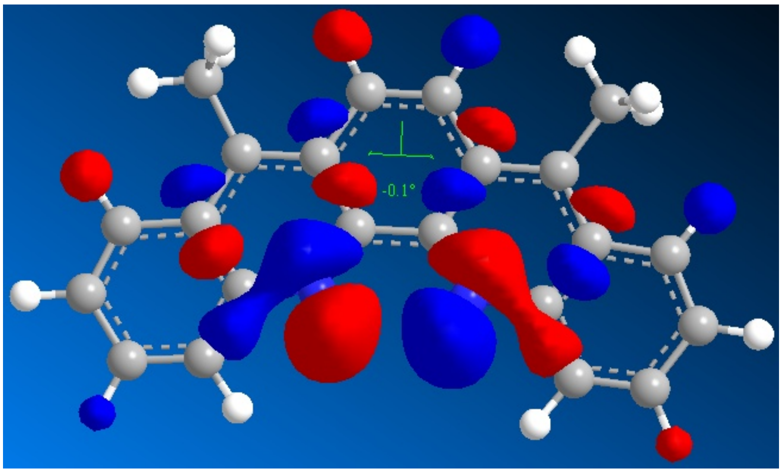

(b) HOMO (-9.126 eV)

Figure 3.10. The calculated HOMO/LUMO of **1**

The first step is a fairly standard Buchwald-Hartwig amination. The use of the Pd(XPhos) precatalyst is necessary in order to prevent beta-hydride elimination from the active acetyl functionality. Less active phenyl ketones can successfully use a simpler $Pd(tBu)_3$ catalyst, or even a copper-catalyzed Ullman-Goldberg amination.

The second step, however, uses an extremely harsh set of conditions for a 6-exo-trig ring closing reaction. Generally, these types of reactions can be carried forward using polyphosphoric acid,[17] sulfuric acid,[18] trifluoroacetic acid,[19] or even Lewis acids[20,21] with moderate to high yields. However, all these techniques either failed to create usable product, or failed to create any product at all. It was surmised that the failure to create a usable product was due to the active acetyl

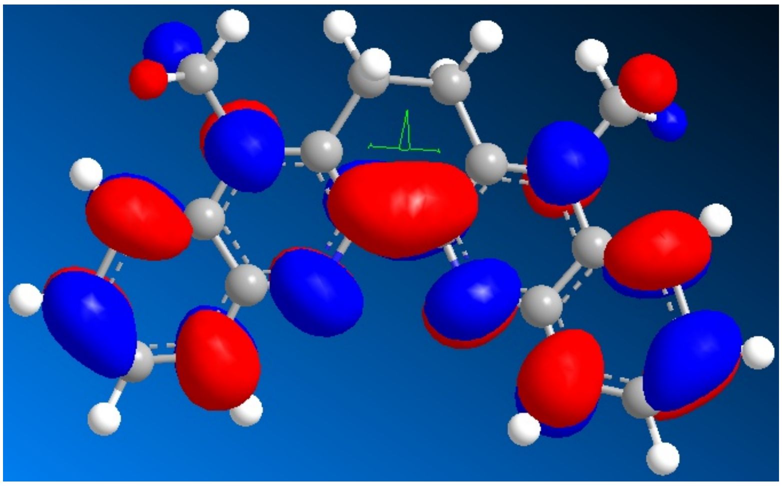

(a) LUMO (-4.112 eV)

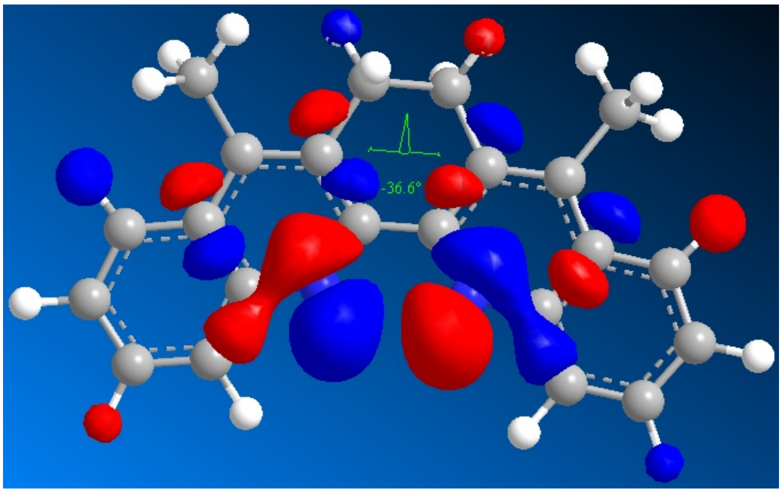

(b) HOMO (-6.646 eV)

Figure 3.11. The calculated HOMO/LUMO of **2**

functionality, which would readily undergo a variety of reactions including aldol condensations, polymerizations, and extraneous ring formations. Thus, a more targeted synthetic method was necessary.

A synthesis listed in a small paper published in 2012 seemed promising,[22] as it used a targeted Lewis acid ($AlCl_3$) along with a strong Brönsted acid. However, every substrate to date using this combination was a substituted anthraquinone,[23–25] which has very different properties from diphenyl ketones. However, with nothing left to lose, the combination was attempted, and turned out to be quite successful. The first step forms an ionic liquid of sorts, using a eutectic mixture of $AlCl_3$ and NaCl that melts at 110°C. This dissolves the substrate, and can then be carefully diluted with 4M HCl to finish the reaction. Yields were surprisingly good, and the reaction yielded a clean product without chromatography. As such, this technique was used moving forward.

The final ruthenium complex was synthesized using $Ru(DMSO)_4Cl_2$ and ethylene glycol at 170°C (to prevent decarboxylation of the dcbpy), followed by a reaction with NH_4NCS in DMF.

3.5 Chemistry

3.5.1 Friedländer

The initial attempt at a synthesis of **1** was based on a literature synthesis from Kempter and Stoss.[26] It involved a Friedländer condensation, followed by a palladium-catalyzed dehydrogenation of the product. The Friedländer synthesis, or the Friedländer annulation, is an old reaction from the late 1800's. The original reaction involved the condensation between 2-aminobenzaldehydes and ketones to form quinolines.[27,28] Since then, the reaction has been greatly improved through the use of a variety of Lewis and Brønsted acids.[29–32] The scope has also been expanded through the use of different carbonyl groups, to form a variety of 4-substituted quinolines. The reaction mechanism has not been fully determined, and proceeds either through an aldol condensation followed by imine formation, or vice versa (Scheme 3.1).

In our scenario, we required a double condensation between 1,2-cyclohexanedione and 2'-aminoacetophenone. This reaction proceeded well using a variety of Lewis and Brønsted acids, but decent yields (˜85%) were achieved using an equivalent of HCl in ethanol (Scheme 3.2).

3.5.2 Palladium-catalyzed dehydrogenation

The Friedlander condensation proceeded with high yields and no difficulty, but yields from literature for the palladium-catalyzed dehydrogenation were quite low

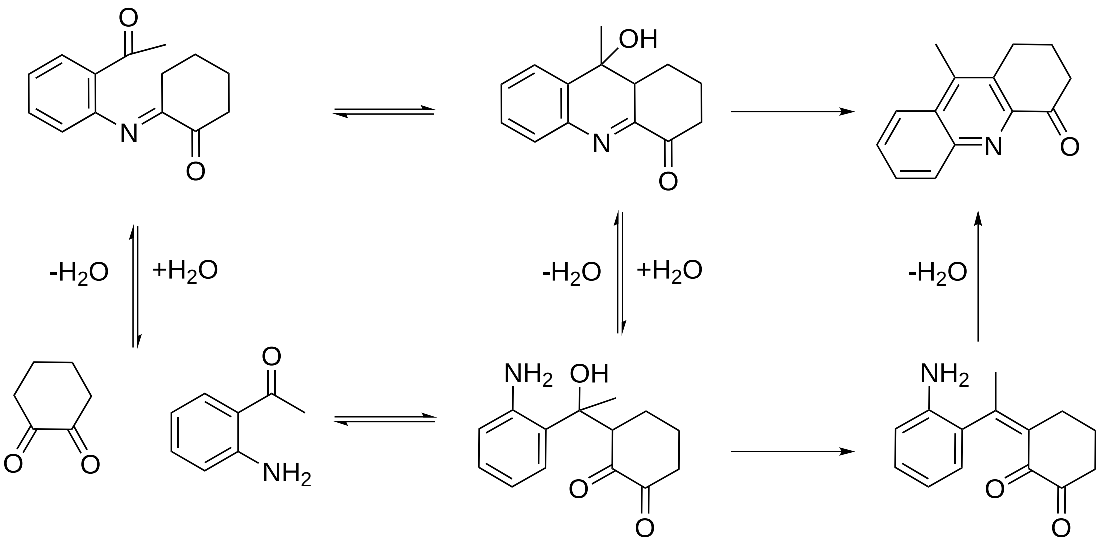

Scheme 3.1. Proposed reaction mechanisms for Friedländer condensation

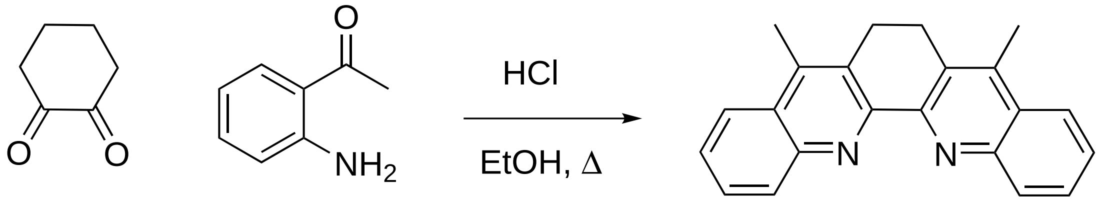

TMP1 TMP2 TMP3

Scheme 3.2. Friedlander condensation between 1,2-cyclohexanedione and 2'-aminoacetophenone

(10-20%). Many different conditions were used to improve the yield, but all proved futile.

Conditions for this reaction relied on elevated temperatures (210 °C), which have a high potential for unwanted side reactions on a compound of this type, potentially explaining the low yield. As such, attempts were made to try carrying out the reaction at lower temperatures. No conversion was seen in methanol, toluene, xylenes, 1,2-dichlorobenezene, acetic acid, and decalin. Decomposition was seen in nitrobenzene, and limited yield (10%) was seen in isocetane. This indicates a high activation energy barrier for the reaction, which wouldn't be expected from the planarity and aromatic nature of the target compound.

Napthalene, anthracene, tetracene, and pentacene are all readily formed from their various dihydro derivatives in boiling xylene, which indicates that molecular size and distribution of aromaticity are not directly relevant to the activation energy barrier.[33] However, the increase in temperature from phenanthrene (110°C)[34] to penthaphene (180°C)[35] indicates that the branched nature of the system is directly relevant to this activation energy barrier. As the catalytic surface shouldn't distinguish between a linear and a curved compound, this would indicate that the branched nature of the system directly impacts the aromaticity of the central double bond. According to Clar's rule, very little aromatic stabilization is gained by this dehydrogenation, but there shouldn't be any particular stabilization of the C-H bond at this position.

3.5.3 Oxidation

Another potential method used on similar systems is oxidative dehydrogenation. This technique can be done with a number of different standard oxidizing agents.[36–38] The most commonly used is MnO_2, and it was the first compound to be tested. Unfortunately, **2** proved surprisingly sensitive to oxidative conditions, considering the usually π-deficient nature of heteroarenes. Exposure to MnO_2 formed a complex mixture of aldehydes, carboxylic acids, and ketones, with none of the target compound (**1**) found.

A milder oxidizing agent was necessary, so we moved on to SeO_2 (Scheme 3.3). This was quite successful in oxidizing the central bond, but unfortunately only after oxidizing the methyl groups. **4** can be isolated after 4 hrs of exposure. Using more equivalents of SeO_2 and reacting overnight forms **7** in high yields. Allowing the reaction to continue with an excess of SeO_2 over two days begins to oxidize the aldehydes to carboxylic acids.

Using mild chromium oxidizing agents such as Jones' reagent and pyridinium chlorochromate avoids oxidizing the methyl group, but leads to the simultaneous formation of the unusual side product of a 6,7-dione (**8**), indicating a very reactive olefinic bond (Scheme 3.4). This was followed by rapid oxidation of the methyl groups to aldehydes and acids, as seen with MnO_2.

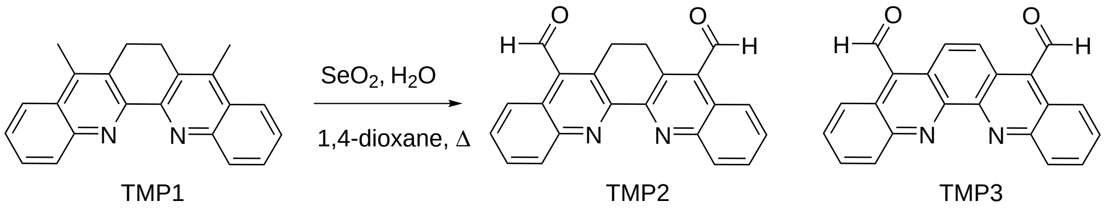

Scheme 3.3. An oxidation of **2** with selenium dioxide

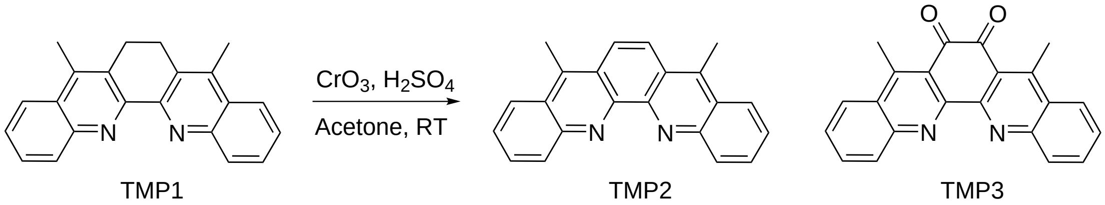

Scheme 3.4. An oxidation of **2** with Jones' reagent

These results indicate that **1** might possess reactivity similar more to phenanthrene than any other compound, which would be highly unusual based on what we know about PAH reactivity.

3.5.4 Bromination

A more effective method of dehdyrogenation was pioneered by Barnes in 1948.[39] It uses N-bromosuccinimide (NBS) under radical conditions to undergo bromination/dehydrobromination. This has been shown to effectively form conjugated π systems on a number of compounds under mild conditions. The mechanism is likely a standard radical bromination, followed by a thermal elimination of hydrogen bromide (Scheme 3.5). Unfortunately, the benzylic positions at C6/C7 and the methyl groups are equally reactive, and full bromination is necessary, using 3-4 equivalents of NBS. This ensures total bromination, with excellent yields of 90+% (Scheme 3.6).

3.5.5 Reduction

The next stage to form the target compound was reduction of **9**. This was expected to be an easy task, as NaBH$_4$ readily displaces bromo functionalities, while olefins

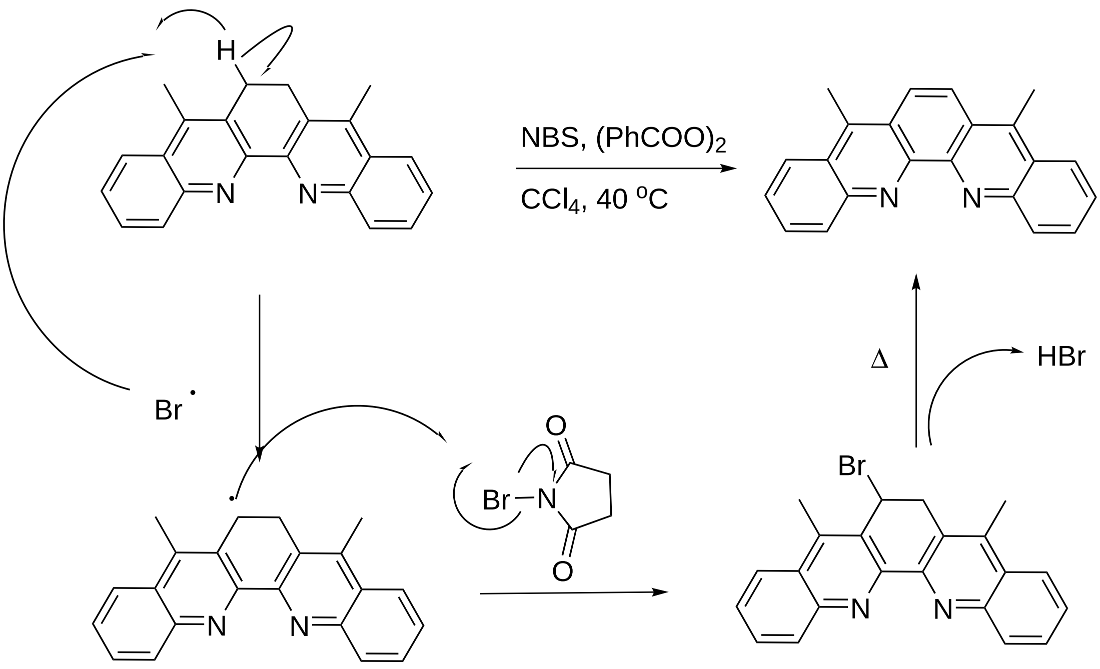

Scheme 3.5. Mechanism for the bromination/dehydrobromination of **2** with NBS

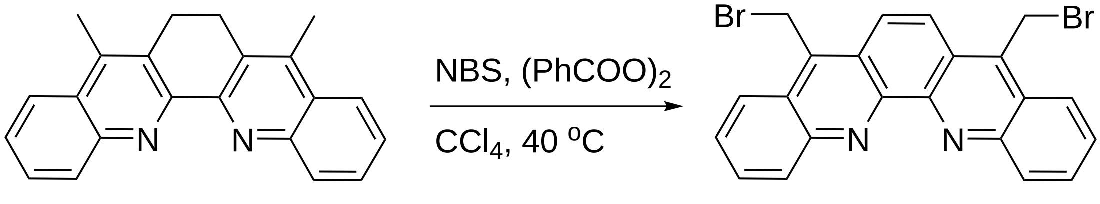

TMP1 TMP2

Scheme 3.6. Bromination/dehydrobromination of **2** with NBS

and aromatics are typically resistant to hydrides in the absence of a catalyst.[40] Therefore, it was very surprising when the addition of $NaBH_4$ in MeOH caused a complete reversal of the bromination reaction, producing **2** as the product rather than the expected **1** (Scheme 3.7)

This result was repeated with $LiAlH_4$, Fe/HCl, Zn/HOAc, and Ni/NH_4HCO_2. All reducing conditions readily displaced the halide functionality, while hydrogenating the central bond. This result indicates a strongly π-deficient system. While heteroaromatic systems like pyridine are already known for this, it is highly unusual that reduction would happen at that position. Heteroarenes, such as quinoline,[41] phenanthroline,[42] and acridine,[16] reduce at the heteroaromatic ring

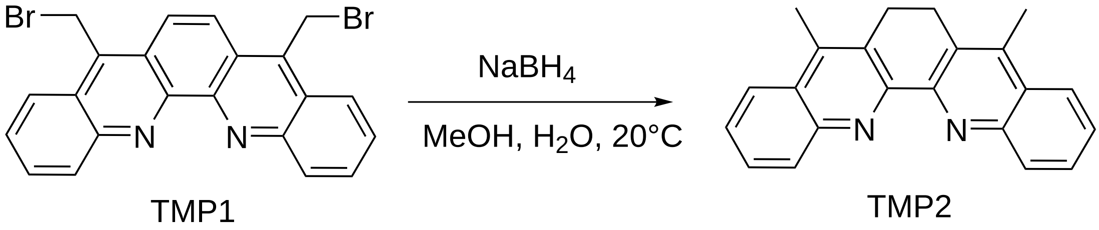

Scheme 3.7. Reduction of **9** with $NaBH_4$

primarily, and few to no exceptions are known to this rule. This reaction lends insight into the unique reactivity of this compound.

While primary reduction at the central ring is unseen in phenanthroline, despite the predictions of Clar's rule, phenanthrene readily reduces at that position, with photoreduction[43] under catalytic hydrogenation,[44] or even using metal hydrides (albeit under extreme conditions).[45] Anthracene initially reduces at the outside ring,[45] which is also consistent with the observed results.

3.5.6 Ullmann-Goldberg

Therefore, we decided to use another reaction scheme, based off of work from Hellwinkel and Ittemann.[46] Under this scheme, metal-catalyzed condensation is used to create 1,1'-((1,2-phenylenebis(azanediyl))bis(2,1-phenylene))bis(ethan-1-one) (**10**), which is then cyclized using a 6-exo-trig ring closing reaction. The initial metal-catalyzed condensation can be either Cu (Ullmann-Goldberg) or Pd-catalyzed (Buchwald-Hartwig). They have a very similar reaction mechanism, going through an oxidative addition, ligand exchange, and reductive elimination (Figure 3.12). The difference between the two is the order of operations, with palladium undergoing oxidative addition before ligand exchange, while copper goes through the catalytic cycle in the opposite direction.

The Ullmann-Goldberg condensation is a very old reaction, centered around the use of copper to mediate the coupling between an aniline and an aryl halide. The Fritz Ullmann published the original Ullmann condensation reaction at the beginning of the 20th century, and it detailed the synthesis of diphenyl ethers

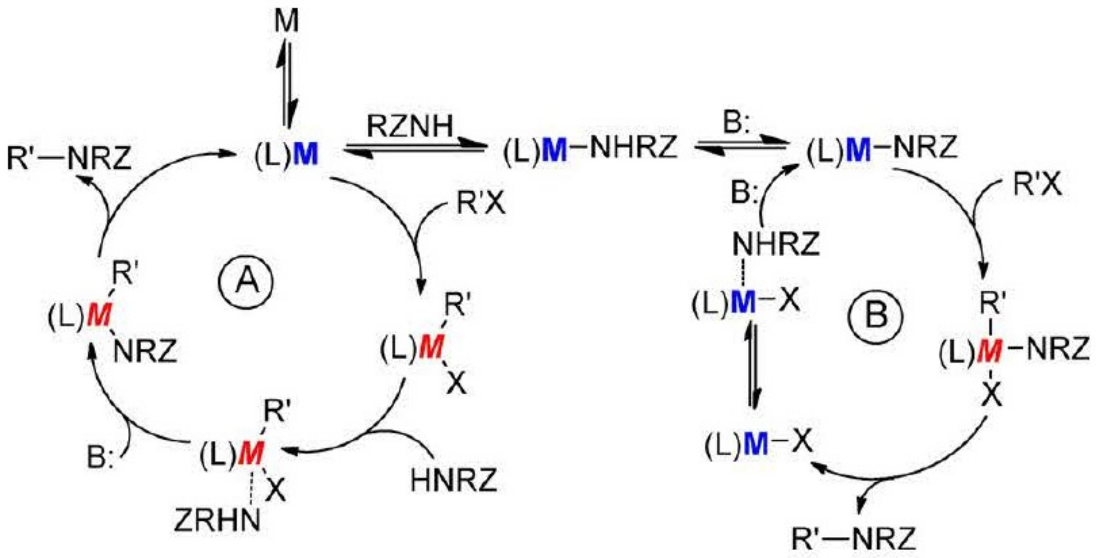

Figure 3.12. Mechanism for a metal-catalyzed condensation using palladium (A), and copper (B).[2]

using a phenol, an aryl halide, copper, and high temperatures.[47] This was quickly followed by the modification by his wife and assistant, Irma Goldberg, which expanded the scope of coupling partners to the anilines.[48] While a very useful reaction, the Ullmann-Goldberg aromatic amination is generally limited by the harsh conditions necessary, and limited scope of substrates. It works best with electronically poor aryl halides, and generally requires high temperatures (150-200°C is not uncommon). And while progress has certainly been made in improving the behavior of the copper catalyst, it still generally requires 5-20% catalyst loading for good yields in less than a few days.[49] Nonetheless, due to the low cost of copper and simplicity of the reaction, this is usually the first reaction attempted when synthesizing diarylamines.

As such, we designed a reaction scheme based on 1,2-diiodobenzene and 2'-aminoacetophenone (Scheme 3.8)

After optimization, this reaction proceeded with decent yields (50%). Unfortunately, our efforts proved unsuccessful in improving the reaction rate or yield, and the long reaction time (4-6 days) made consistency quite difficult. Experimental difficulties caused an unusually high number of failed reactions due to lost solvent,

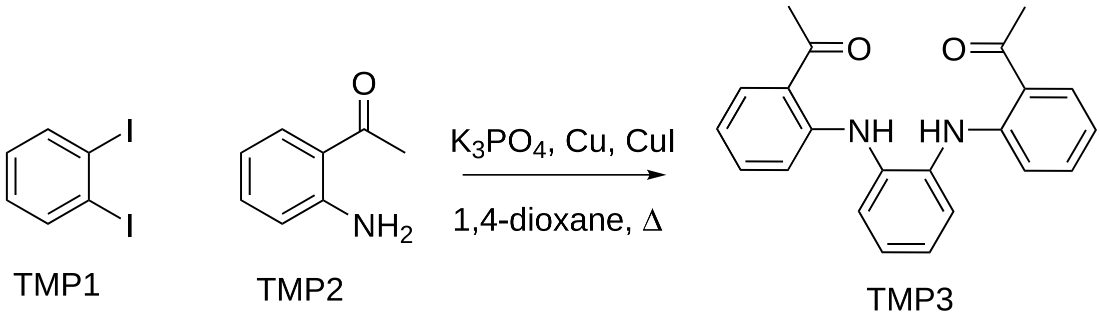

Scheme 3.8. Ullmann condensation of 1,2-diiodobenzene with 2'-aminoacetophenone

air leaks, and changes in water pressure. Therefore, a new reaction was needed.

3.5.7 Buchwald-Hartwig

The Buchwald-Hartwig reaction is an expansion of the current set of palladium-catalyzed coupling reactions, simultaneously discovered by John Hartwig, then at Yale, and Stephen Buchwald of MIT. The groundwork for the reaction was laid in the Stille reaction, also known as the Migita-Kosugi-Stille coupling. While attempting to expand the scope of this reaction, Toshihiko Migita and coworkers discovered in 1983 that diethylamine could be used in place of the normal aromatic and allylic compounds that had been used thus far.[50] They used a Pd(II) compound in catalytic quantities to couple a small number of sterically unhindered aryl bromides to N,N-diethylaminotributyltin, which was the first example of Pd-catalyzed amination. The next year, Dale Boger of the University of Kansas used a Pd(0) compound in an intramolecular amination reaction, but it required stoichiometric $Pd(PPh_3)_4$.[51] For ten years the field remained undeveloped, with no further forays made into this branch of chemistry. Then, in 1994, the Hartwig group and the Buchwald group made nearly back-to-back publications on the Migita publication. Hartwig made a fundamental breakthrough on the reaction, discovering that the active catalytic species was a Pd(0) complex that formed in situ, rather than the added Pd(II) complex.[52] He also proposed a mechanism for the reaction, which included an important oxidative addition of the aryl halide to the Pd(0).

Buchwald, by contrast, made a practical breakthrough for the reaction.[53] By cleverly utilizing the volatility of diethylamine, he was able to expand the variety of secondary amines available through transamination, and simultaneously expanded the scope of the aryl halide beyond electronically neutral ones using different reaction conditions. The big breakthrough occurred next year, when both groups simultaneously discovered that a bulky base eliminated the need for an organotin compound.[54,55] The scope of the reaction was then expanded to free amines, which made this an incredibly useful reaction for synthetic chemistry. Since then, the Buchwald-Hartwig amination has been constantly improved, and can couple a wide variety of amines and aryl halides whether they are electronically rich or poor.[49] However, while the reaction is quite robust, the conditions are strongly dependent on substrate. This requires careful selection of catalyst, solvent, and base to account for steric bulk, N-H acidity, electronic properties, and sensitive side groups.[49]

Attempts to use $(tBu)_3P$ as the ligand failed, as β-arylation proved to be an inescapable byproduct from the reactive acetyl functionalities. As such, more containment of the metal center was needed, and 2,2'-bis(diphenylphosphino)-1,1'-binaphthyl (BINAP) was chosen (Figure 3.13).

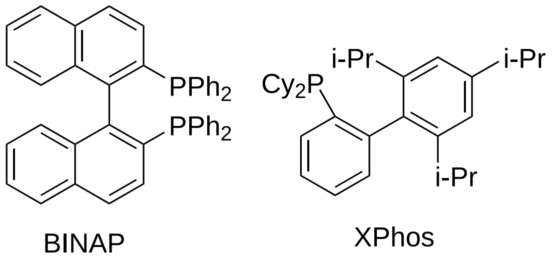

Figure 3.13. Ligands for the Buchwald-Hartwig amination of 1,2-dibromobenzene with 2'-aminoacetophenone

This worked well, providing yields up to 60%, but 2-dicyclohexylphosphino-2',4',6'-triisopropylbiphenyl (XPhos) proved far more successful, with yields up to

80% under the proper conditions (Scheme 3.9).

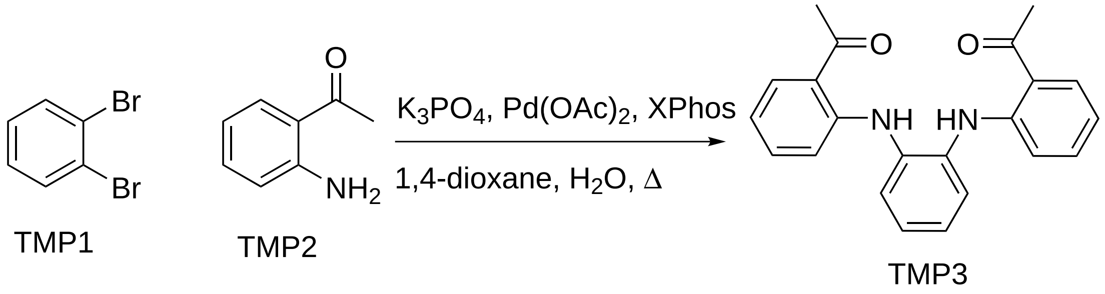

Scheme 3.9. Buchwald-Hartwig amination of 1,2-dibromobenzene with 2'-aminoacetophenone

The reaction was optimized using a procedure developed for this ligand in Buchwald's lab, using stoichiometric amounts of water to activate the $Pd(OAc)_2$/XPhos precatalyst system.[56] This allowed the reaction time to be accelerated from 4-6 days using the Ullmann reaction to overnight. NMR analysis of the reaction mixture shows that the individual displacements behave semi-sequentially, with monosubstitution being preferentially followed by monosubstitution of another molecule, rather than disubstitution of the same.

3.5.8 Ring closing

Generally, these types of reactions can be carried forward using polyphosphoric acid,[17] sulfuric acid,[18] trifluoroacetic acid,[19] or even Lewis acids[20,21] with moderate to high yields. This was not the case in our situation. Sulfuric acid, phosphoric acid, and Eaton's reagent produced total decomposition of the products. Nothing was able to be identified. Acetic acid catalyzed by sulfuric acid caused the formation of carboxylic acid byproducts before the desired target could be formed. Trifluoroacetic acid formed an unidentified product upon reaction with **10**. Weak Lewis acids such as In(III), Sn(II), and even Fe(III) produced no results either. Imidazolium-based ionic liquids and deep eutectic salts, such as that formed between choline chloride and $ZnCl_2$, also failed to react. All in all, it took nearly a year and a half of work, off and on, to find a set of conditions that would successfully carry out the 6-exo-trig ring closing reaction.

A synthesis listed in a small paper published in 2012 seemed promising,[22] as it used a targeted Lewis acid ($AlCl_3$) along with a strong Brönsted acid. However, every substrate to date using this combination was a substituted anthraquinone of some kind,[23–25] which has very different properties from diphenyl ketones or diphenylamines. However, with nothing left to lose, the combination was attempted, and turned out to be quite successful. The first step forms an ionic liquid of sorts, using a eutectic mixture of $AlCl_3$ and NaCl that melts at 110°C. This dissolves the substrate, and can then be carefully diluted with 4M HCl to finish the reaction (Scheme 3.10).

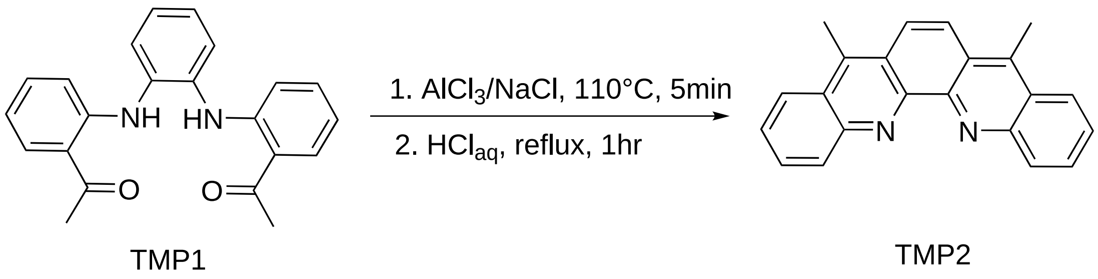

Scheme 3.10. 6-exo-trig ring closing reaction of **10**

Yields were surprisingly good (75%), and the reaction yielded a clean product without chromatography. As such, this technique was used moving forward.

3.5.9 Complexation

Complexation reactions are chemically quite straightforward. A metal precursor is chosen with coordinating ligands sufficiently labile to be displaced by the incoming nucleophile. Successful formation of the product (assuming standard $2\,e^-$ donors) is mainly determined by simple sterics. Unfortunately, **1** is a rigid planar system, with a bent conformation that forces extension of the aromatic rings into the coordination sphere of the metal center.

Minimum necessary conditions were tested by mixing one equivalent of **1** with one equivalent of Ru(DMSO)$_4$Cl$_2$ in polar solvent systems with ever increasing boiling points. While 2,2'-bipyridine-4,4'-dicarboxylic acid (**13**) would readily coordinate in as mild conditions as refluxing 1,2-dichloroethane, **1** failed to coordinate until refluxing N,N-dimethylformamide (DMF). Even then, coordination was so slow as to take multiple days, so conditions were increased to ethylene glycol. In hot (170°C) ethylene glycol, the coordination takes less than 30 minutes. Therefore, these conditions were used to create the chloride salt of the final ruthenium complex, with a final reaction in DMF to make the thiocyanate (Scheme 3.11).

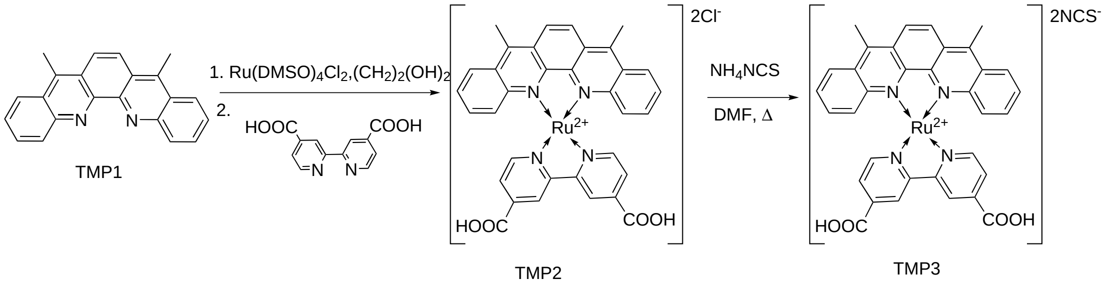

Scheme 3.11. Coordination of **1** to ruthenium

Under these conditions, it's also possible to make the homoleptic system (**15**), offering the possibility for some future derivatives (Scheme 3.12).

3.6 Solar Cell Characteristics

Unfortunately, the compound did not perform well as a DSSC. With an overall conversion efficiency of only 0.015% (compared to 1.9% for N-719), this compound will not serve as a good solar cell dye.

The main issue is the J_{sc} of only 0.06 $\mathrm{mA\,cm^{-2}}$. This indicates that there is a severe problem with the electron injection efficiency in this compound, which is

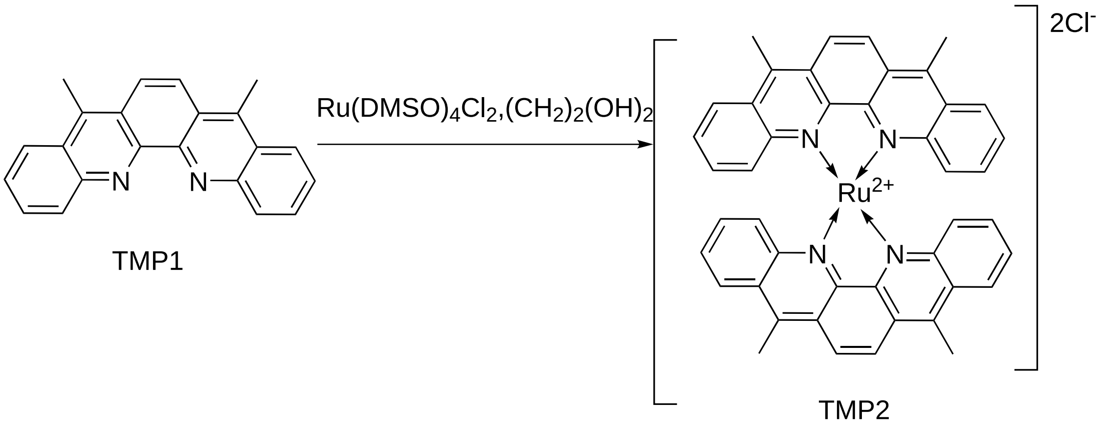

Scheme 3.12. Coordination of **1** to ruthenium

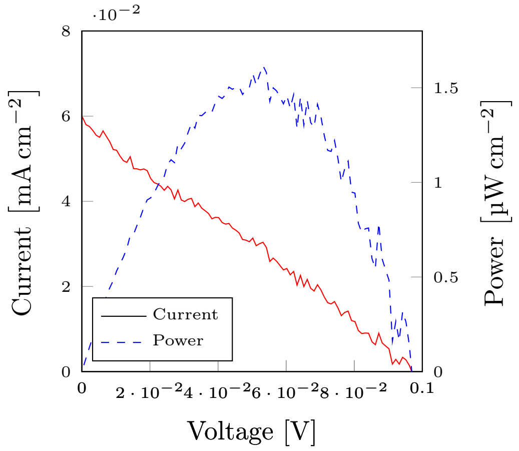

Figure 3.14. Power and JV curves of a DSSC loaded with **3** in a nonpolar solvent

supported by prior results. As stated earlier, another group using C6-C7 dihydro derivatives found that their compound had a low electron injection efficiency of 1.36 mA cm^{-2}.[3] They ascribed this to the LUMO of their compound being too close in energy to the conduction band of TiO_2. While there was some reason to doubt their conclusion (Section 3.2), this seems consistent with their findings. As was seen with the DFT calculations, the dehydrogenation of the central double bond leads to a large stabilization of the compound compared to the dihydro compound. Therefore, our ruthenium complex based on this ligand would likely be lowered in energy as well. This should decrease the driving force for electron injection in the compound, and increase the number of electrons lost to relaxation.

The V_{oc} is 0.1 V, which is relatively similar to that found by Islam et al with their dihydro derivative.[3]

3.7 Future Work

3.7.1 Aromaticity

As contradictory results were found related to the reactivity of the dibenzophenanthrolines, more study is certainly merited. Specifically, the question as to the nature of the central double bond needs to answered. To that end, a more in-depth DFT study could show how the electrons behave during simple reactions. More reactions could also be used to determine reactivity, including halogenation and ozonolysis.

3.7.2 Derivatives

The original purpose of this project was to create a library of compounds, but the chemistry was unique enough to slow synthesis, and merit study on its own. With this in-depth knowledge in hand, further synthesis could create a library of derivatives that could yield much more insight into this system. A Horner-Wadsworth-Emmons synthesis is commonly used in the creation of DSSCs to couple two aromatic systems, thereby redshifting absorption and localizing the HOMO. As we have the means to create an aldehyde derivative, this could be coupled to any number of aromatic phosphonate esters to create multiple derivatives (Scheme 3.13)

Moreover, this could be used to compare the effect of planarity on the efficiency of the solar cell. By comparing dibenzophenanthroline, dihydrodibenzophenanthroline, and biquinoline derivatives, a more complete picture could be drawn as to the interaction of highly aromatic compounds in DSSCs (Figure 3.15).

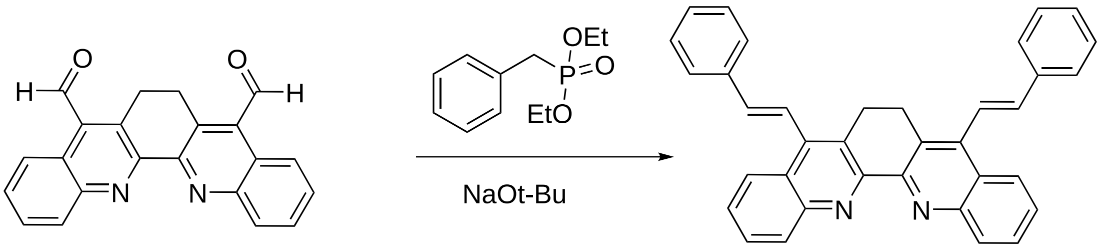

Scheme 3.13. Horner-Wadsworth-Emmons reaction of **4**

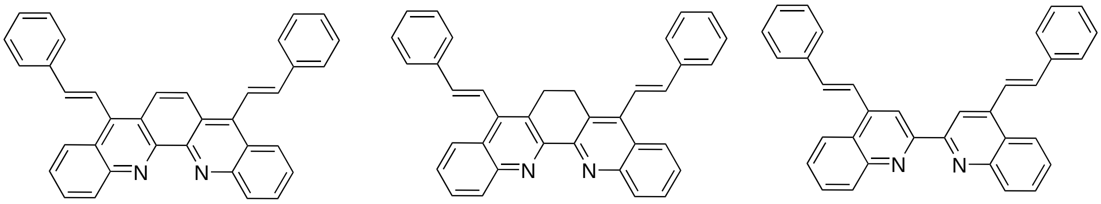

Figure 3.15. Library for comparing the effect of planarity

3.8 Conclusions

Within this chapter, I have detailed the extensive synthesis of a polycyclic heteroaromatic hydrocarbon, **1**. The reaction chemistry of this class of compounds was explored, leading to a number of insights about the unique nature of their aromaticity. Contradicting results were found, each indicating reactivity at different positions on the compound, which merits further investigation.

The compound was used as a ligand in the creation of a ruthenium complex, which was in turn used as a sensitizing dye for a dye-sensitized solar cell. The efficiency, while limited, does lend insight into what could be done to improve their efficiency if future derivatives were made. In particular, better matching of the dye's energy level to that of its electrolyte and semiconductor could afford a drastic improvement in efficiency, as well as derivation of the compound.

3.9 Experimental

3.9.1 Density Functional Theory

Energy minimization was done using the MMF94 forcefield to obtain the initial approximation, followed by the B3LYP/6-31G* basis set, with the General Atomic and Molecular Electronic Structure System (GAMESS) package in the ChemBio3D software.

3.9.2 Solar Cell Assembly and Testing

The solar cells were prepared according to the procedure described previously[57]. A titanium dioxide paste was purchased from Solaronix (Ti-Nanoxide T/SP). The paste was then doctor bladed onto FTO glass (Hartford Glass, 7 Ω/□) and sintered at 500 °C for 1 h and cooled to 80 °C, at which point it was immersed in 0.5 mM solution of dye in methanol for 48 h. Next, the photoanode was rinsed with ethanol and dried. The cell was completed by sandwiching an electrolyte solution consisting of 0.5 M lithium iodide (Aldrich 99.9%) and 0.05 M iodine (Aldrich 99%) in acetonitrile together with the photoanode and a counter electrode. The cathode was prepared by spin coating 50 µL of a 5 mM solution consisting of chloroplatinic acid hydrate (Aldrich, 99.9%) in 2-propanol (Aldrich, 99%) onto FTO glass (Hartford Glass, 15 Ω/□) and annealing at 400 °C for 40 min. The cells were assembled using standard published procedures[58].

The photoanode thickness, as determined by SEM, was 13 µm.

The solar cells were tested with a Gamry Reference 600 potentiostat, using a 300 W Xe lamp and 0.25 cm^2 mask, filtered to 1.5 AM (100 mW/cm^2).

3.9.3 Synthesis

All reactions were performed under nitrogen unless specified otherwise. All chemicals were purchased from Fisher Scientific and were used as received. Deuterated solvents were purchased from Acros Organics. Nuclear Magnetic Resonance

(NMR) spectra were obtained on Varian INNOVA 300 MHz and 500 MHz NMR spectrometers. Mass spectrometry (HRMS) experiments were conducted using Micromass AutoSpec M magnetic sector using chemical ionization (CI) in methane.

1,1'-((1,2-phenylenebis(azanediyl))bis(2,1-phenylene))bis(ethan-1-one) (**10**)

Ullmann-Goldberg

0.5041 g (1.54 mmol) of 1,2-diiodobenzene, 0.5219 g (3.87 mmol) of 2'-aminoacetophenone, 0.4958 g of K_2CO_3, 18 mg of CuI, and 10.4 mg of freshly washed Cu powder were added to a round-bottom flask, along with 25 mL of 1,4-dioxane. The solution was stirred vigorously and allowed to reflux. After 6 days, the solution was brought to room temperature and diethyl ether (50 mL) was added. The solution was filtered, and the filter cake was washed sequentially with water and cold acetone. Recrystallization in MeOH yielded 417.3 mg (79%)

Buchwald-Hartwig

Into a round bottom was added palladium (II) acetate (6.6 mg, 29.4 µmol), 2-Dicyclohexylphosphino-2',4',6'-triisopropylbiphenyl (Xphos) (41.7 mg, 87.4 µmol), and potassium phosphate (921 mg, 4.34 mmol), and an inert atmosphere was established. 3 mL of dioxane with 2 µL of water was then added to the round bottom, and the orange solution was heated until the color had deepened to a dark red. The 1,2-dibromobenzene (327.4 mg, 1.39 mmol) and 2'-aminoacetophenone (420.6 mg, 3.11 mmol) were then added along with an addition 3 mL of dioxane, and the reaction was heated to reflux. The dioxane was removed in the rotary evaporator, and the reaction mixture was resuspended in dichloromethane with added Celite. This was filtered and washed with an additional 20 mL of dichloromethane. The dark red solution was then washed with 3 portions of 30 mL of 0.8 M HCl to remove the excess amine, followed by 2 portions of 30 mL of water. The resulting brownish solution was dried over magnesium sulfate, rotovapped, and chromatographed on silica (30:70 ethyl acetate:hexanes) to yield 428.8 mg of yellow solid (90%).

^{1}H-NMR (499 MHz, Chloroform-d) δ 10.33 (s, 2H, N-H), 7.73 (dd, J = 8.1, 1.6 Hz, 2H), 7.43 (dd, J = 5.9, 3.6 Hz, 2H), 7.27 – 7.21 (m, 2H), 7.14 (dd, J = 5.9, 3.6 Hz, 2H), 7.03 (dd, J = 8.5, 1.1 Hz, 2H), 6.69 (ddd, J = 8.1, 7.0, 1.1 Hz, 2H), 2.55 (s, 6H, Me).

5,8-dimethyldibenzo[b,j][1,10]phenanthroline (**1**)

A round-bottomed flask was placed in a nitrogen glove box and loaded with 21.245 g of a finely ground 4:1 mixture (by weight) of dried $AlCl_3$ and NaCl, respectively. This was then heated at 110 °C until a clear liquid was formed, and then cooled. 2.043 g (5.94 mmol) of **10** was added, and the mixture was re-heated until a dark brown solution was formed. This was heated for 5 minutes before cooling. Finally, 150mL of 4M HCl was slowly added until the solution was completely neutralized, and it was reheated for 1 hr. The resulting solution was filtered, poured on ice, slowly neutralized with $NaHCO_3$, and filtered again to collect the precipitate. The filter cake was washed with water and cold methanol to yield 1.283 mg (4.17 mmol) of yellow solid (70.2%). This can be recrystallized from CH_2Cl_2/MeOH to yield yellow needles. ^{1}H-NMR (498 MHz, Chloroform-d) δ 8.70 (d, J = 8.5 Hz, 2H), 8.31 (d, J = 8.7 Hz, 3H), 8.09 (s, 2H, C6/C7), 7.87 (t, J = 7.5 Hz, 2H), 7.70 (t, J = 7.6 Hz, 2H), 3.16 (s, 6H, Me).

6,7-dihydrodibenzo[b,j][1,10]phenanthroline-5,8-dicarbaldehyde (**4**)

Into a round-bottomed flask was added 312.5 mg (1.01 mmol) **2**, 275.3 mg (2.50 mmol) of freshly sublimed SeO_2, and 40 mL of wet 1,4-dioxane. This was refluxed for 16 hours. The resulting red suspension was filtered through Celite, and the filtrate was concentrated 50% under vacuum. The solution was then diluted with ether, and the precipitate was filtered and washed with acetone and ether to yield 274.5 mg (81%) of product. ^{1}H-NMR (500 MHz, Chloroform-d) δ 11.15 (d, J = 1.0 Hz, 2H, COH), 8.59 (d, J = 8.9 Hz, 2H), 8.53 (d, J = 8.7 Hz, 2H), 7.83 (ddd, J = 8.4, 6.9, 1.4 Hz, 2H), 7.74 (ddd, J = 8.2, 6.8, 1.3 Hz, 2H), 3.61 (d, J = 1.1 Hz, 5H, CH2).

Dibenzo[b,j][1,10]phenanthroline-5,8-dicarbaldehyde (**7**)

Into a round-bottomed flask was added 310.7 mg (1.01 mmol) of **1**, 267.1 mg (2.41 mmol) of freshly sublimed SeO_2, and 40 mL of wet 1,4-dioxane. This was refluxed for 16 hours. The resulting red suspension was filtered through Celite, and the filtrate was concentrated 50% under vacuum. The solution was then diluted with ether, and the precipitate was filtered and washed with acetone and ether to yield 292.4 mg (87%) of product. ^{1}H-NMR (498 MHz, Chloroform-d) δ 11.54 (s, 2H, COH), 8.79 (t, J = 7.9 Hz, 4H), 8.68 (s, 2H), 8.00 (td, J = 8.6, 7.3, 1.6 Hz, 2H), 7.88 (td, J = 7.7, 1.6 Hz, 2H).

5,8-dimethyldibenzo[b,j][1,10]phenanthroline-6,7-dione (**8**)

450.1 mg (1.53 mmol) of $K_2Cr_2O_7$ was dissolved in 5 mL of H_2SO_4. This solution was then slowly added to a vigorously stirred solution of 156.2 mg (0.504 mmol) of **2** in 20 mL of acetone. After 2 hours, the green solution was diluted with water, filtered and washed with water and aqueous $NaHCO_3$. The solid was then chromatographed on neutral alumina (80:20 ethyl acetate/hexanes) to yield 155.3 mg of yellowish solid (30% yield). ^{1}H-NMR (499 MHz, DMSO-d6) δ 8.76 (d, J = 4.3 Hz, 2H), 8.11 (dd, J = 8.4, 1.3 Hz, 2H), 8.03 – 7.99 (m, 4H), 7.76 (ddd, J = 8.3, 6.9, 1.4 Hz, 2H), 7.64 (ddd, J = 8.2, 6.8, 1.3 Hz, 2H), 7.41 – 7.36 (m, 1H), 2.69 (d, J = 0.9 Hz, 6H, Me).

5,8-bis(bromomethyl)dibenzo[b,j][1,10]phenanthroline (**9**)

Into a round-bottomed flask was added **2** (932.2 mg, 3.10 mmol), N-bromosuccinimide (1.769 mg, 3.79 mmol) benzoyl peroxide (184.5 mg, 0.76 mmol), and 35 mL of CCl_4. The solution was refluxed overnight. The resulting orange solution was concentrated, dissolved in EtOAc, and washed with sodium metabisulfite, water, and brine. The solution was then concentrated under vacuum and the resulting solid recrystallized in MeOH/Et_2O to yield 1.448 g (82%) of product. ^{1}H-NMR (500 MHz, Chloroform-d) δ 8.73 (dd, J = 8.5, 1.0 Hz, 2H), 8.33 (dd, J = 8.3, 1.1 Hz, 2H), 8.21 (s, 2H, C6/C7), 7.92 (ddd, J = 8.3, 6.7, 1.3 Hz, 2H), 7.82 (ddd, J = 8.2, 6.7, 1.3 Hz, 2H), 5.41 (s, 4H, CH2Br).

*Reduction of **9***

156.7 mg (0.336 mmol) of **9** was added to a round-bottomed flask, along with 40.2 mg (1.06 mmol) of $NaBH_4$ and 15 mL of methanol. The solution was stirred overnight at room temperature, and then concentrated and diluted with EtOAc. This was washed with water and brine, and the organic layer was concentrated again. The product was determined to be **2**.

Dichlorotetrakis(dimethylsulfoxide)ruthenium(II)

Into a round-bottomed flask was added 1.53 g (6.80 mmol) of $RuCl_3$ and 15 mL of dry DMSO. The deep red solution was refluxed for 30 min, cooled, and diluted with acetone. The precipitated solid was filtered and washed with acetone to yield 2.145 g (4.43 mmol) of yellow solid (65%). The compound was used without further purification.

*Ru(**1**)(dcbpy)NCS*$_2$ (**3**)

$Ru(DMSO)_4(Cl)_2$ (241.3 mg, 0.499 mmol) was added to a round-bottomed flask, along with 155.2 mg (0.504 mmol) of **1** and 20 mL of dry ethylene glycol. This was heated at 170 °C for 30 min. 4,4'-dicarboxy-2,2'-bipyridine (125.3 mg, 0.514 mmol) was then added, and heating continued for another 2 hours. Finally, 253.2 mg (3.33 mmol) of NH_4NCS was added, and heating continued for another 3 hours. Once the reaction was cooled, it was diluted with 0.1 M HNO_3, and placed at 4 °C overnight. The resulting deep red precipitate was filtered, washed with water and acetone, and dissolved in 0.1 M Na_2CO_3. This was then reprecipitated with HNO_3, filtered, and washed again with water and acetone to yield 174.1 mg of red solid (45%) ^{1}H-NMR (500 MHz, DMSO-d6) δ 10.04 (d, J = 7.9 Hz, 1H), 9.91 (d, J = 8.8 Hz, 1H), 8.83 (d, J = 3.1 Hz, 1H), 8.82 (d, J = 1.6 Hz, 1H), 8.57 (d, J = 3.2 Hz, 1H), 8.56 (d, J = 0.6 Hz, 1H), 8.46 (d, J = 5.4 Hz, 1H), 8.21 – 8.18 (m, 2H), 7.73 (d, J = 5.4 Hz, 1H), 7.47 (s, 1H), 7.28 – 7.21 (m, 2H), 7.20 – 7.11 (m, 2H), 6.18 (d, J = 8.2 Hz, 1H), 3.90 (s, 6H).

3.10 References

(1) Pérez León, C.; Kador, L.; Peng, B.; Thelakkat, M. *J. Phys. Chem. B* **May 2006**, *110*, 8723–30.

(2) Yin, J.-F.; Velayudham, M.; Bhattacharya, D.; Lin, H.-C.; Lu, K.-L. *Coord. Chem. Rev.* **Dec. 2012**, *256*, 3008–3035.

(3) Islam, A.; Sugihara, H.; Singh, L. P.; Hara, K.; Katoh, R.; Nagawa, Y.; Yanagida, M.; Takahashi, Y.; Murata, S.; Arakawa, H. *Inorganica Chim. Acta* **Oct. 2001**, *322*, 7–16.

(4) Hückel, E. *Z. Für Phys. Hadrons Nucl.* **1931**, *70*, 204.

(5) Roberts, J. D.; Streitwieser, A.; Regan, C. M. *J. Am. Chem. Soc.* **1952**, *74*, 4579–4582.

(6) Clar, E., *The aromatic sextet*; J. Wiley: 1972; 144 pp.

(7) Kumar, B.; Viboh, R. L.; Bonifacio, M. C.; Thompson, W. B.; Buttrick, J. C.; Westlake, B. C.; Kim, M.-S.; Zoellner, R. W.; Varganov, S. A.; Mörschel, P.; Teteruk, J.; Schmidt, M. U.; King, B. T. *Angew. Chem. Int. Ed.* **Dec. 14, 2012**, *51*, 12795–12800.

(8) Wendland, R.; LaLonde, J. *Org Synth* **1954**, *34*, 76.

(9) Ma, K.; Li, S.; Weiss, R. G. *Org. Lett.* **Oct. 2, 2008**, *10*, 4155–4158.

(10) Phillips, D. D. *Org Synth* **1954**, *34*, 31.

(11) Bailey, P. S. *Erickson Ronald E* **1961**, *41*, 41.

(12) Yamada, M.; Tanaka, Y.; Yoshimoto, Y.; Kuroda, S.; Shimao, I. *Bull. Chem. Soc. Jpn.* **1992**, *65*, 1006–1011.

(13) Chesneau, B.; Passelande, A.; Hudhomme, P. *Org. Lett.* **Feb. 5, 2009**, *11*, 649–652.

(14) Kipping, F. B.; Wren, J. J. *J. Chem. Soc.* **Jan. 1, 1957**, 1733–1740.

(15) Graebe, L. *Justus Liebigs Ann. Chem.* *276*, 48.

(16) Sakanishi, K.; Mochida, I.; Okazaki, H.; Soeda, M. *Chem. Lett.* **1990**, 319–322.

(17) Sugasawa, T.; Toyoda, T.; Adachi, M.; Sasakura, K. *J. Am. Chem. Soc.* **July 1978**, *100*, 4842–4852.

(18) Ruediger, E. H.; Kaldas, M. L.; Gandhi, S. S.; Fedryna, C.; Gibson, M. S. *J. Org. Chem.* **May 1980**, *45*, 1974–1978.

(19) Shidlovskii, A. F.; Golubev, A. S.; Gusev, D. V.; Suponitsky, K. Y.; Peregudov, A. S.; Chkanikov, N. D. *J. Fluor. Chem.* **Nov. 2012**, *143*, 272–280.

(20) Han, X.-D.; Zhao, Y.-L.; Meng, J.; Ren, C.-Q.; Liu, Q. *J. Org. Chem.* **June 2012**, *77*, 5173–8.

(21) Kuninobu, Y.; Tatsuzaki, T.; Matsuki, T.; Takai, K. *J. Org. Chem.* **Sept. 2011**, *76*, 7005–9.

(22) Park, B. S.; Lee, S. W.; Kim, I. T.; Tae, J. S.; Lee, S. H. *Heteroat. Chem.* **Oct. 2012**, *23*, 66–73.

(23) Cook, A. H.; Waddington, W. *J. Chem. Soc. Resumed* **Jan. 1945**, 402.

(24) Sokolyuk, N. T.; Pisulina, L. P. *Russ. J. Org. Chem.* **2002**, *38*, 1212–1213.

(25) Waldmann, H.; Hindenburg, K.-G. *J. Für Prakt. Chem.* **Aug. 1940**, *156*, 157–168.

(26) Kempter, G.; Stoss, W. *J. Prakt. Chem.* **Sept. 1, 1963**, *21*, 198–203.

(27) Friedlaender, P. *Berichte Dtsch. Chem. Ges.* **July 1882**, *15*, 2572–2575.

(28) Friedländer, P.; Gohring, C. F. *Berichte Dtsch. Chem. Ges.* **July 1883**, *16*, 1833–1839.

(29) Jia, C.-S.; Zhang, Z.; Tu, S.-J.; Wang, G.-W. *Org. Biomol. Chem.* **2006**, *4*, 104–110.

(30) Shaabani, A.; Soleimani, E.; Badri, Z. *Synth. Commun.* **2007**, *37*, 629–635.

(31) Sridharan, V.; Ribelles, P.; Ramos, M. T.; Menéndez, J. C. *J. Org. Chem.* **Aug. 2009**, *74*, 5715–8.

(32) Varala, R.; Enugala, R.; Adapa, S. R. *Synthesis* **2006**, 3825–3830.

(33) Luo, J.; Hart, H. *J. Org. Chem.* **Oct. 1, 1987**, *52*, 4833–4836.

(34) Cosmo, R.; Sternhell, S. *Aust. J. Chem.* **Jan. 1, 1987**, *40*, 2137–2142.

(35) Badger, G. M.; Jefferies, P. R.; Kimber, R. W. L. *J. Chem. Soc.* **Jan. 1, 1957**, 1837–1841.

(36) Yoshida, M.; Nagayama, S.; Minabe, M.; Suzuki, K. *J. Org. Chem.* **1979**, *44*, 1915–1917.

(37) Minabe, M.; Yoshida, M.; Kimura, O. *Bull. Chem. Soc. Jpn.* **1985**, *58*, 385–386.

(38) Míšek, J.; Teplý, F.; Stará, I.; Tichý, M.; Šaman, D.; Císařová, I.; Vojtíšek, P.; Starý, I. *Angewandte Chemie International Edition* **Apr. 14, 2008**, *47*, 3188–3191.

(39) Barnes, R. A. **Jan. 1948**, *70*, 145–147.

(40) Tran, A. T.; Huynh, V. A.; Friz, E. M.; Whitney, S. K.; Cordes, D. B. *Tetrahedron Letters* **Apr. 22, 2009**, *50*, 1817–1819.

(41) Fish, R. H.; Tan, J. L.; Thormodsen, A. D. *J. Org. Chem.* **1984**, *49*, 4500–4505.

(42) Metallinos, C.; Barrett, F. B.; Wang, Y.; Xu, S.; Taylor, N. J. *Tetrahedron* **Nov. 27, 2006**, *62*, 11145–11157.

(43) Yang, N.-c. C.; Wei-Long, C.; Langan, J. R. *Tetrahedron Letters* **Jan. 1, 1984**, *25*, 2855–2858.

(44) Lawton, R. G.; Barth, W. E. *J. Am. Chem. Soc.* **1971**, *93*, 1730–1745.

(45) Newman, M. S.; Beal, P. *J. Am. Chem. Soc.* **1949**, *71*, 1506–1507.

(46) Hellwinkel, D.; Ittemann, P. *Liebigs Ann. Chem.* **July 12, 1985**, *1985*, 1501–1507.

(47) Ullmann, F.; Sponagel, P. *Ber Dtsch Chem Ges* **1905**, *38*, 2211–2212.

(48) Goldberg, I. *Berichte Dtsch. Chem. Ges.* **1906**, *39*, 1691–1692.

(49) Beletskaya, I. P.; Cheprakov, A. V. *Organometallics* **Nov. 2012**, *31*, 7753–7808.

(50) Kosugi, M.; Kameyama, M.; Migita, T. *Chem. Lett.* **1983**, 927–928.

(51) Dale Boger, L.; Panek, J. S. *Tetrahedron Lett.* **1984**, *25*, 3175–3178.

(52) Paul, F.; Patt, J.; Hartwig, J. F. *J. Am. Chem. Soc.* **1994**, *116*, 5969.

(53) Guram, A.; Buchwald, S. *J Am Chem Soc* **1994**, *116*, 7901–7902.

(54) Guram, A. S.; Rennels, R. A.; Buchwald, S. L. *Angew. Chem. Int. Ed.* **1995**, *34*, 1348.

(55) Louie, J.; Hartwig, J. F. *Tetrahedron Lett.* **1995**, *36*, 3609–3612.

(56) Fors, B. P.; Krattiger, P.; Strieter, E.; Buchwald, S. L. *Org. Lett.* **Aug. 2008**, *10*, 3505–8.

(57) Ito, S.; Murakami, T.; Comte, P.; Liska, P.; Gratzel, C.; Nazeeruddin, M.; Gratzel, M. *Thin Solid Films* **May 2008**, *516*, 4613–4619.

(58) Smestad, G. P. *J. Chem. Educ.* **June 1998**, *75*, 752–756.

.

Appendix

NMR

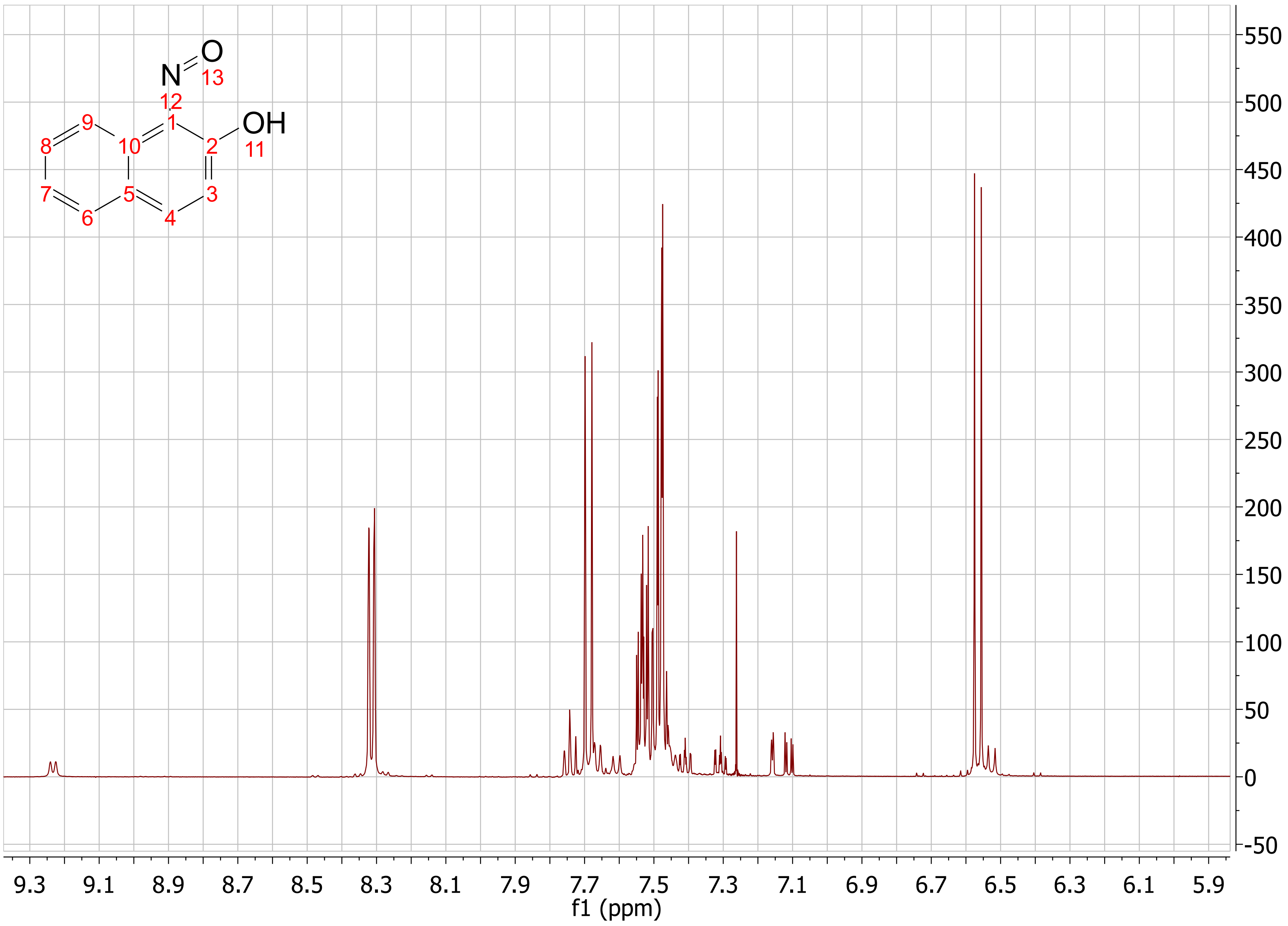
N
O
13
12
OH
11
1
2
3
4
5
6
7
8
9
10
550
500
450
400
350
300
250
200
150
100
50
0
-50
9.3
9.1
8.9
8.7
8.5
8.3
8.1
7.9
7.7
7.5
7.3
7.1
6.9
6.7
6.5
6.3
6.1
5.9
f1 (ppm)

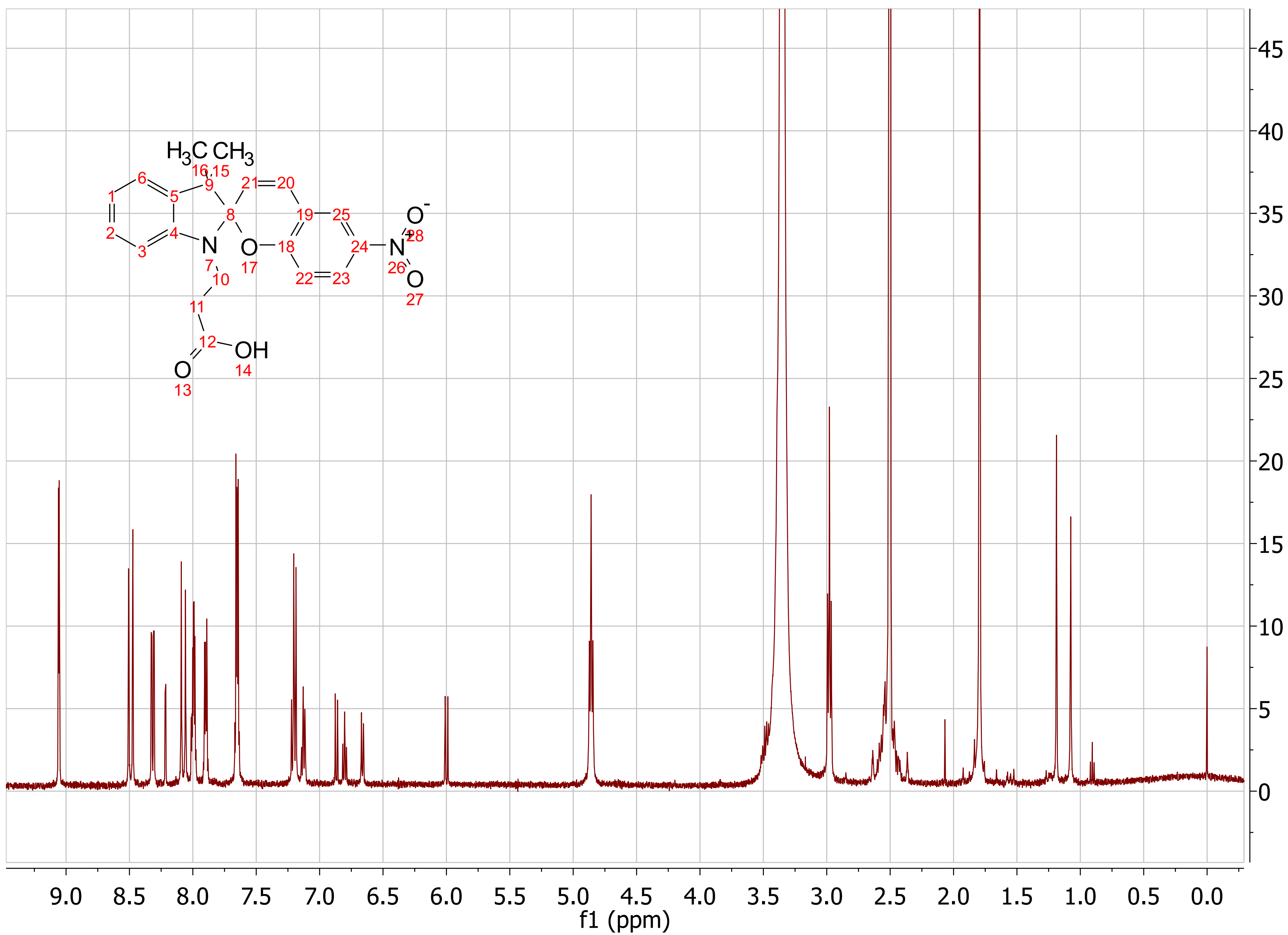

H3C CH3
16 15
1 2 3 4 5 6 7 8 9 10 11 12 13 14 17 18 19 20 21 22 23 24 25 26 27 28
N
O
O-
N
O
OH
O
45
40
35
30
25
20
15
10
5
0
9.0 8.5 8.0 7.5 7.0 6.5 6.0 5.5 5.0 4.5 4.0 3.5 3.0 2.5 2.0 1.5 1.0 0.5 0.0
f1 (ppm)

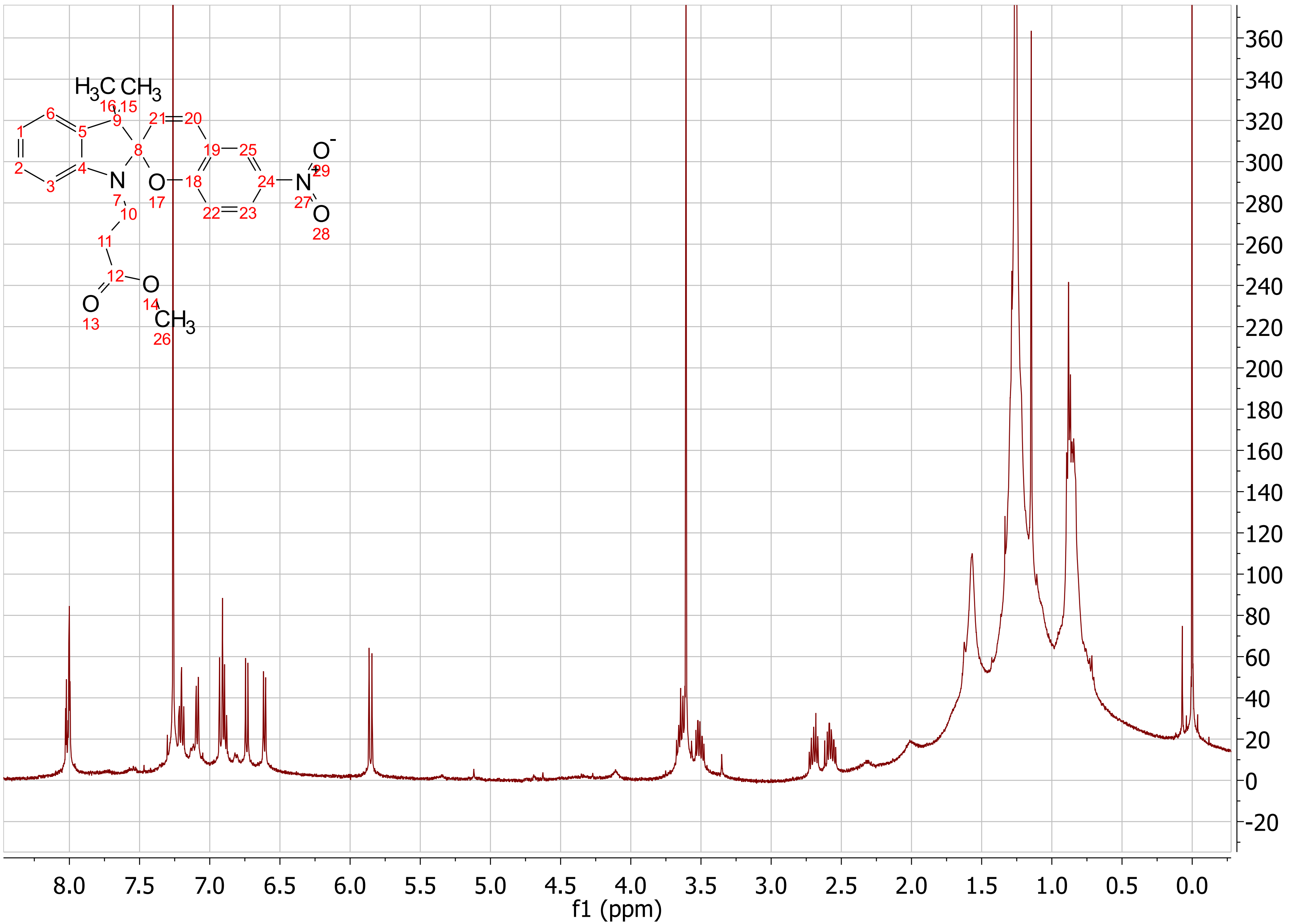
H3C CH3
O-
N+
O
O
O
CH3
N
O
8.0
7.5
7.0
6.5
6.0
5.5
5.0
4.5
4.0
3.5
3.0
2.5
2.0
1.5
1.0
0.5
0.0
f1 (ppm)
360
340
320
300
280
260
240
220
200
180
160
140
120
100
80
60
40
20
0
-20

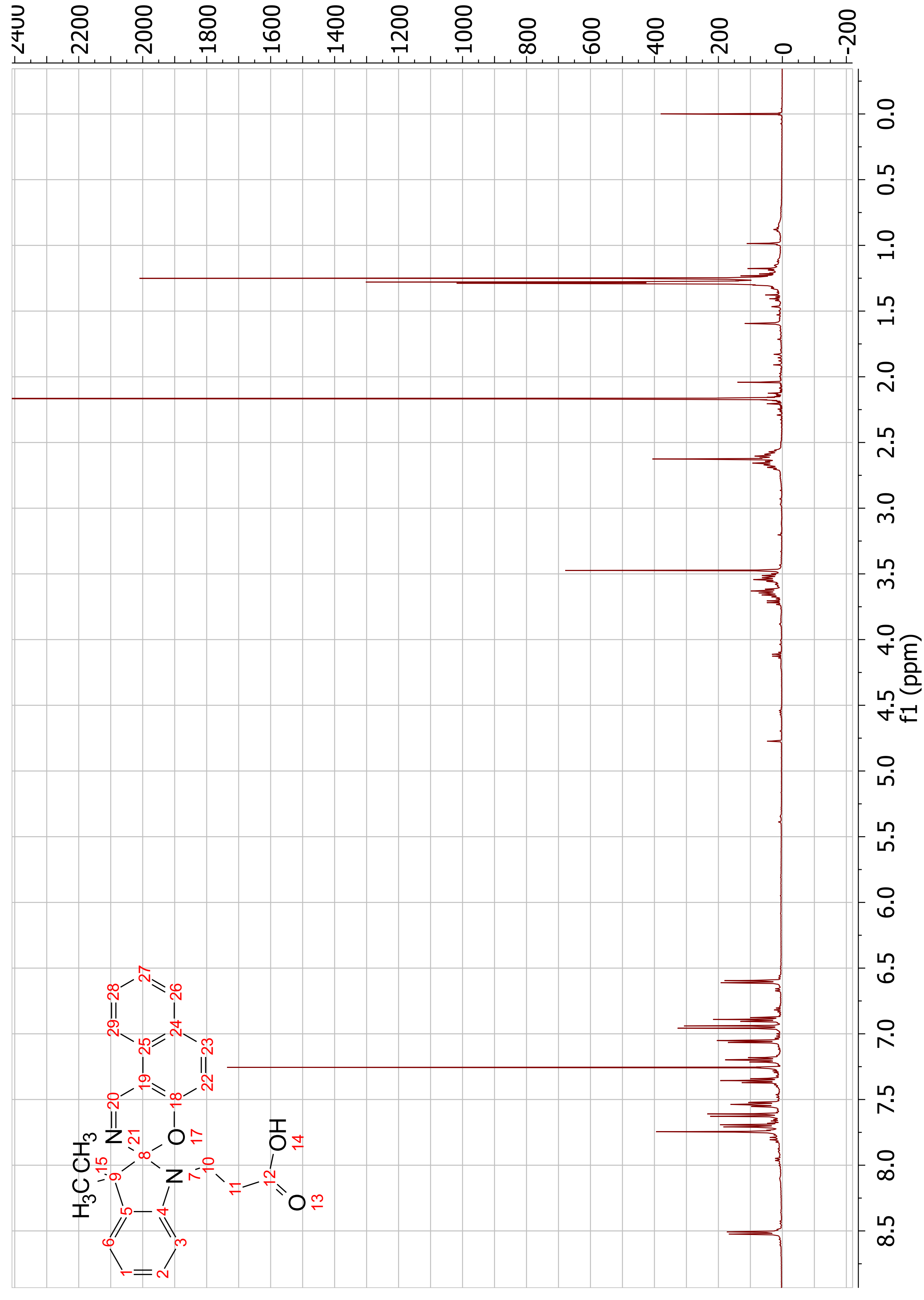
f1 (ppm)
8.5
8.0
7.5
7.0
6.5
6.0
5.5
5.0
4.5
4.0
3.5
3.0
2.5
2.0
1.5
1.0
0.5
0.0
2200
2000
1800
1600
1400
1200
1000
800
600
400
200
0
-200
H3C CH3
N
O
OH
O

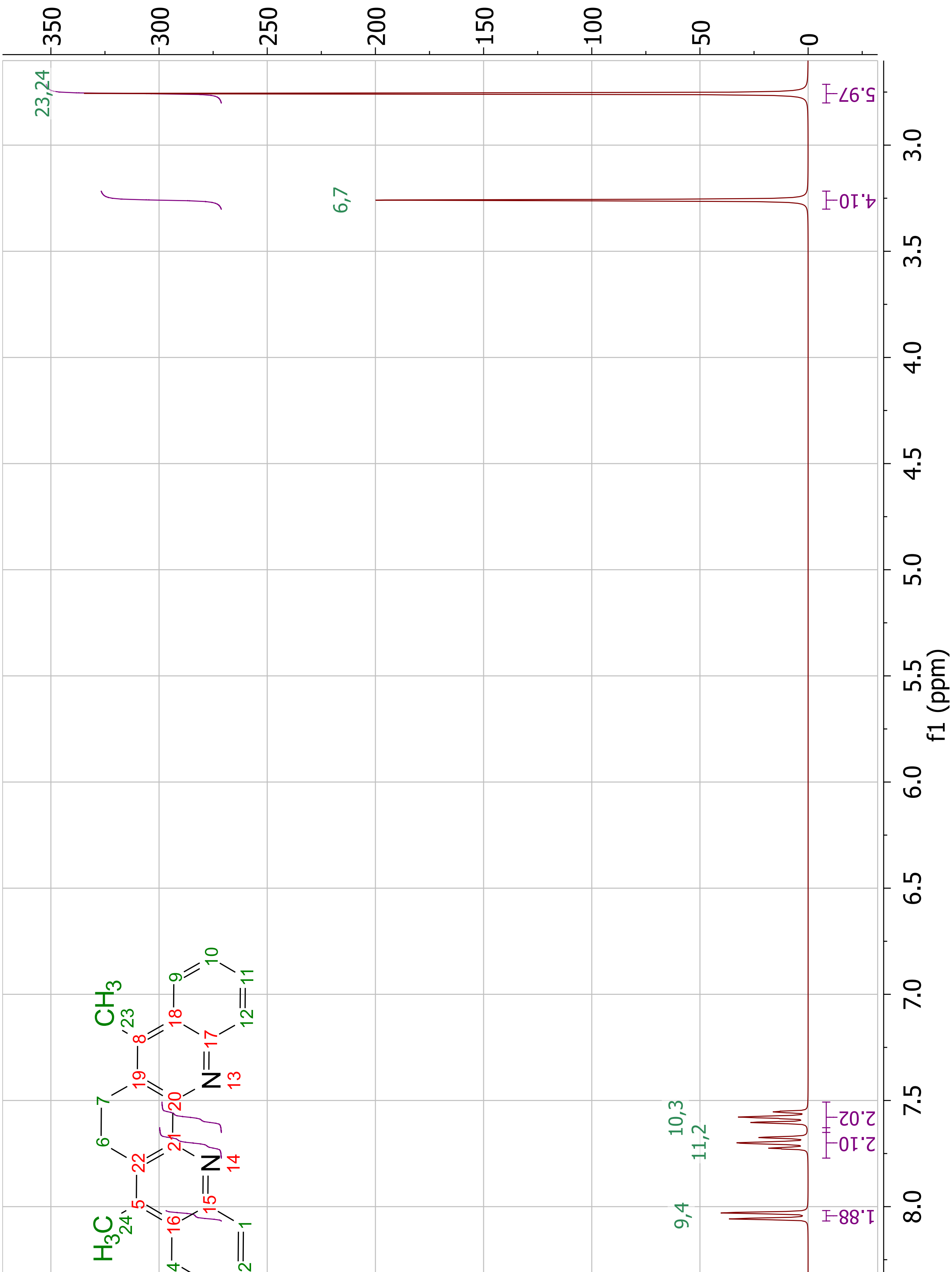
23,24
6,7
10,3
11,2
9,4
12,1
5.97
4.10
2.02
2.10
1.88
1.76
H3C
CH3
N
N
1
2
3
4
5
6
7
8
9
10
11
12
13
14
15
16
17
18
19
20
21
22
23
24
350
300
250
200
150
100
50
0
3.0
3.5
4.0
4.5
5.0
5.5
6.0
6.5
7.0
7.5
8.0
8.5
f1 (ppm)

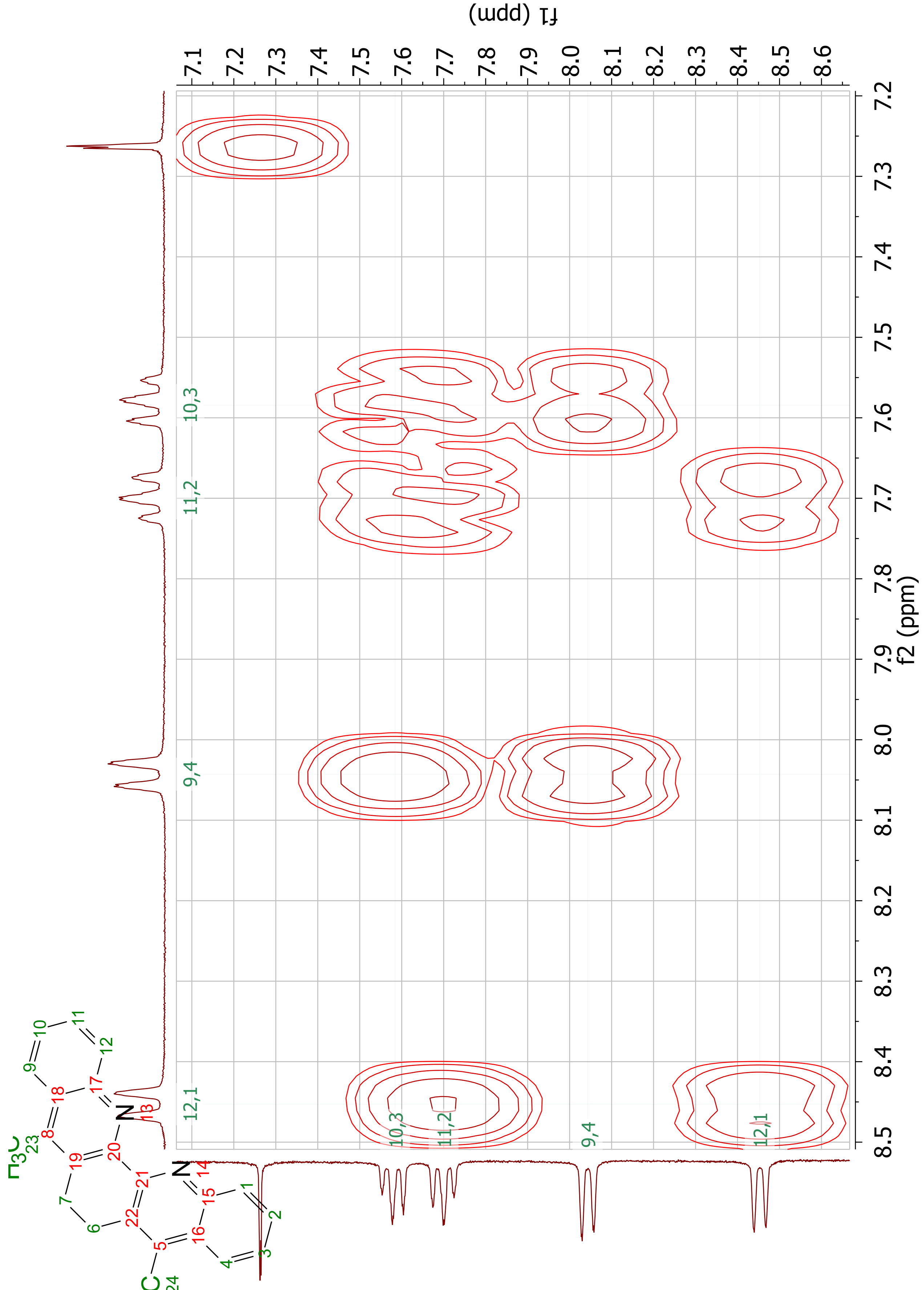
f1 (ppm)
7.1
7.2
7.3
7.4
7.5
7.6
7.7
7.8
7.9
8.0
8.1
8.2
8.3
8.4
8.5
8.6
f2 (ppm)
7.2
7.3
7.4
7.5
7.6
7.7
7.8
7.9
8.0
8.1
8.2
8.3
8.4
8.5
10,3
11,2
9,4
12,1
10,3
11,2
9,4
12,1
H3C 23
H3C 24
N 13
N 14
1
2
3
4
5
6
7
8
9
10
11
12
15
16
17
18
19
20
21
22

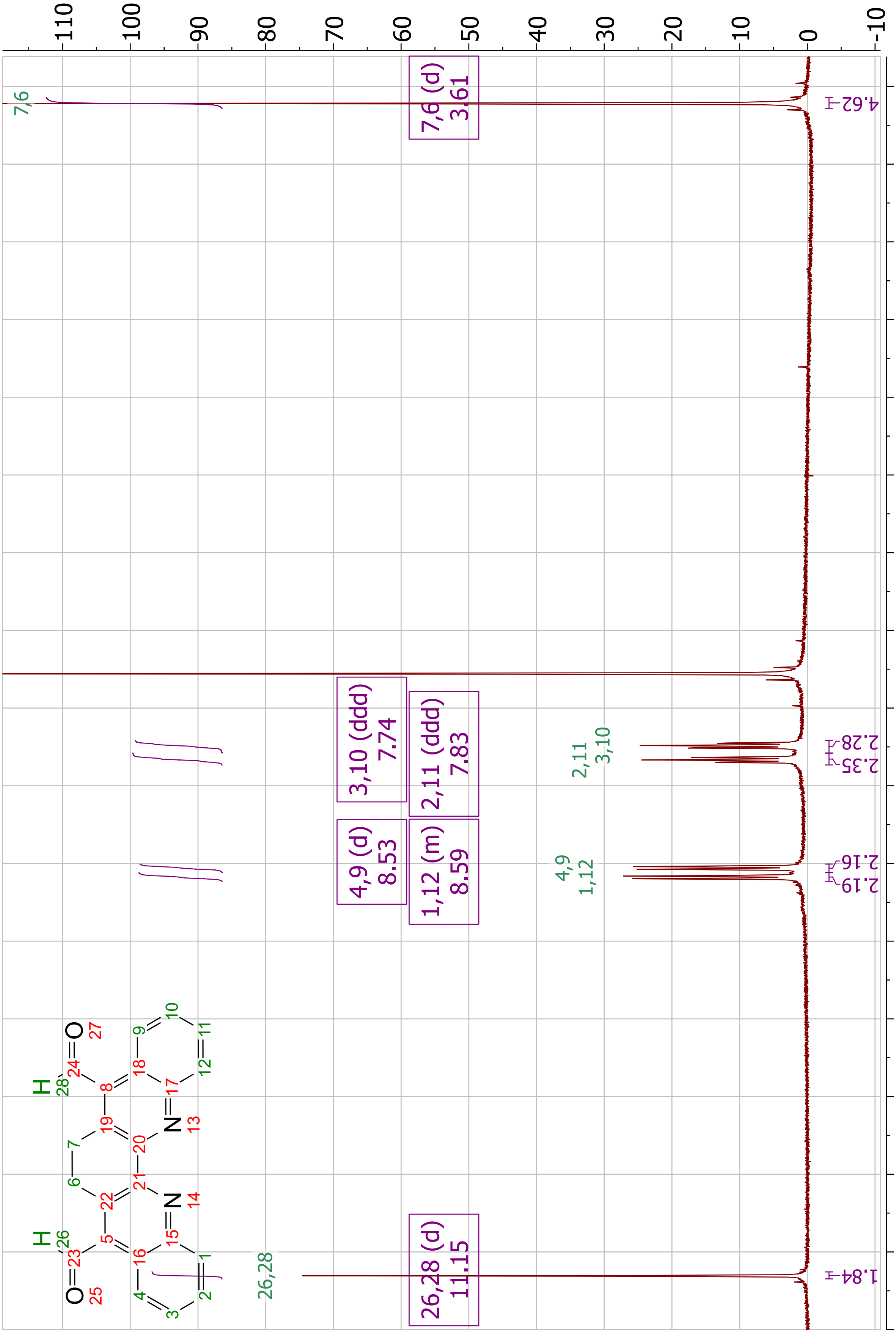
26,28 (d)
11.15
1,12 (m)
8.59
4,9 (d)
8.53
2,11 (ddd)
7.83
3,10 (ddd)
7.74
7,6 (d)
3.61
26,28
4,9
1,12
2,11
3,10
7,6
1.84
2.19
2.16
2.35
2.28
4.62
f1 (ppm)
11.5
11.0
10.5
10.0
9.5
9.0
8.5
8.0
7.5
7.0
6.5
6.0
5.5
5.0
4.5
4.0
3.5
110
100
90
80
70
60
50
40
30
20
10
0
-10

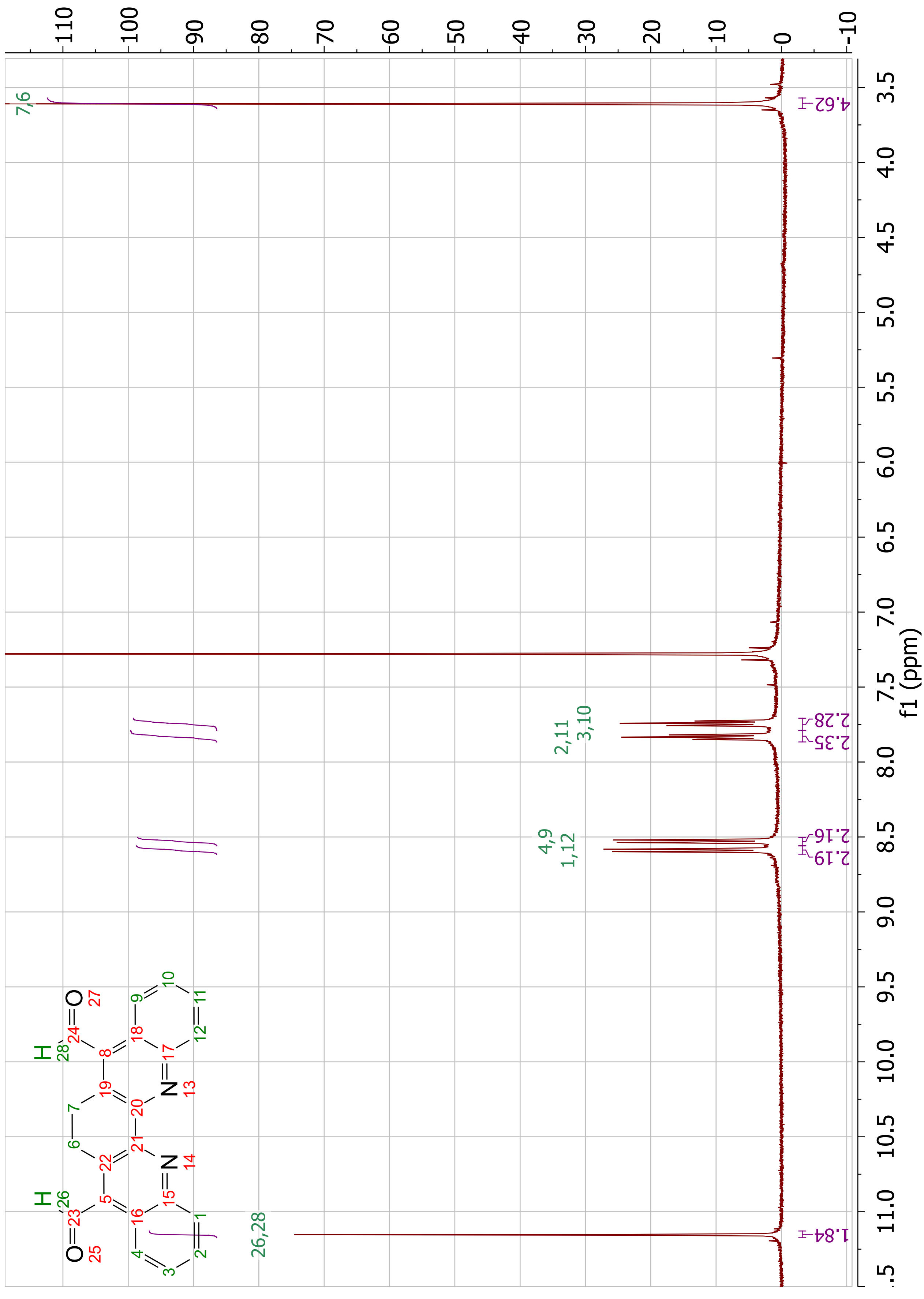f1 (ppm)
3.5
4.0
4.5
5.0
5.5
6.0
6.5
7.0
7.5
8.0
8.5
9.0
9.5
10.0
10.5
11.0
.5
110
100
90
80
70
60
50
40
30
20
10
0
-10
7,6
2,11
3,10
4,9
1,12
26,28
4.62
2.28
2.35
2.16
2.19
1.84
O
H
N
25
26
27
28
13
14

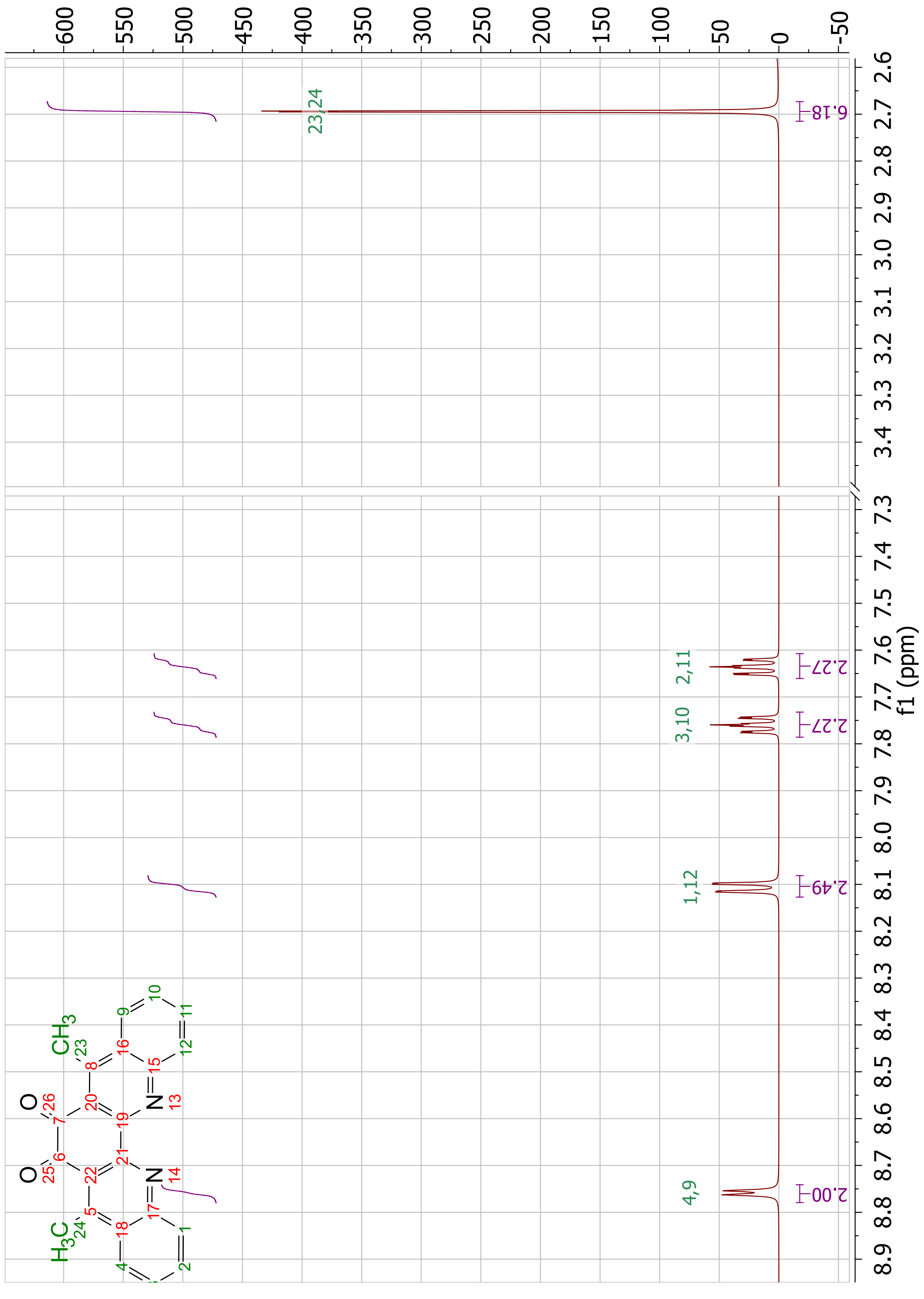23,24
6.18
2,11
2.27
3,10
2.27
1,12
2.49
4,9
2.00
H3C
CH3
O
O
N
N
f1 (ppm)
2.6
2.7
2.8
2.9
3.0
3.1
3.2
3.3
3.4
7.3
7.4
7.5
7.6
7.7
7.8
7.9
8.0
8.1
8.2
8.3
8.4
8.5
8.6
8.7
8.8
8.9
600
550
500
450
400
350
300
250
200
150
100
50
0
-50

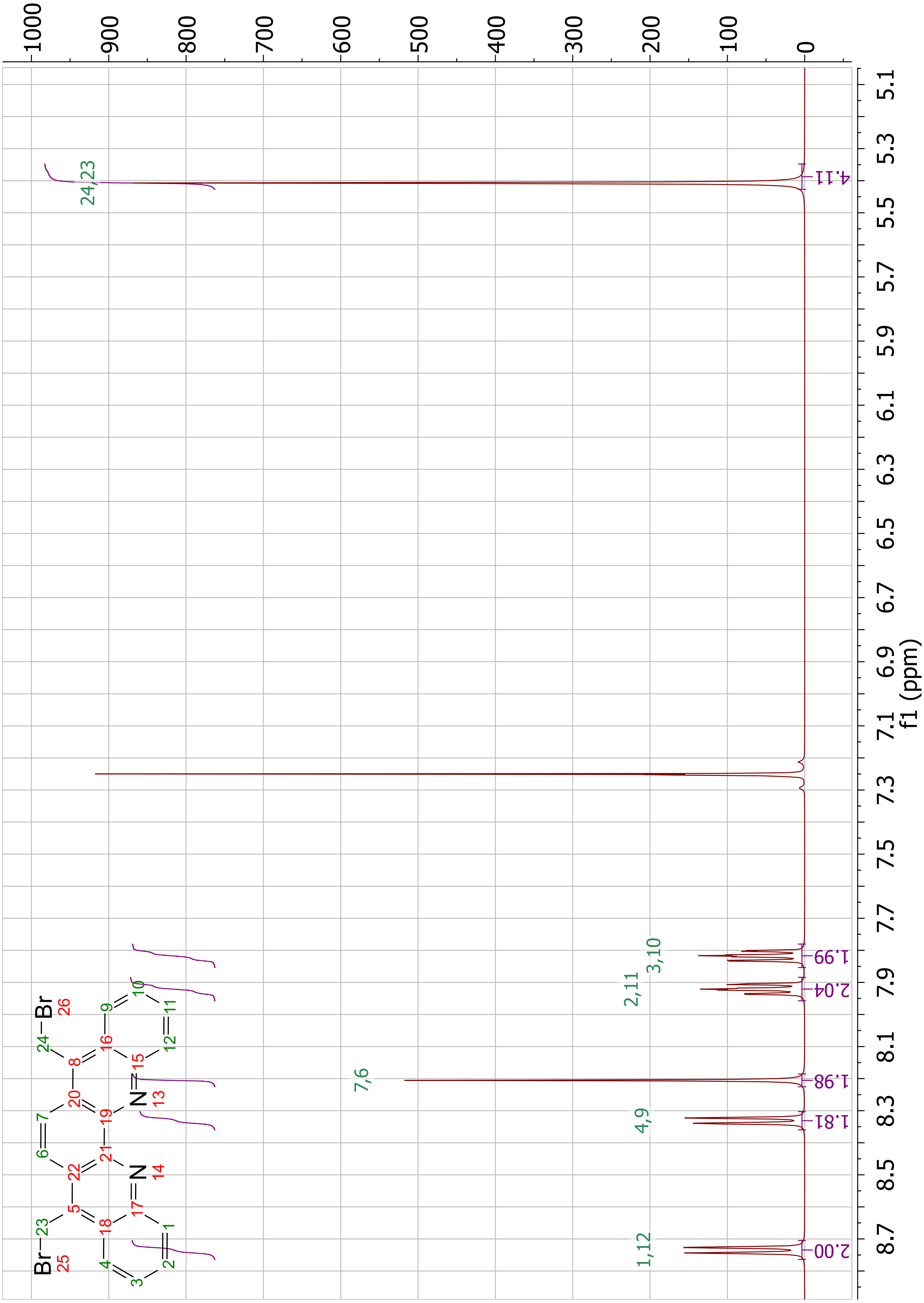
Br
25
23
24
Br
26
N
13
N
14
24,23
3,10
2,11
7,6
4,9
1,12
4.11
1.99
2.04
1.98
1.81
2.00
5.1
5.3
5.5
5.7
5.9
6.1
6.3
6.5
6.7
6.9
7.1
7.3
7.5
7.7
7.9
8.1
8.3
8.5
8.7
f1 (ppm)
1000
900
800
700
600
500
400
300
200
100
0

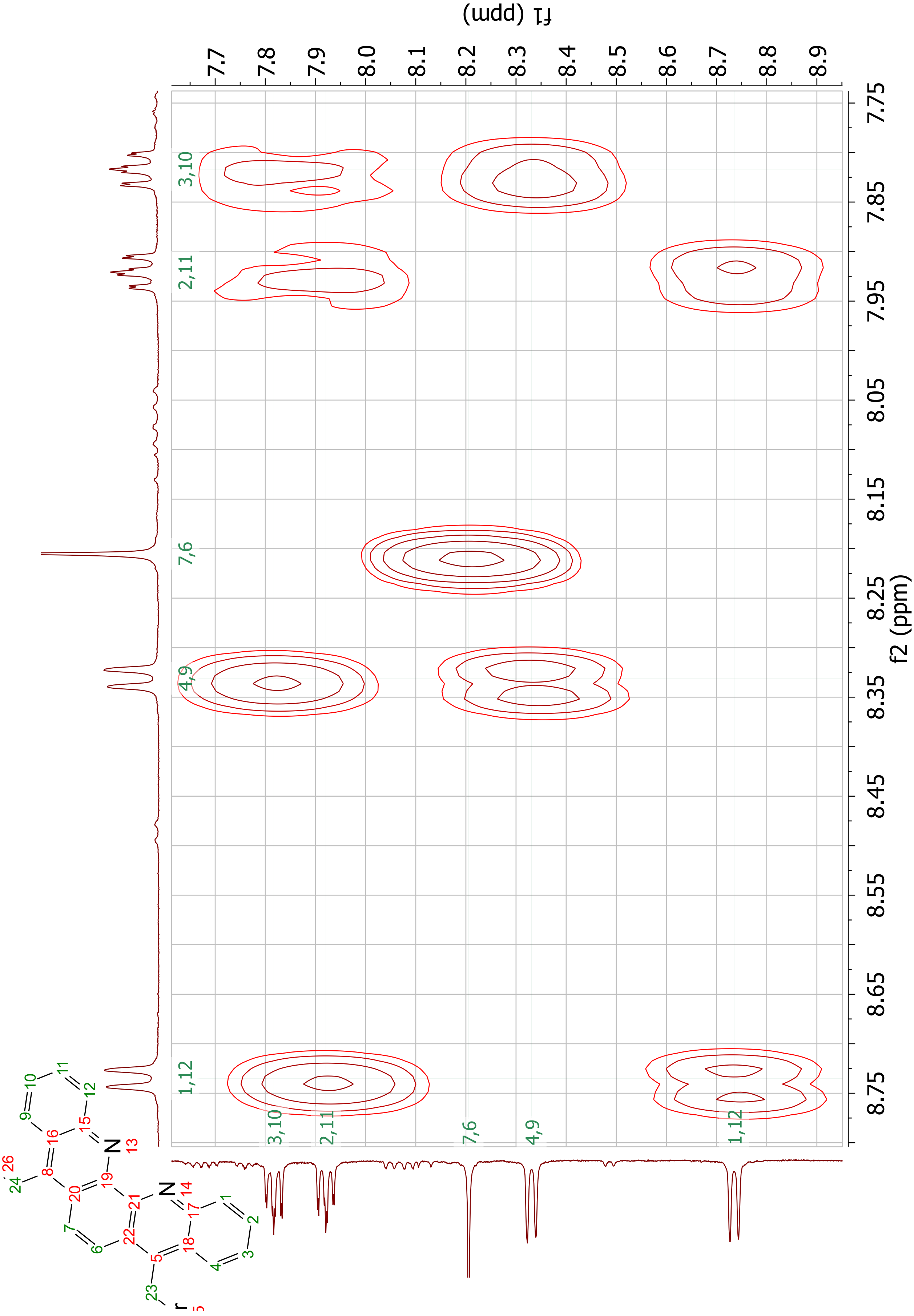
f1 (ppm)
7.7
7.8
7.9
8.0
8.1
8.2
8.3
8.4
8.5
8.6
8.7
8.8
8.9
f2 (ppm)
7.75
7.85
7.95
8.05
8.15
8.25
8.35
8.45
8.55
8.65
8.75
3,10
2,11
7,6
4,9
1,12
N
N
13
14
1
2
3
4
5
6
7
8
9
10
11
12
15
16
17
18
19
20
21
22
23
24
26

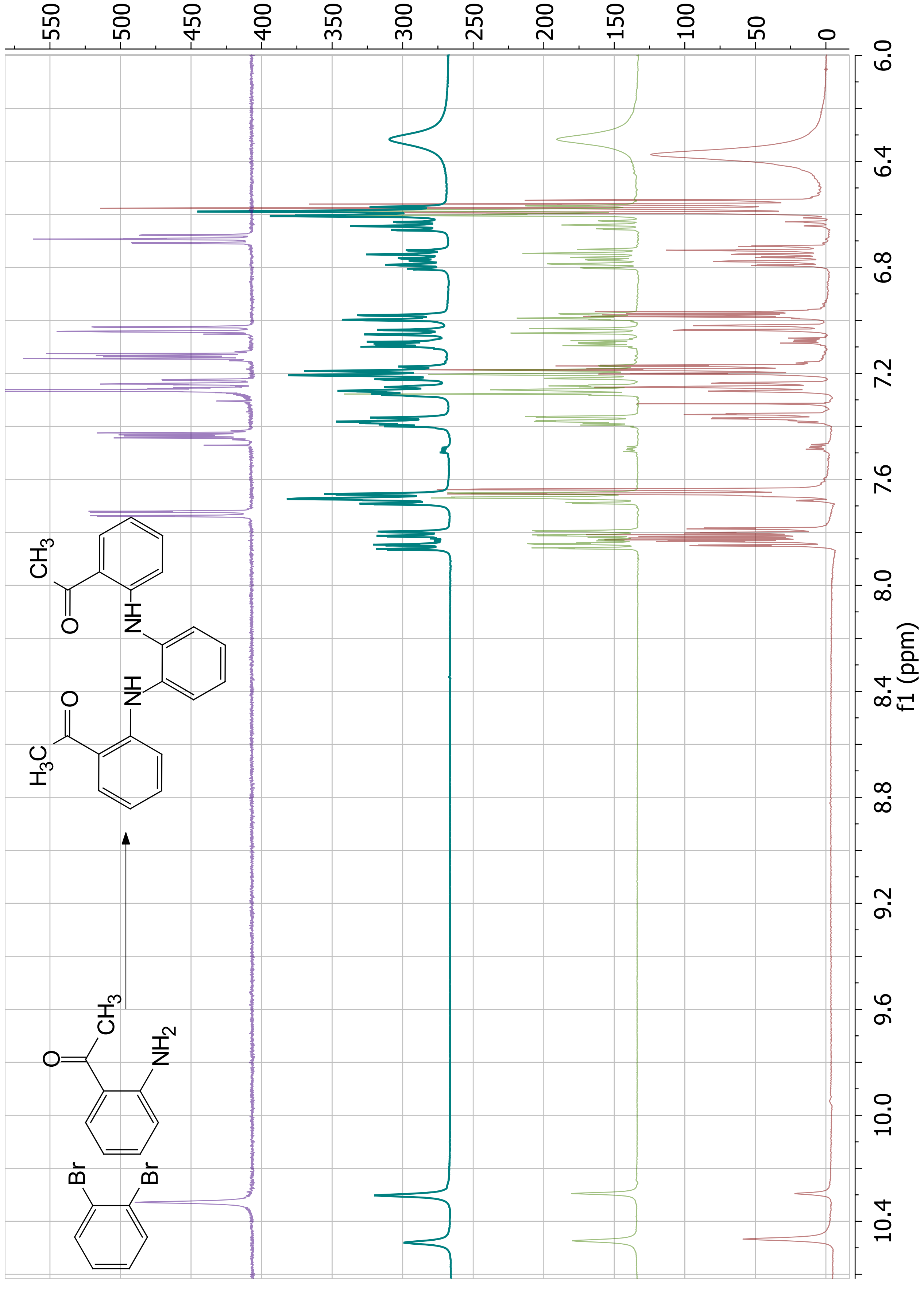
Br
Br
O
CH3
NH2
H3C
O
NH
NH
O
CH3
f1 (ppm)
6.0
6.4
6.8
7.2
7.6
8.0
8.4
8.8
9.2
9.6
10.0
10.4
550
500
450
400
350
300
250
200
150
100
50
0

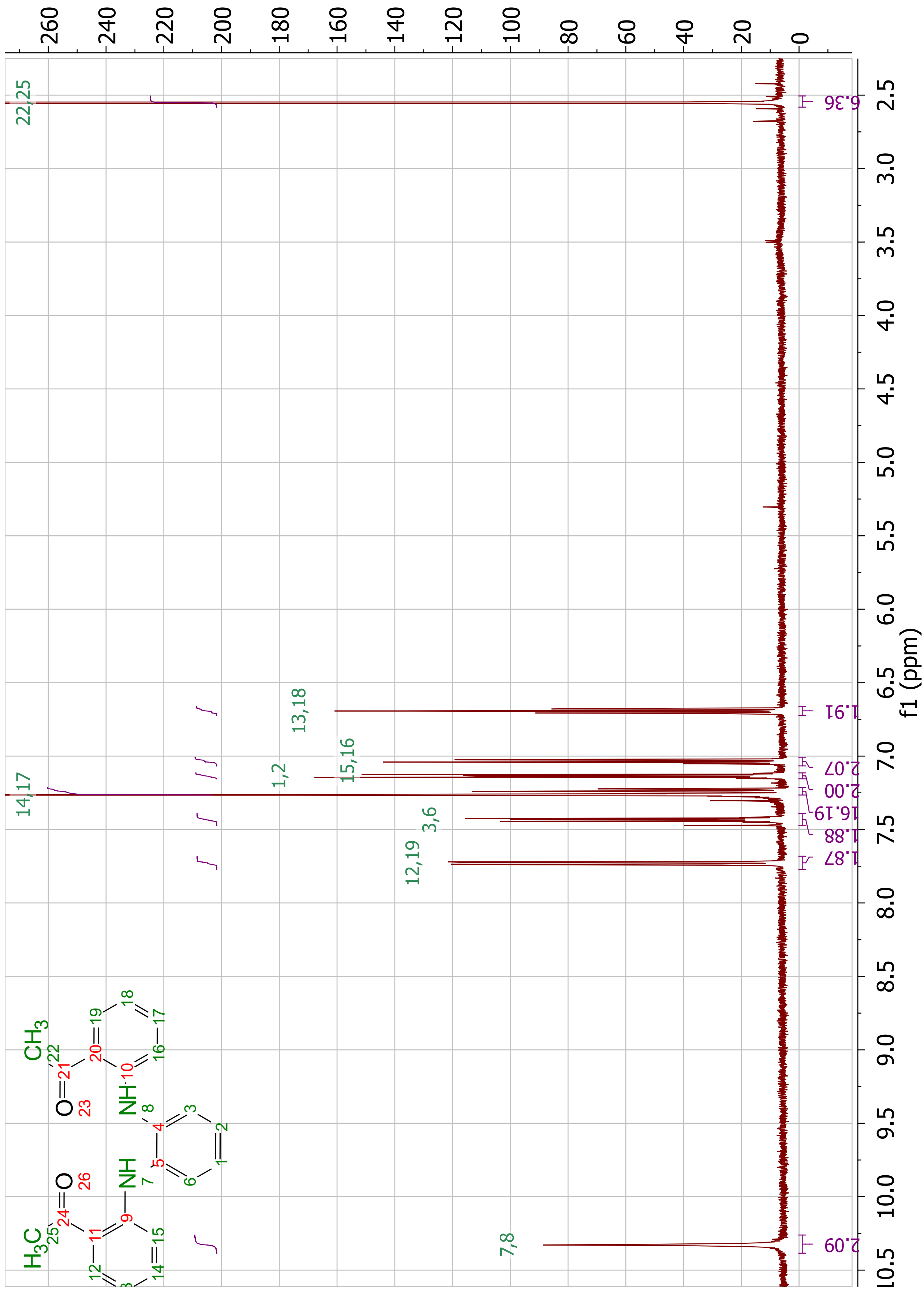
H3C
25
24
O
26
11
12
14
15
9
NH
7
5
4
6
1
2
3
NH
8
10
O
23
21
22
CH3
20
19
18
16
17
22,25
14,17
1,2
15,16
13,18
3,6
12,19
7,8
6.36
1.91
2.07
2.00
16.19
1.88
1.87
2.09
f1 (ppm)
2.5
3.0
3.5
4.0
4.5
5.0
5.5
6.0
6.5
7.0
7.5
8.0
8.5
9.0
9.5
10.0
10.5
260
240
220
200
180
160
140
120
100
80
60
40
20
0

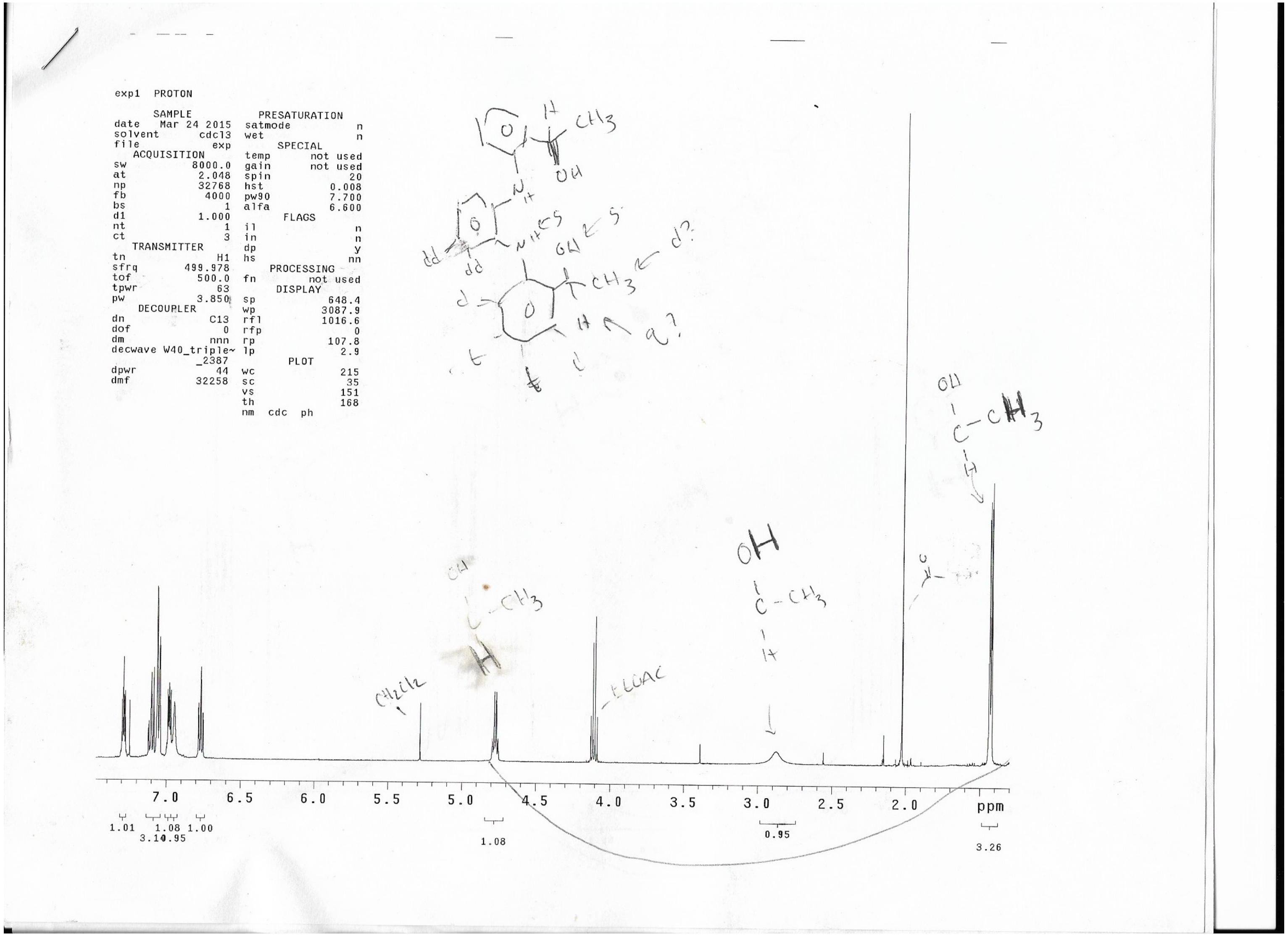

```
exp1  PROTON

      SAMPLE               PRESATURATION
date   Mar 24 2015   satmode            n
solvent       cdcl3   wet                n
file            exp        SPECIAL
   ACQUISITION        temp        not used
sw           8000.0   gain        not used
at            2.048   spin              20
np            32768   hst            0.008
fb             4000   pw90           7.700
bs                1   alfa           6.600
d1            1.000          FLAGS
nt                1   il                 n
ct                3   in                 n
   TRANSMITTER        dp                 y
tn               H1   hs                nn
sfrq        499.978       PROCESSING
tof           500.0   fn          not used
tpwr             63         DISPLAY
pw            3.850   sp             648.4
    DECOUPLER         wp            3087.9
dn              C13   rfl           1016.6
dof               0   rfp                0
dm              nnn   rp             107.8
decwave W40_triple~   lp               2.9
              _2387          PLOT
dpwr             44   wc               215
dmf           32258   sc                35
                      vs               151
                      th               168
                      nm   cdc   ph
```

7.0
6.5
6.0
5.5
5.0
4.5
4.0
3.5
3.0
2.5
2.0
ppm
1.01
1.08
1.00
3.10
0.95
1.08
0.95
3.26
H
CH3
OH
N
H
dd
dd
NHCS
OH
s
CH3
d?
d
H
q?
t
t
CH2Cl2
OH
C
CH3
H
EtOAc
OH
C
CH3
H
OH
C
CH3
H

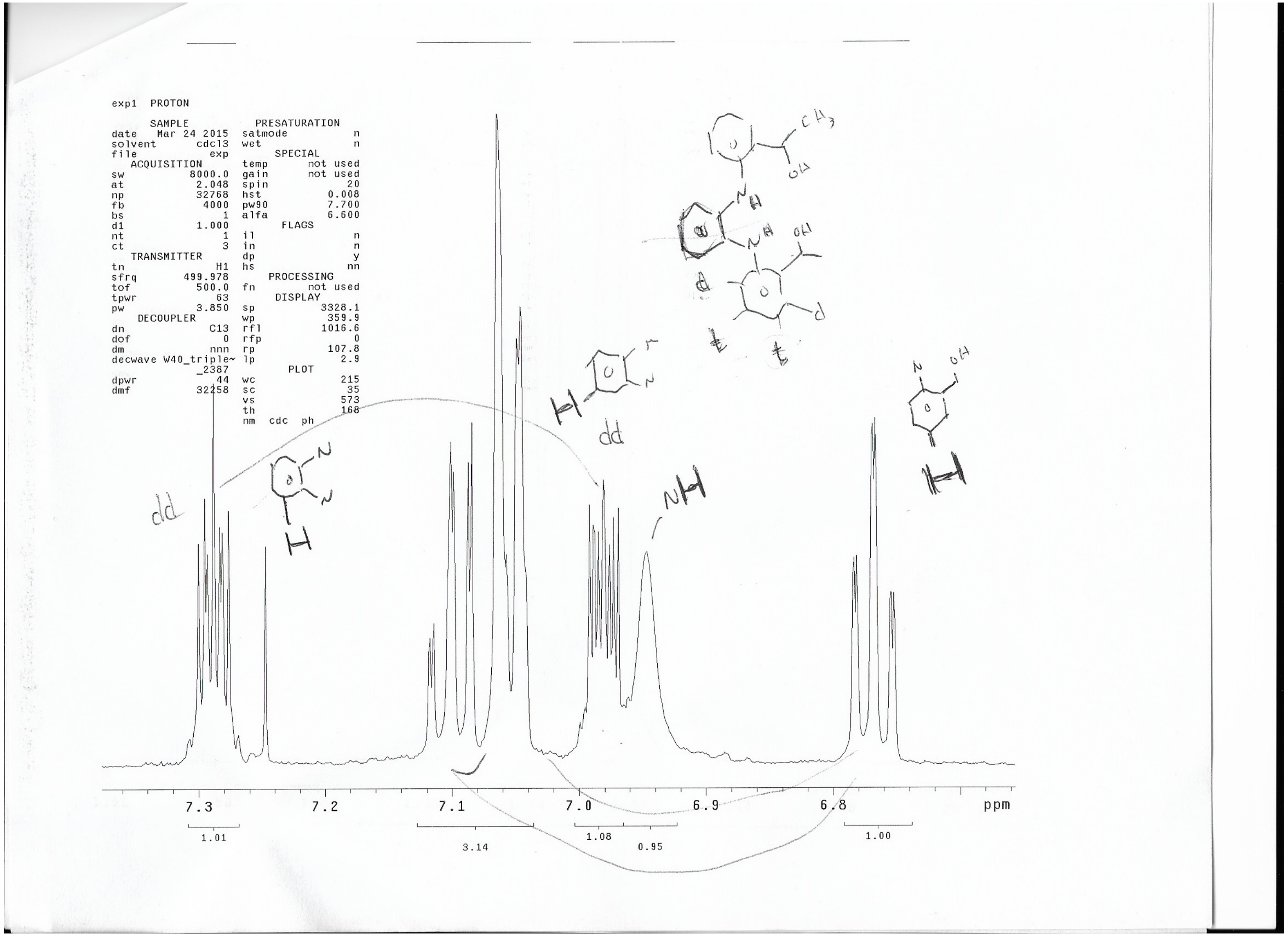

```
exp1  PROTON

     SAMPLE            PRESATURATION
date   Mar 24 2015   satmode          n
solvent      cdcl3   wet              n
file           exp         SPECIAL
   ACQUISITION       temp      not used
sw          8000.0   gain      not used
at           2.048   spin            20
np           32768   hst          0.008
fb            4000   pw90         7.700
bs               1   alfa         6.600
d1           1.000          FLAGS
nt               1   il               n
ct               3   in               n
   TRANSMITTER       dp               y
tn              H1   hs              nn
sfrq       499.978        PROCESSING
tof          500.0   fn        not used
tpwr            63         DISPLAY
pw           3.850   sp          3328.1
    DECOUPLER        wp           359.9
dn             C13   rfl         1016.6
dof              0   rfp              0
dm             nnn   rp           107.8
decwave W40_triple~  lp             2.9
             _2387           PLOT
dpwr            44   wc             215
dmf          32258   sc              35
                     vs             573
                     th             168
                     nm   cdc   ph
```

7.3
7.2
7.1
7.0
6.9
6.8
ppm
1.01
3.14
1.08
0.95
1.00
dd
H
dd
H
NH
H
CH3
OH
NH
NH
OH
d
t
t
d
OH

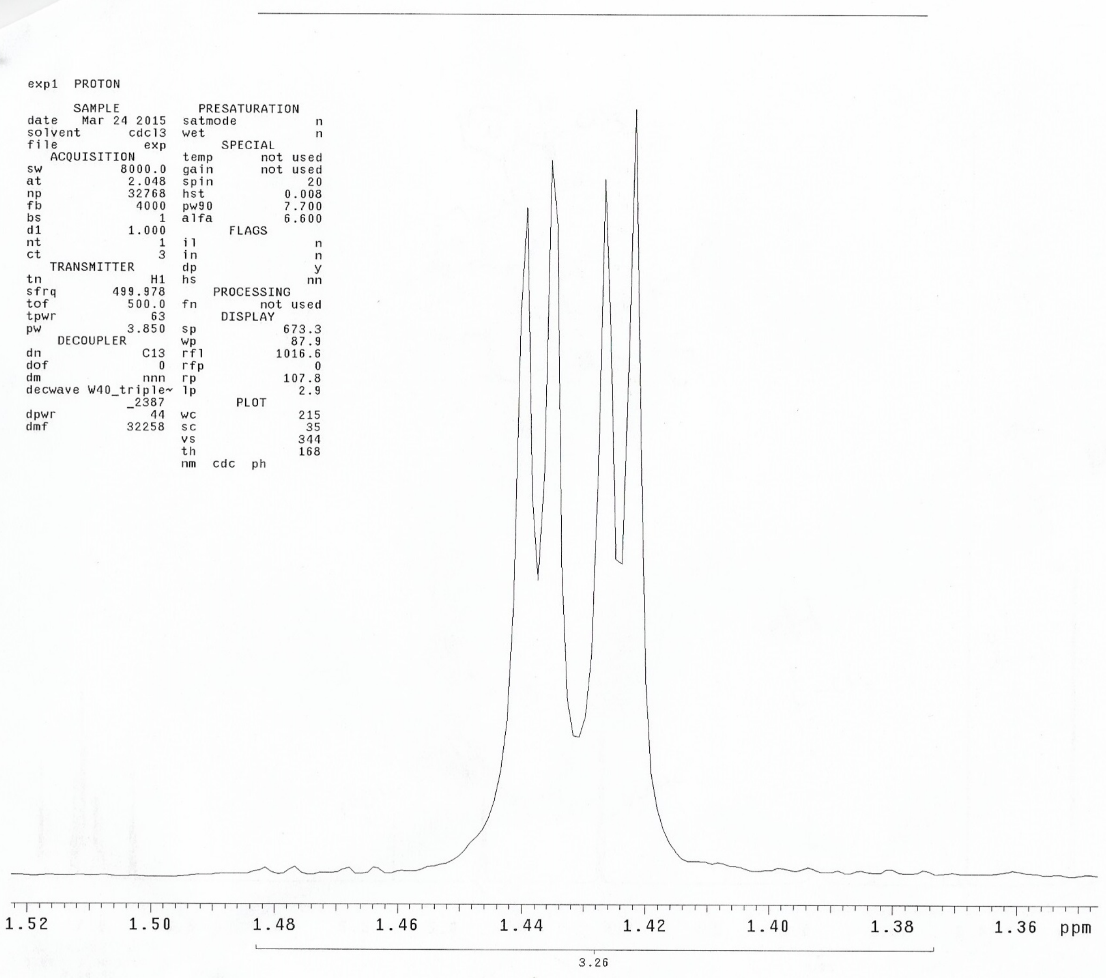

```
exp1  PROTON

      SAMPLE              PRESATURATION
date   Mar 24 2015   satmode            n
solvent      cdcl3   wet                n
file           exp        SPECIAL
   ACQUISITION       temp        not used
sw          8000.0   gain        not used
at           2.048   spin              20
np           32768   hst            0.008
fb            4000   pw90           7.700
bs               1   alfa           6.600
d1           1.000         FLAGS
nt               1   il                 n
ct               3   in                 n
   TRANSMITTER       dp                 y
tn              H1   hs                nn
sfrq       499.978       PROCESSING
tof          500.0   fn          not used
tpwr            63         DISPLAY
pw           3.850   sp             673.3
    DECOUPLER        wp              87.9
dn             C13   rfl           1016.6
dof              0   rfp                0
dm             nnn   rp             107.8
decwave W40_triple~  lp               2.9
             _2387           PLOT
dpwr            44   wc               215
dmf          32258   sc                35
                     vs               344
                     th               168
                     nm  cdc  ph
```

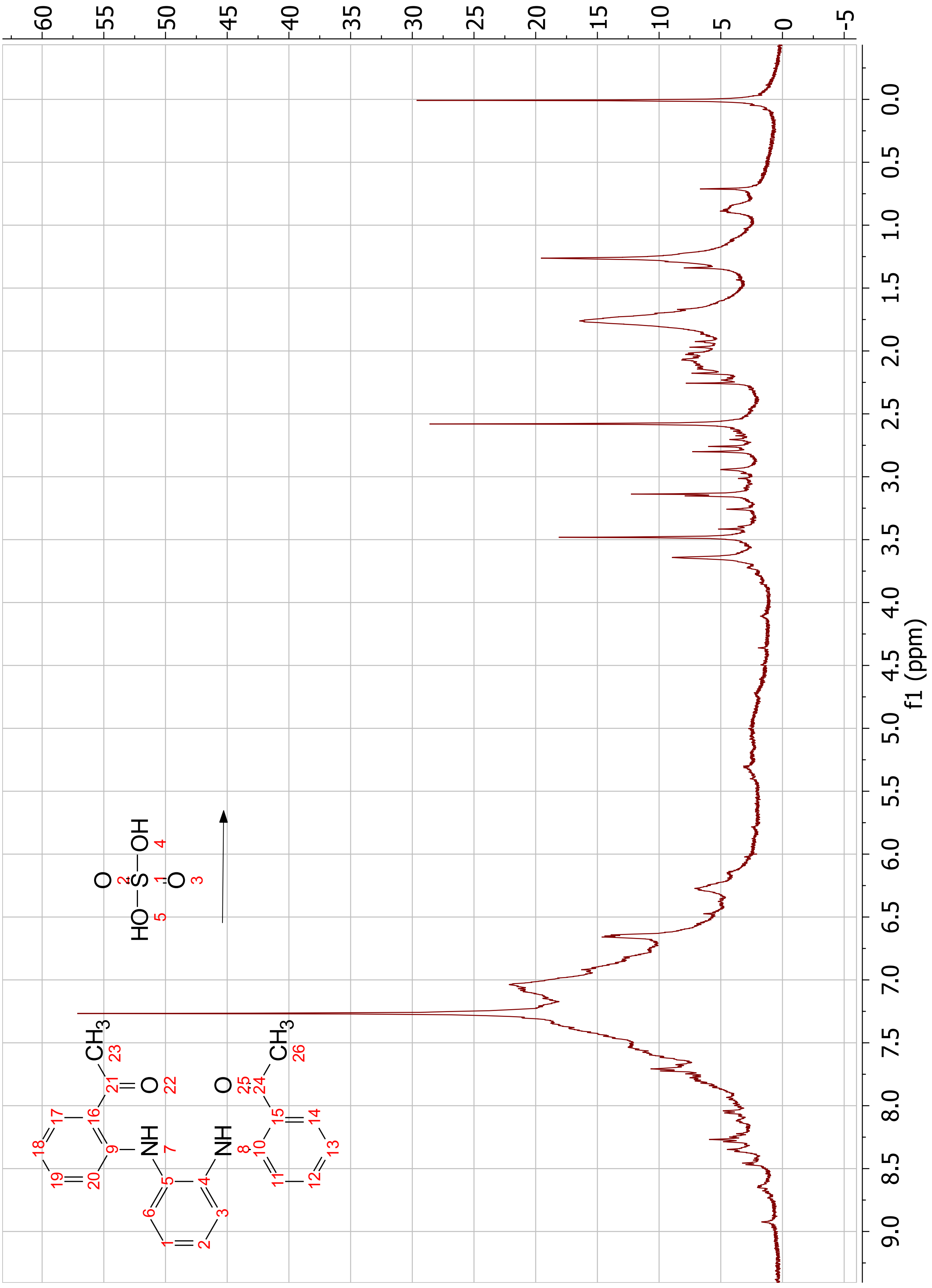

f1 (ppm)
9.0
8.5
8.0
7.5
7.0
6.5
6.0
5.5
5.0
4.5
4.0
3.5
3.0
2.5
2.0
1.5
1.0
0.5
0.0
60
55
50
45
40
35
30
25
20
15
10
5
0
-5
NH
NH
O
O
CH3
CH3
HO
S
OH
O
O

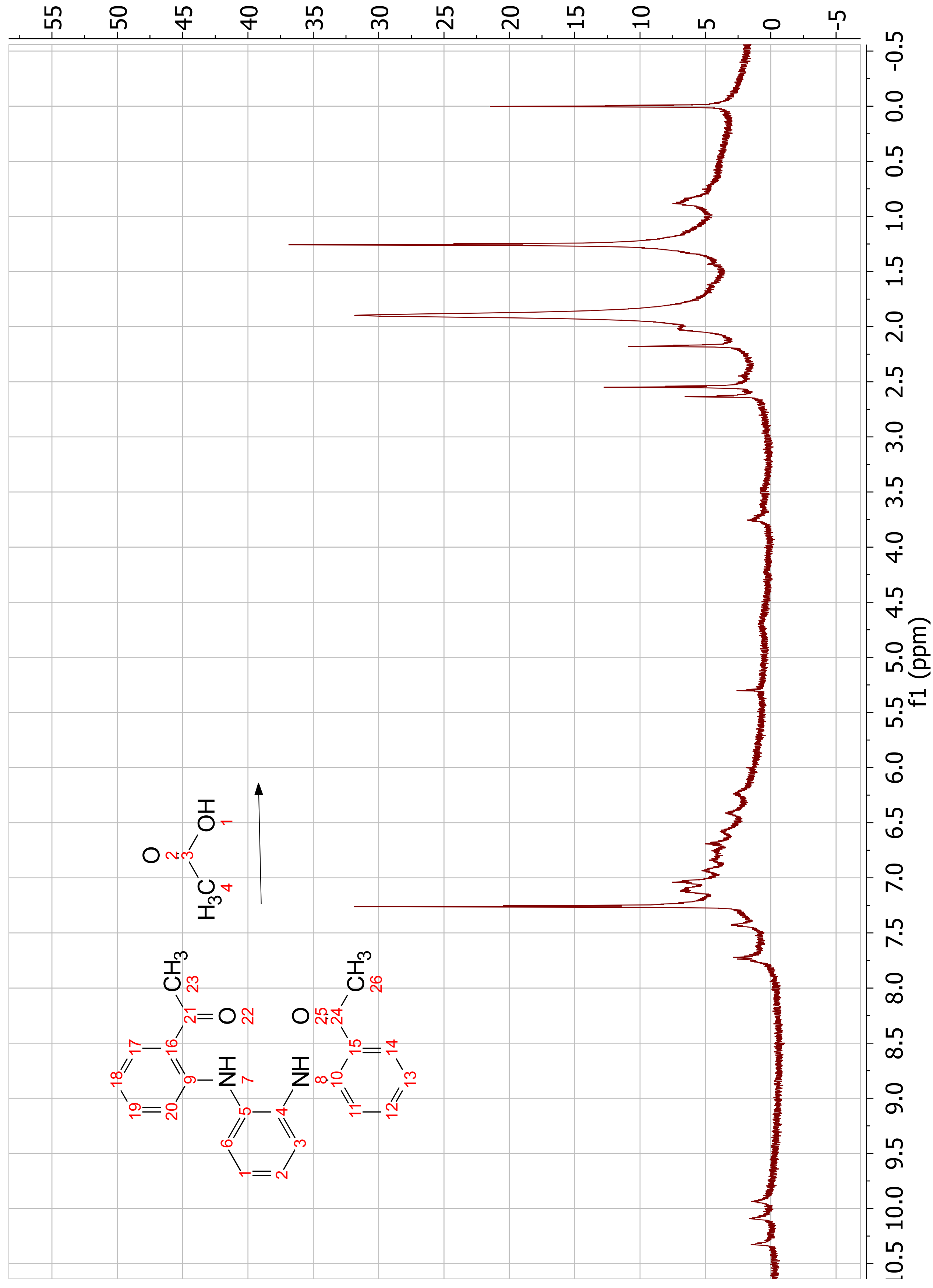
O
H3C
OH
1
2
3
4
NH
NH
O
O
CH3
CH3
1
2
3
4
5
6
7
8
9
10
11
12
13
14
15
16
17
18
19
20
21
22
23
24
25
26
f1 (ppm)
10.5
10.0
9.5
9.0
8.5
8.0
7.5
7.0
6.5
6.0
5.5
5.0
4.5
4.0
3.5
3.0
2.5
2.0
1.5
1.0
0.5
0.0
-0.5
55
50
45
40
35
30
25
20
15
10
5
0
-5

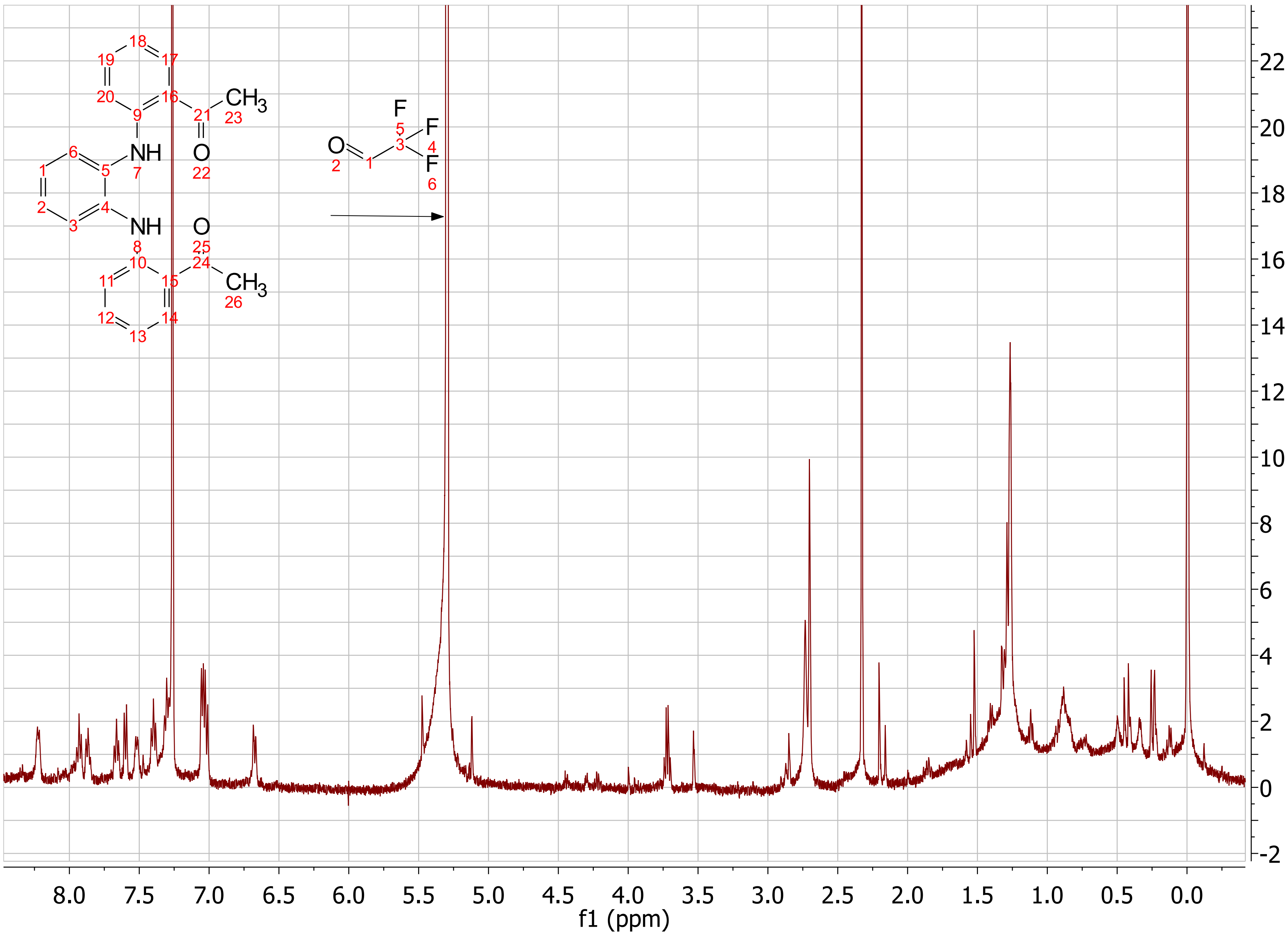
CH3
23
21
O
22
NH
7
NH
8
O
25
24
CH3
26
1
2
3
4
5
6
9
10
11
12
13
14
15
16
17
18
19
20
O
2
1
3
5
F
F
4
F
6
22
20
18
16
14
12
10
8
6
4
2
0
-2
8.0
7.5
7.0
6.5
6.0
5.5
5.0
4.5
4.0
3.5
3.0
2.5
2.0
1.5
1.0
0.5
0.0
f1 (ppm)

```
exp1  PROTON

     SAMPLE            PRESATURATION
date   Jan 21 2015  satmode          n
solvent        cdcl3  wet              n
file /home/nmj37/v~       SPECIAL
nmrsys/data/Noah/D~ temp      not used
ye/Complexation/Te~ gain      not used
mp2_RuBidMe_rc-012~ spin            20
           115.fid  hst          0.008
   ACQUISITION      pw90         6.900
sw          7977.7  alfa         6.600
at           2.054        FLAGS
np           32768  il               n
fb            4000  in               n
bs               1  dp               y
d1           1.000  hs              nn
nt              32       PROCESSING
ct              32  fn        not used
   TRANSMITTER            DISPLAY
tn              H1  sp          3374.3
sfrq       499.978  wp          1380.4
tof          498.6  rfl         1000.1
tpwr            60  rfp              0
pw           3.450  rp            98.1
    DECOUPLER       lp            18.0
dn             C13          PLOT
dof              0  wc             250
dm             nnn  sc               0
decwave W40_triple~ vs             864
             _2387  th             168
dpwr            44  ai  cdc  ph
dmf          32258
```

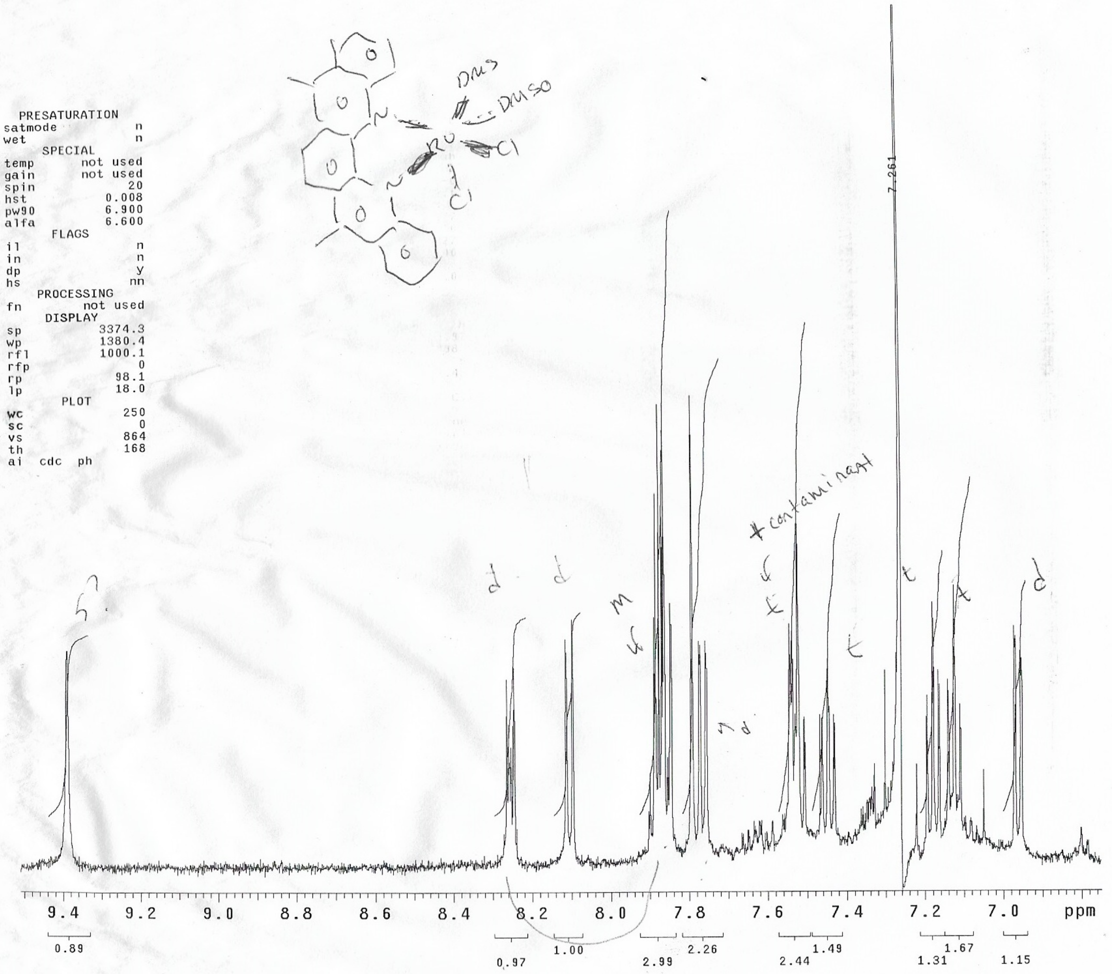

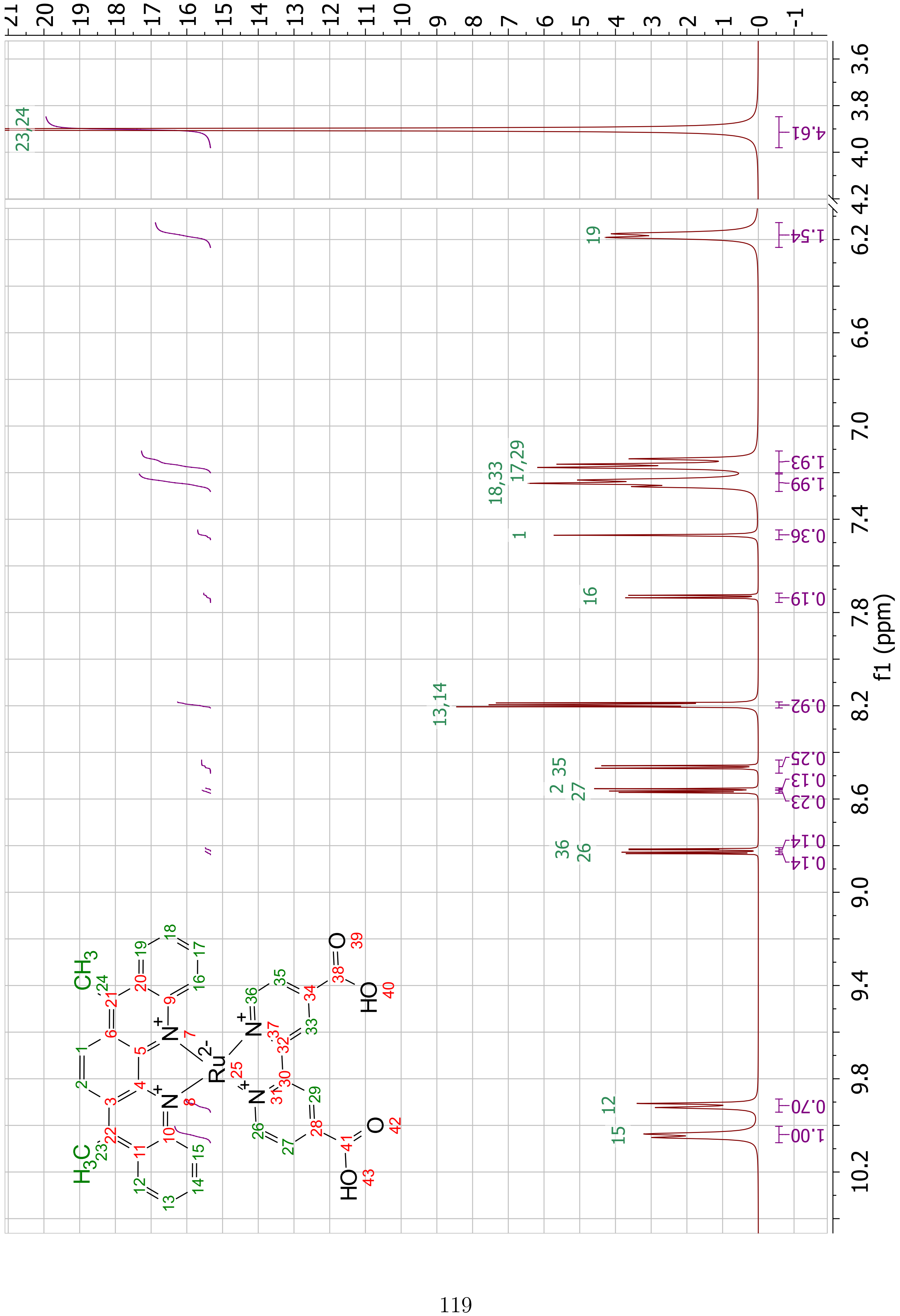

23,24
19
17,29
18,33
1
16
13,14
2 35
27
36
26
12
15
4.61
1.54
1.93
1.99
0.36
0.19
0.92
0.25
0.13
0.23
0.14
0.14
0.70
1.00
f1 (ppm)
3.6
3.8
4.0
4.2
6.2
6.6
7.0
7.4
7.8
8.2
8.6
9.0
9.4
9.8
10.2
-1
0
1
2
3
4
5
6
7
8
9
10
11
12
13
14
15
16
17
18
19
20
21
H3C
CH3
Ru
2-
N+
HO
O

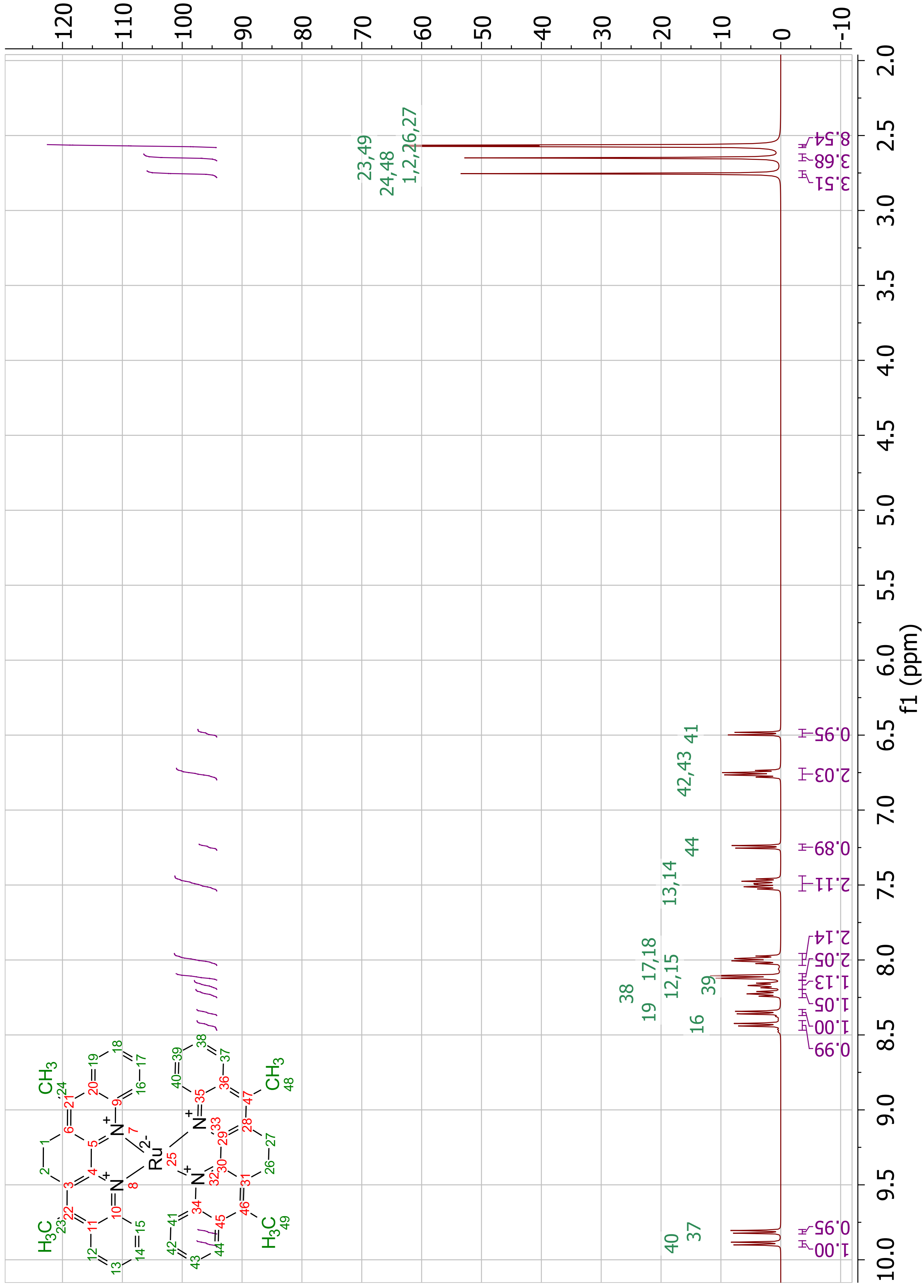
f1 (ppm)
2.0
2.5
3.0
3.5
4.0
4.5
5.0
5.5
6.0
6.5
7.0
7.5
8.0
8.5
9.0
9.5
10.0
120
110
100
90
80
70
60
50
40
30
20
10
0
-10
23,49
24,48
1,2,26,27
41
42,43
44
13,14
38
19
17,18
12,15
39
16
40
37
8.54
3.68
3.51
0.95
2.03
0.89
2.11
2.14
2.05
1.13
1.05
1.00
0.99
0.95
1.00
H_3C
CH_3
Ru
2-

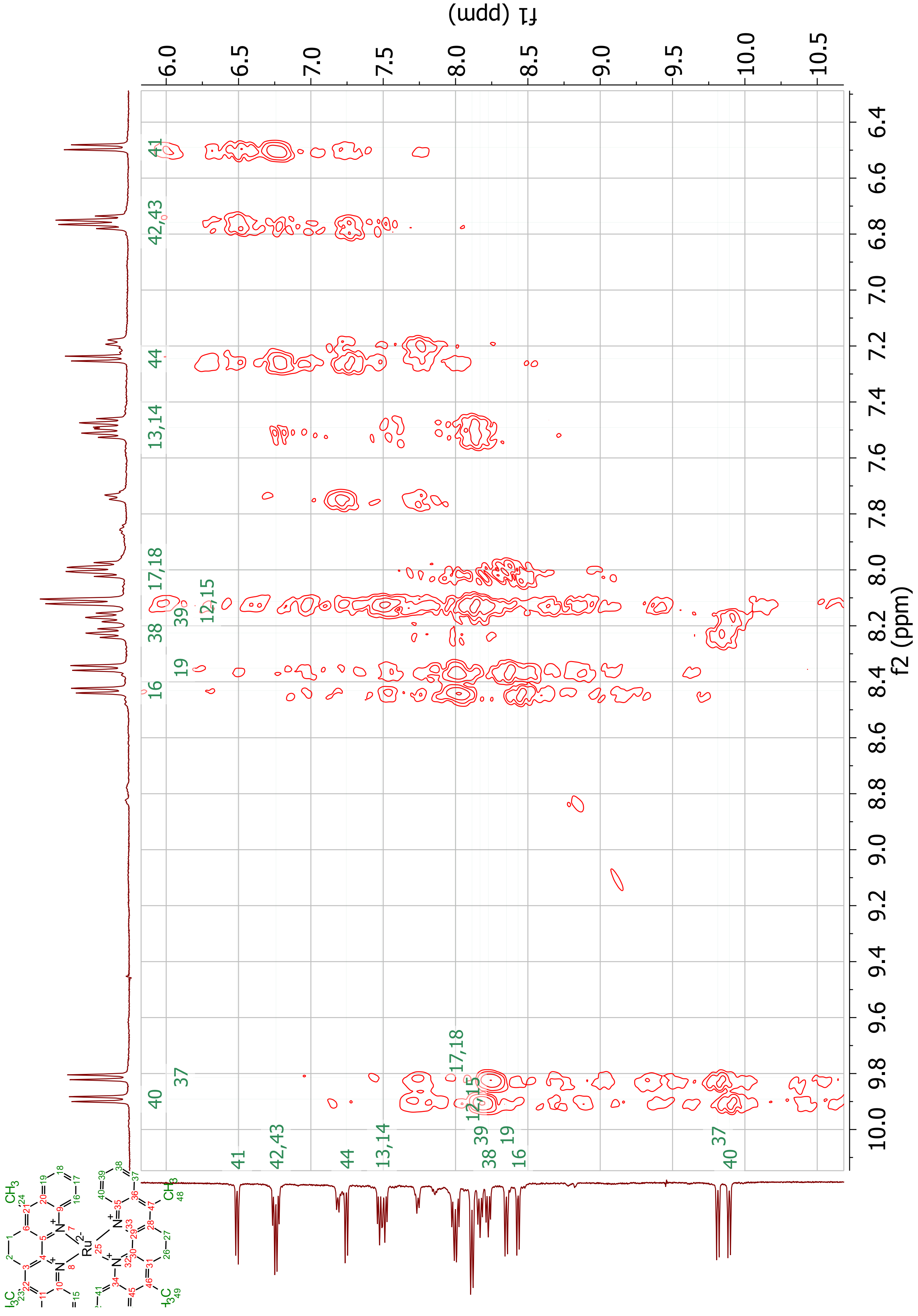
f1 (ppm)
6.0
6.5
7.0
7.5
8.0
8.5
9.0
9.5
10.0
10.5
f2 (ppm)
6.4
6.6
6.8
7.0
7.2
7.4
7.6
7.8
8.0
8.2
8.4
8.6
8.8
9.0
9.2
9.4
9.6
9.8
10.0
41
42,43
44
13,14
17,18
39
12,15
38
19
16
37
40
17,18
12,15
39
38
19
16
37
40
41
42,43
44
13,14
CH3
H3C
Ru2-
N+
CH3
H3C

MS

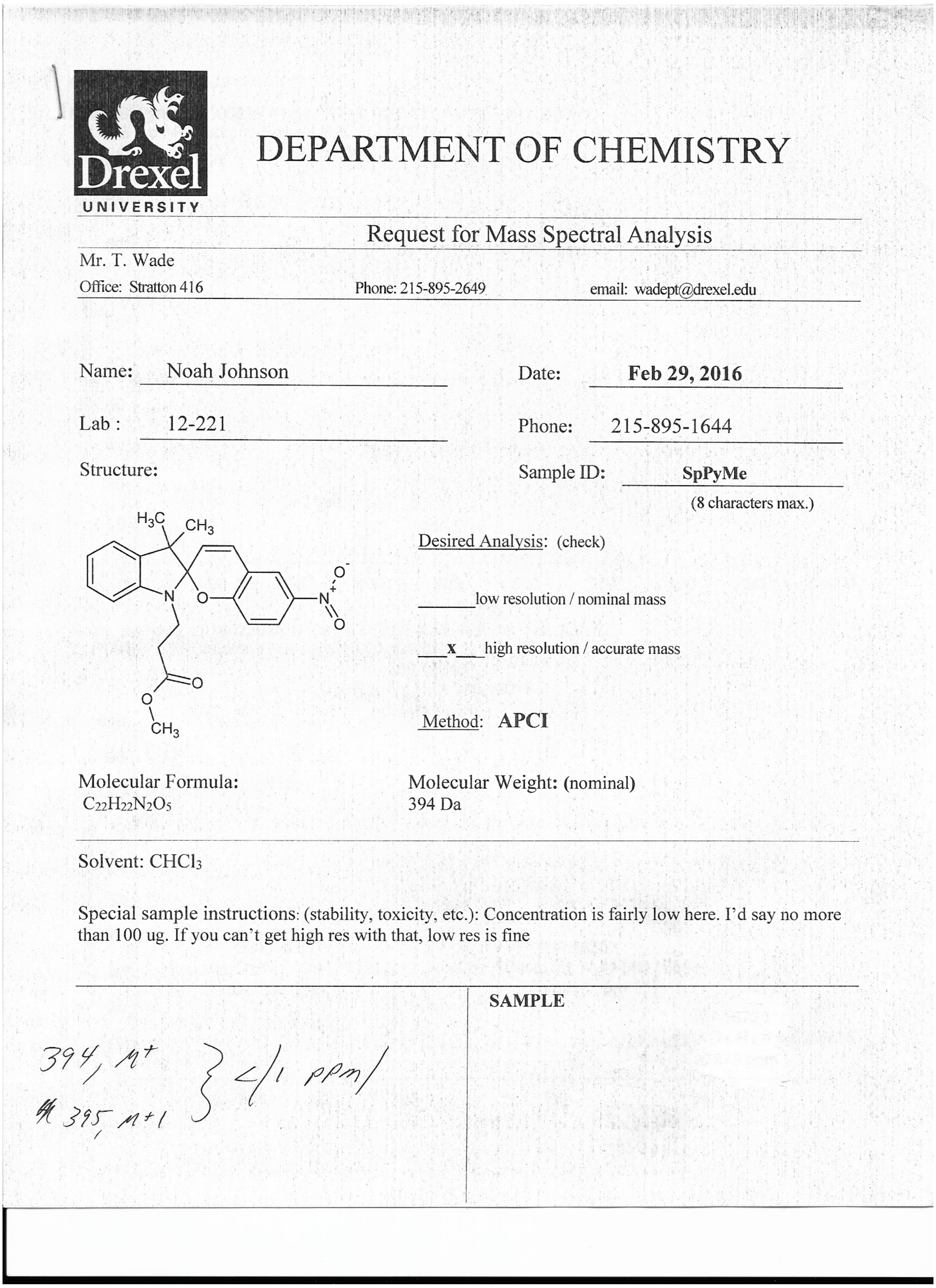

Drexel UNIVERSITY

DEPARTMENT OF CHEMISTRY

Request for Mass Spectral Analysis

Mr. T. Wade
Office: Stratton 416 Phone: 215-895-2649 email: wadept@drexel.edu

Name: Noah Johnson

Date: **Feb 29, 2016**

Lab : 12-221

Phone: 215-895-1644

Structure:

H_3C
CH_3
N
O
N^+
O^-
O
O
O
CH_3

Sample ID: **SpPyMe**
(8 characters max.)

Desired Analysis: (check)

______low resolution / nominal mass

__**x**__high resolution / accurate mass

Method: **APCI**

Molecular Formula:
$C_{22}H_{22}N_2O_5$

Molecular Weight: **(nominal)**
394 Da

Solvent: $CHCl_3$

Special sample instructions: (stability, toxicity, etc.): Concentration is fairly low here. I'd say no more than 100 ug. If you can't get high res with that, low res is fine

SAMPLE

394, M+
~~M~~ 395, M+1
} <1 ppm

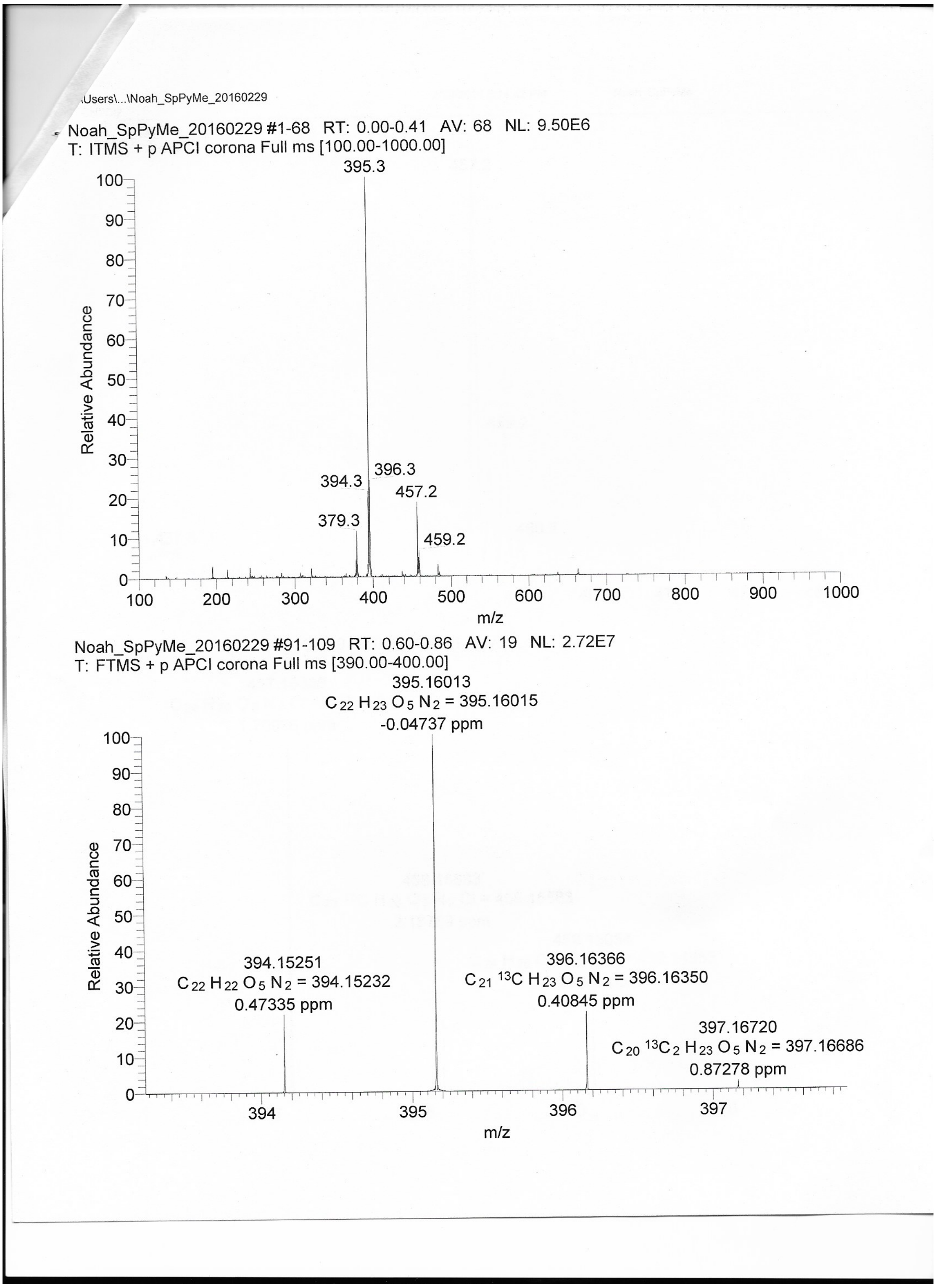

\Users\...\Noah_SpPyMe_20160229

Noah_SpPyMe_20160229 #1-68 RT: 0.00-0.41 AV: 68 NL: 9.50E6
T: ITMS + p APCI corona Full ms [100.00-1000.00]

Noah_SpPyMe_20160229 #91-109 RT: 0.60-0.86 AV: 19 NL: 2.72E7
T: FTMS + p APCI corona Full ms [390.00-400.00]

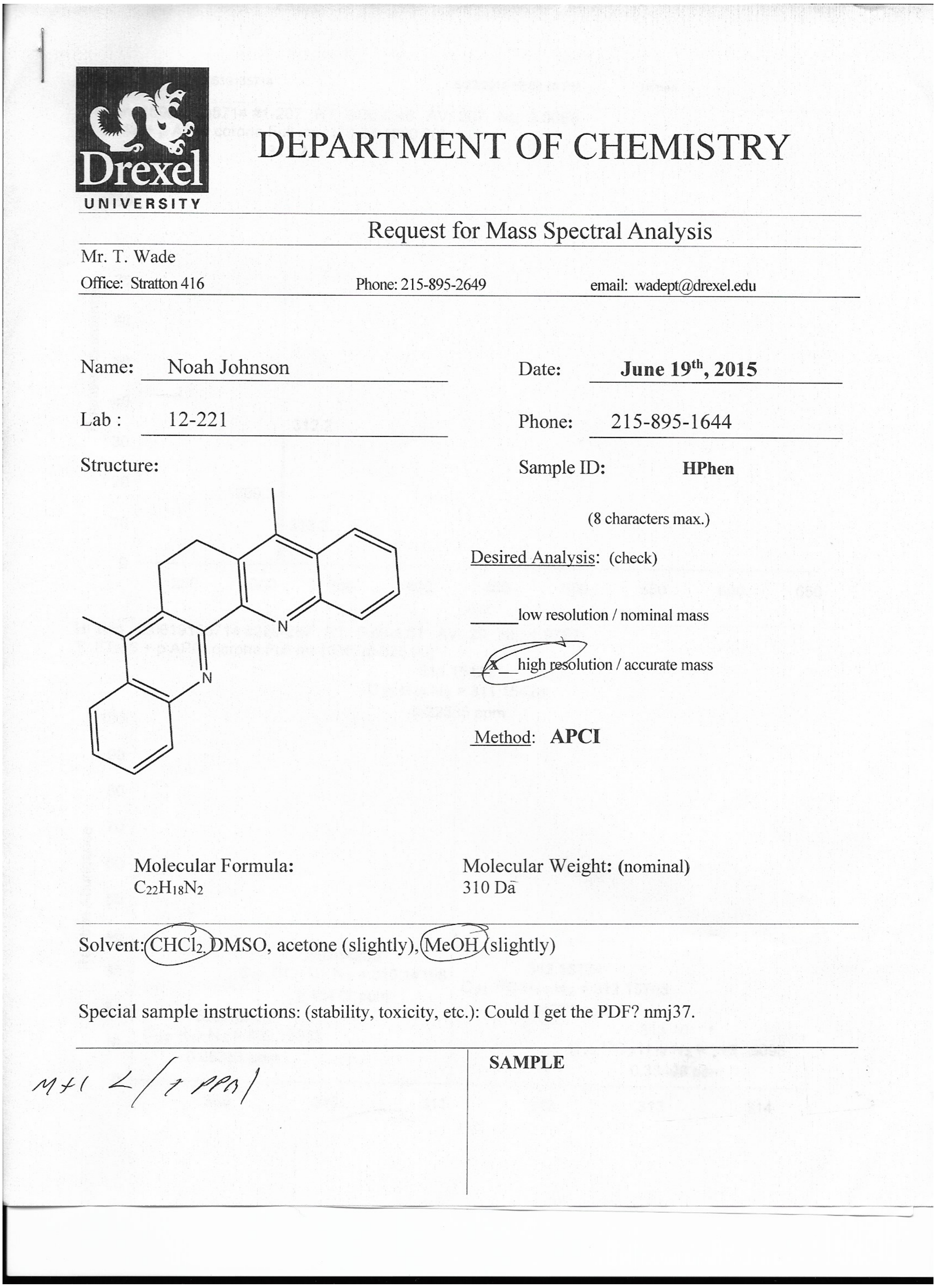

Drexel UNIVERSITY

DEPARTMENT OF CHEMISTRY

Request for Mass Spectral Analysis

Mr. T. Wade
Office: Stratton 416 Phone: 215-895-2649 email: wadept@drexel.edu

Name: Noah Johnson
Date: **June 19th, 2015**
Lab : 12-221
Phone: 215-895-1644
Structure:
Sample ID: **HPhen**
(8 characters max.)

Desired Analysis: (check)

____ low resolution / nominal mass

[✓ _X_] high resolution / accurate mass

Method: **APCI**

Molecular Formula: $C_{22}H_{18}N_2$

Molecular Weight: (nominal) 310 Da

Solvent: [✓ $CHCl_2$], DMSO, acetone (slightly), [✓ MeOH] (slightly)

Special sample instructions: (stability, toxicity, etc.): Could I get the PDF? nmj37.

M+1 ∠ (1 ppm)

SAMPLE

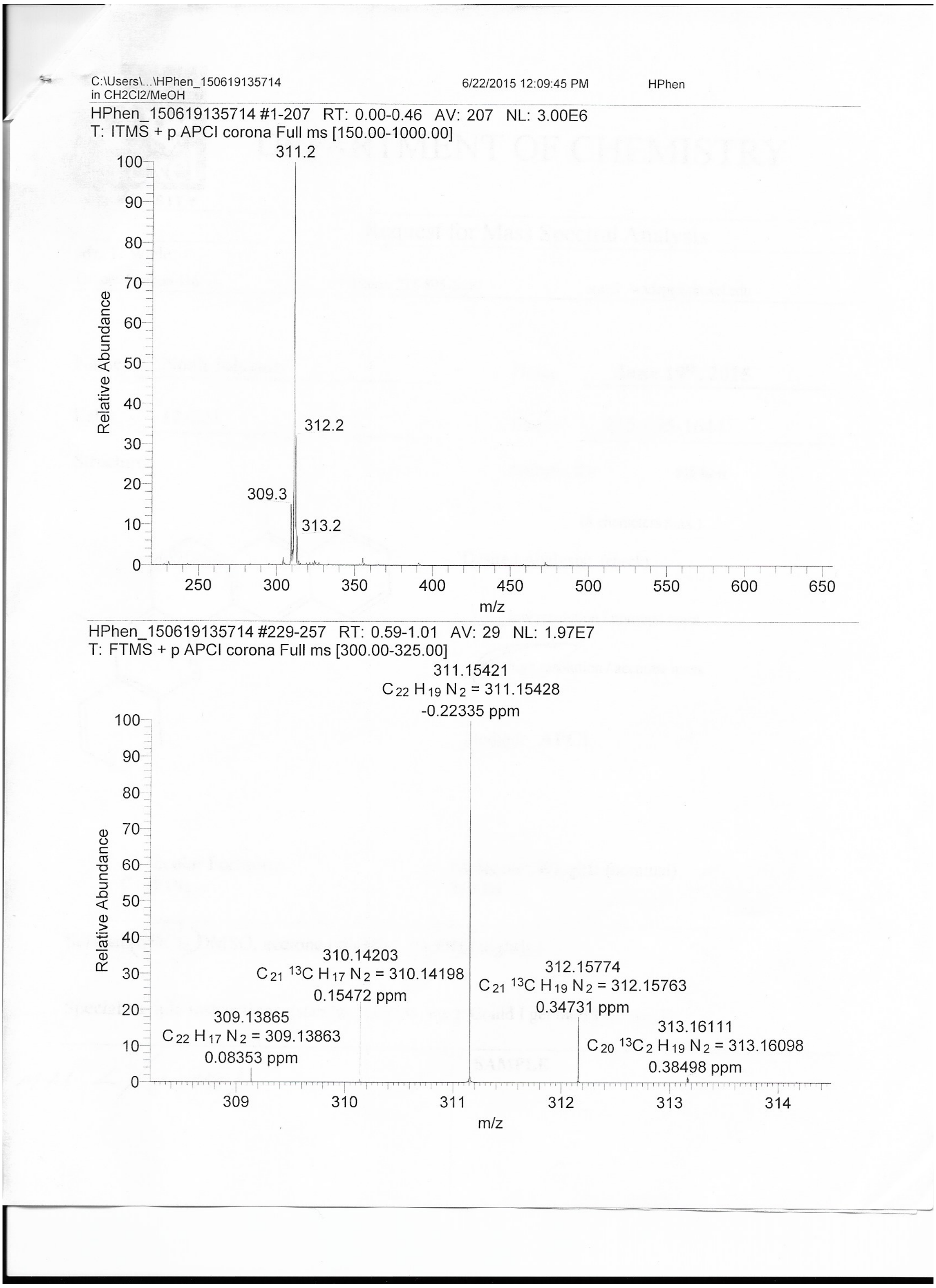

C:\Users\...\HPhen_150619135714 6/22/2015 12:09:45 PM HPhen
in CH2Cl2/MeOH

HPhen_150619135714 #1-207 RT: 0.00-0.46 AV: 207 NL: 3.00E6
T: ITMS + p APCI corona Full ms [150.00-1000.00]

HPhen_150619135714 #229-257 RT: 0.59-1.01 AV: 29 NL: 1.97E7
T: FTMS + p APCI corona Full ms [300.00-325.00]

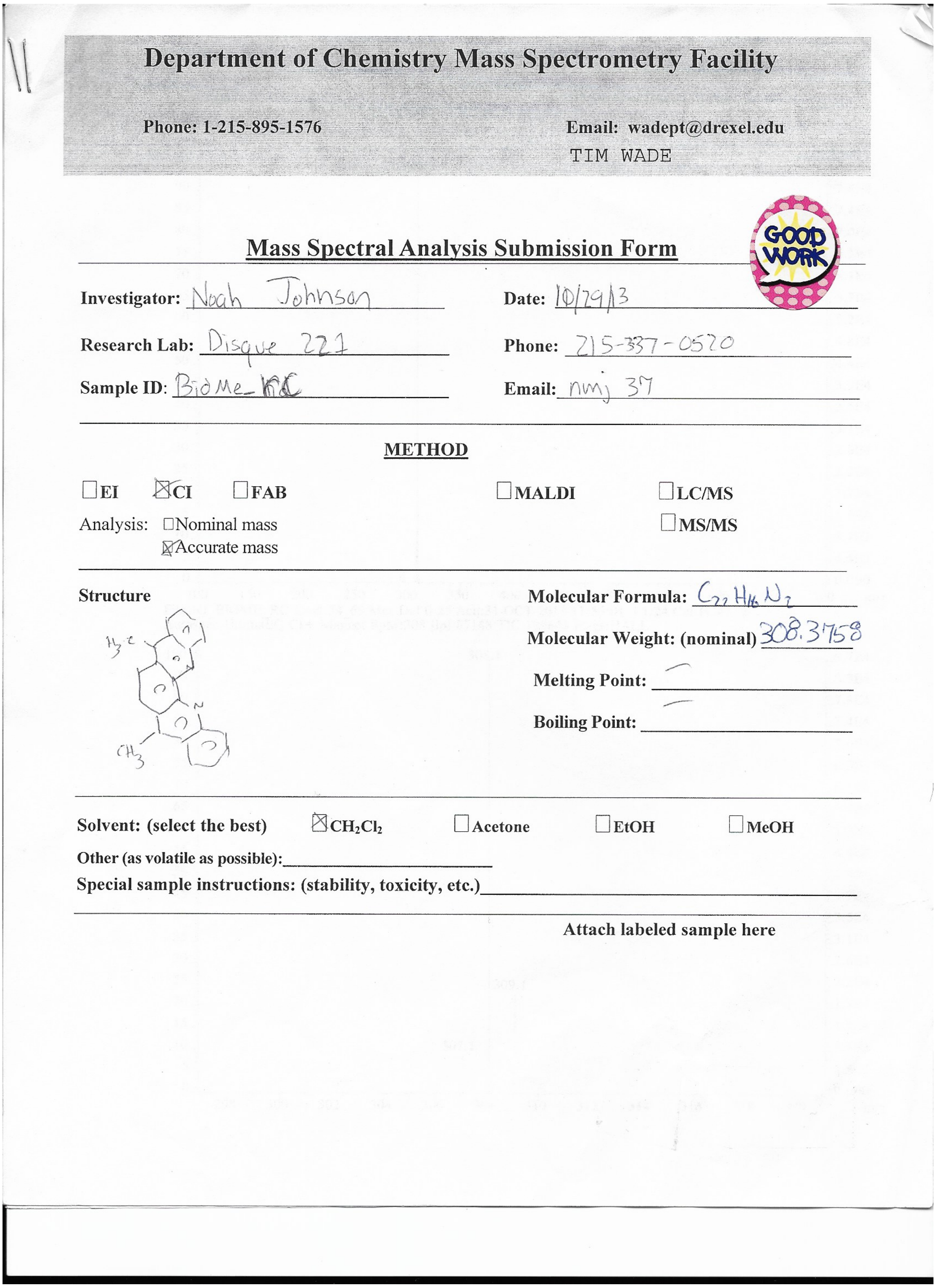

Department of Chemistry Mass Spectrometry Facility

Phone: 1-215-895-1576 **Email: wadept@drexel.edu**
TIM WADE

GOOD WORK

Mass Spectral Analysis Submission Form

Investigator: Noah Johnson
Date: 10/29/13
Research Lab: Disque 221
Phone: 215-337-0520
Sample ID: BiOMe_[illegible]
Email: nmj 37

METHOD

☐**EI** ☒**CI** ☐**FAB** ☐**MALDI** ☐**LC/MS**

Analysis: ☐Nominal mass ☐**MS/MS**
☒Accurate mass

Structure

Molecular Formula: $C_{22}H_{16}N_2$
Molecular Weight: (nominal) 308.3758
Melting Point: —
Boiling Point: —

Solvent: (select the best) ☒$\mathbf{CH_2Cl_2}$ ☐**Acetone** ☐**EtOH** ☐**MeOH**

Other (as volatile as possible):

Special sample instructions: (stability, toxicity, etc.)

Attach labeled sample here

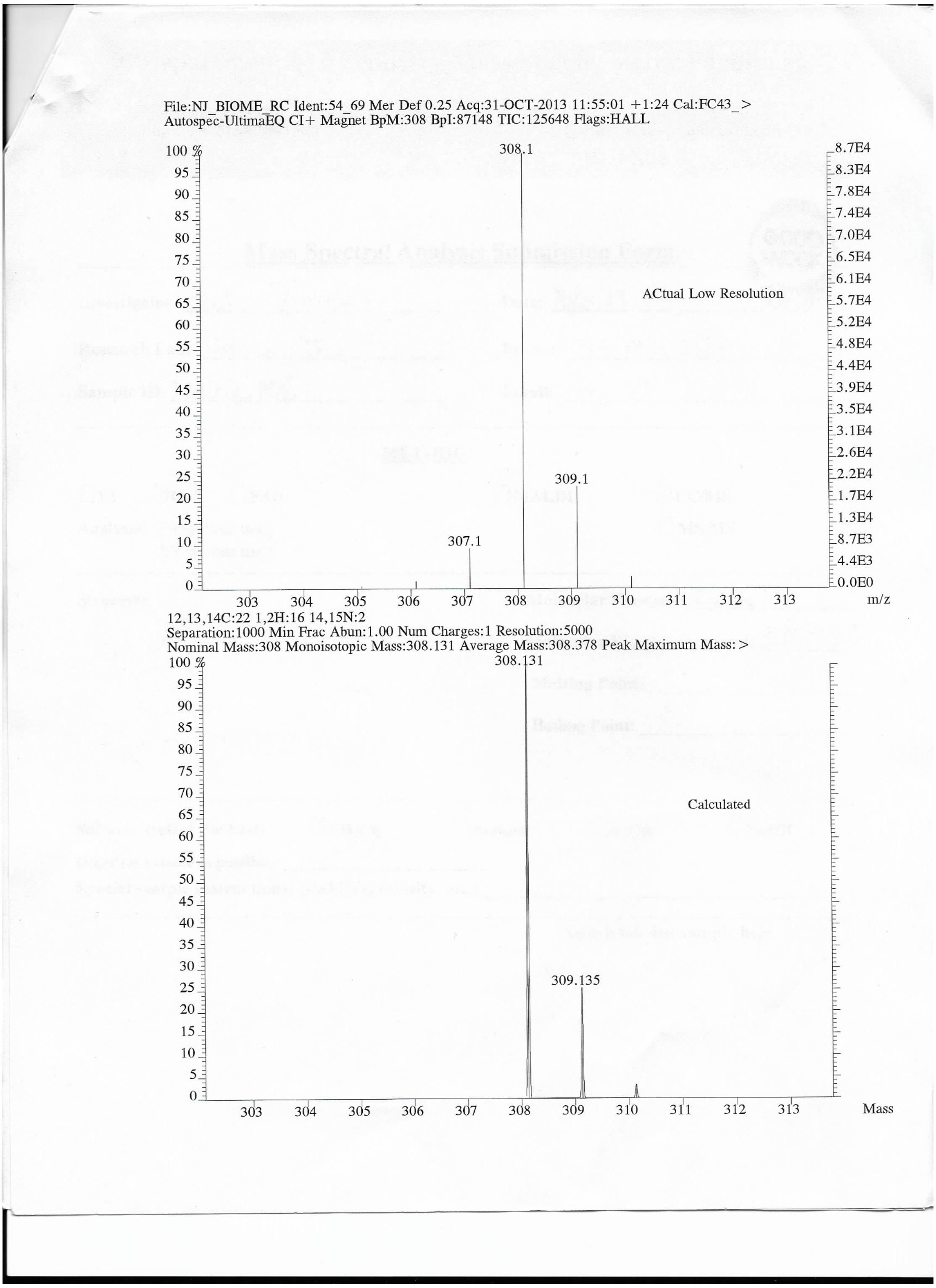

File:NJ_BIOME_RC Ident:54_69 Mer Def 0.25 Acq:31-OCT-2013 11:55:01 +1:24 Cal:FC43_>
Autospec-UltimaEQ CI+ Magnet BpM:308 BpI:87148 TIC:125648 Flags:HALL

12,13,14C:22 1,2H:16 14,15N:2
Separation:1000 Min Frac Abun:1.00 Num Charges:1 Resolution:5000
Nominal Mass:308 Monoisotopic Mass:308.131 Average Mass:308.378 Peak Maximum Mass: >

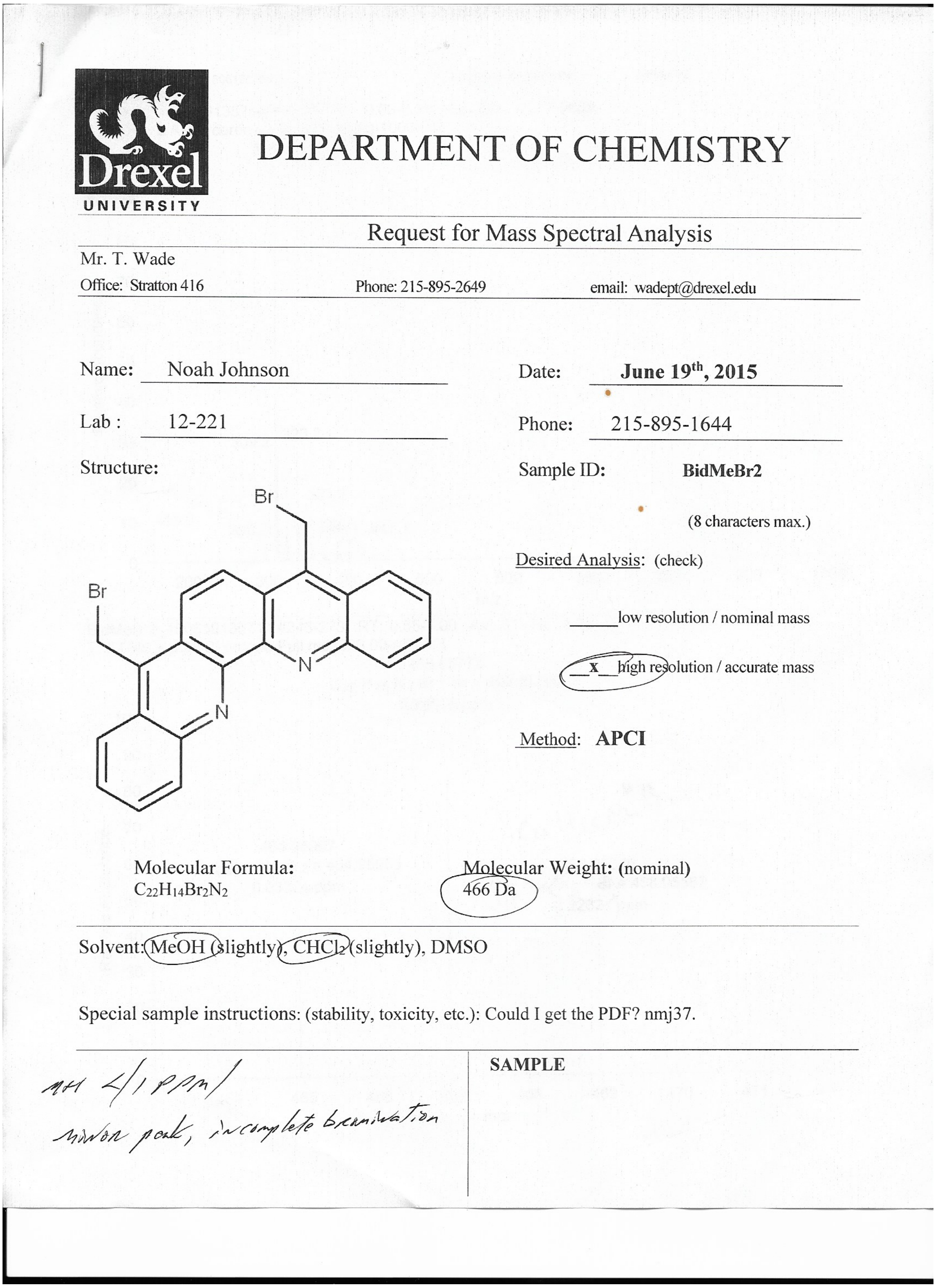

DEPARTMENT OF CHEMISTRY

Drexel UNIVERSITY

Request for Mass Spectral Analysis

Mr. T. Wade
Office: Stratton 416 Phone: 215-895-2649 email: wadept@drexel.edu

Name: Noah Johnson

Date: **June 19th, 2015**

Lab : 12-221

Phone: 215-895-1644

Structure:

Sample ID: **BidMeBr2**

(8 characters max.)

Desired Analysis: (check)

_____ low resolution / nominal mass

[✓ __x__ high resolution / accurate mass]

Method: **APCI**

Molecular Formula: $C_{22}H_{14}Br_2N_2$

Molecular Weight: (nominal) 466 Da

Solvent: [✓ MeOH] (slightly), [✓ $CHCl_3$] (slightly), DMSO

Special sample instructions: (stability, toxicity, etc.): Could I get the PDF? nmj37.

MH <1 ppm/
minor peak, incomplete bromination

SAMPLE

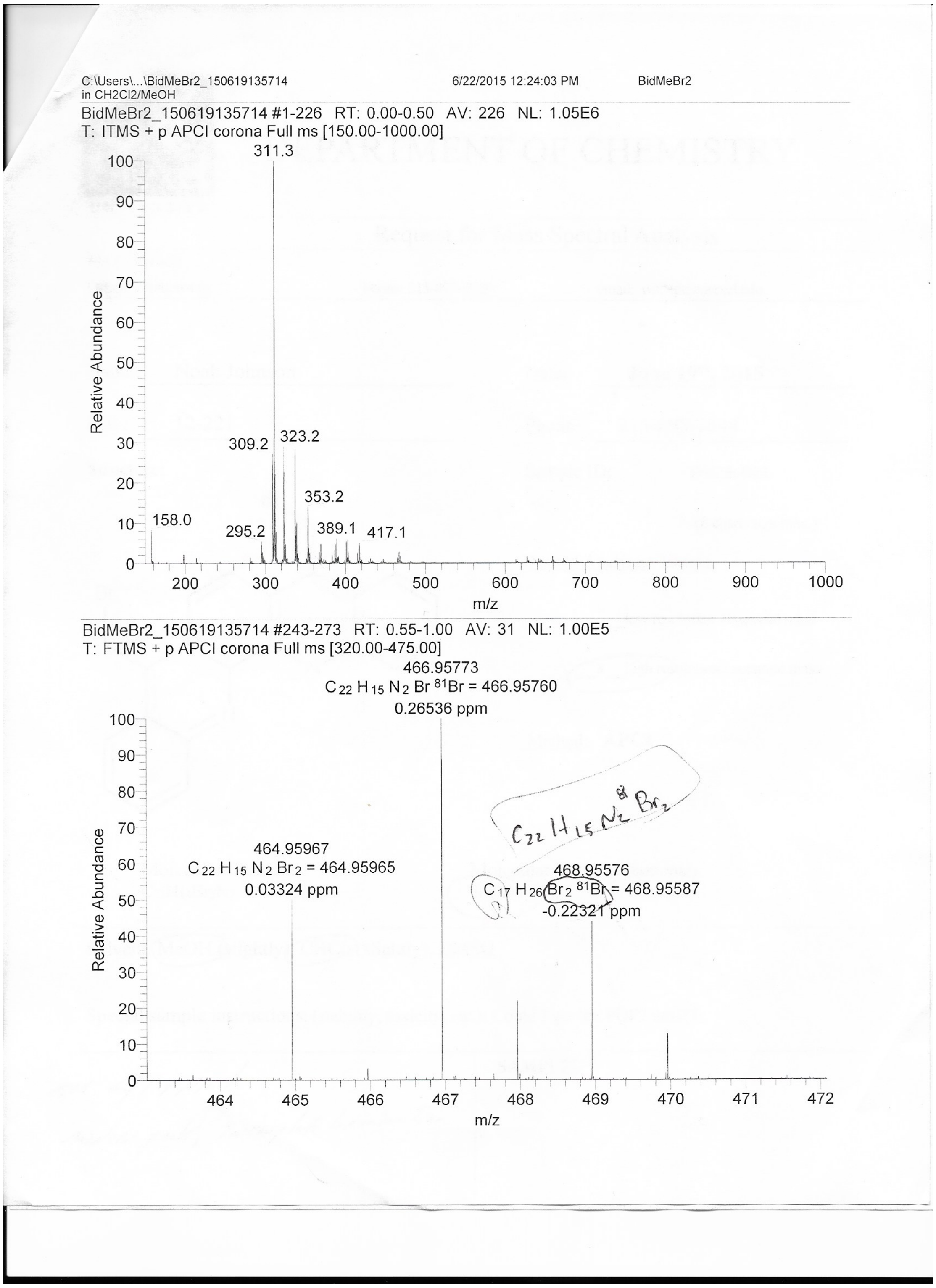

C:\Users\...\BidMeBr2_150619135714 6/22/2015 12:24:03 PM BidMeBr2
in CH2Cl2/MeOH

BidMeBr2_150619135714 #1-226 RT: 0.00-0.50 AV: 226 NL: 1.05E6
T: ITMS + p APCI corona Full ms [150.00-1000.00]

BidMeBr2_150619135714 #243-273 RT: 0.55-1.00 AV: 31 NL: 1.00E5
T: FTMS + p APCI corona Full ms [320.00-475.00]

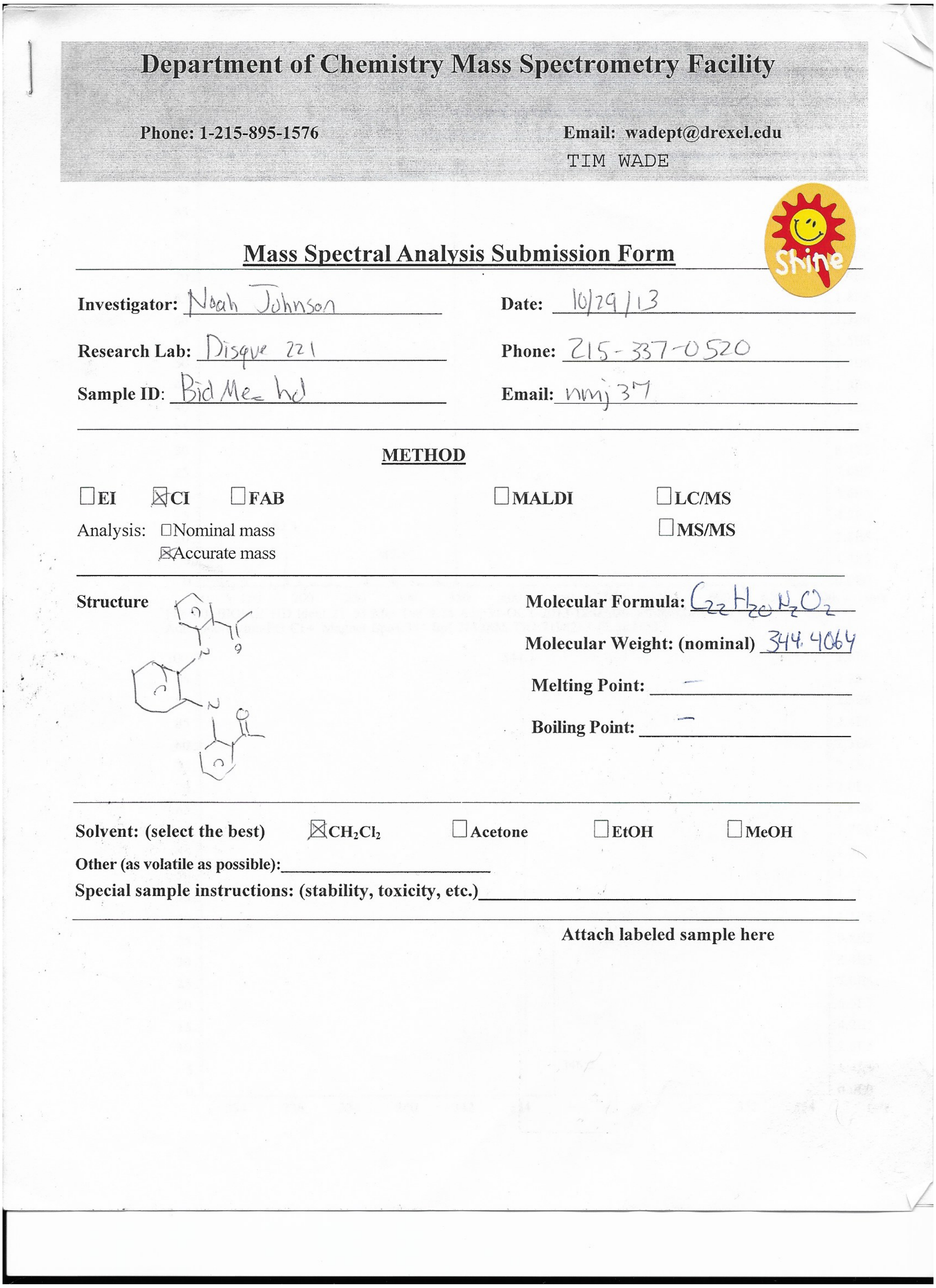

Department of Chemistry Mass Spectrometry Facility

Phone: 1-215-895-1576 **Email: wadept@drexel.edu**
TIM WADE

Mass Spectral Analysis Submission Form

Investigator: Noah Johnson
Date: 10/29/13
Research Lab: Disque 221
Phone: 215-337-0520
Sample ID: Bid Me= hd
Email: nmj37

METHOD

☐**EI** ☒**CI** ☐**FAB** ☐**MALDI** ☐**LC/MS**

Analysis: ☐Nominal mass ☒Accurate mass ☐**MS/MS**

Structure

Molecular Formula: $C_{22}H_{20}N_2O_2$
Molecular Weight: (nominal) 344.4064
Melting Point: –
Boiling Point: –

Solvent: (select the best) ☒CH_2Cl_2 ☐**Acetone** ☐**EtOH** ☐**MeOH**

Other (as volatile as possible):
Special sample instructions: (stability, toxicity, etc.)

Attach labeled sample here

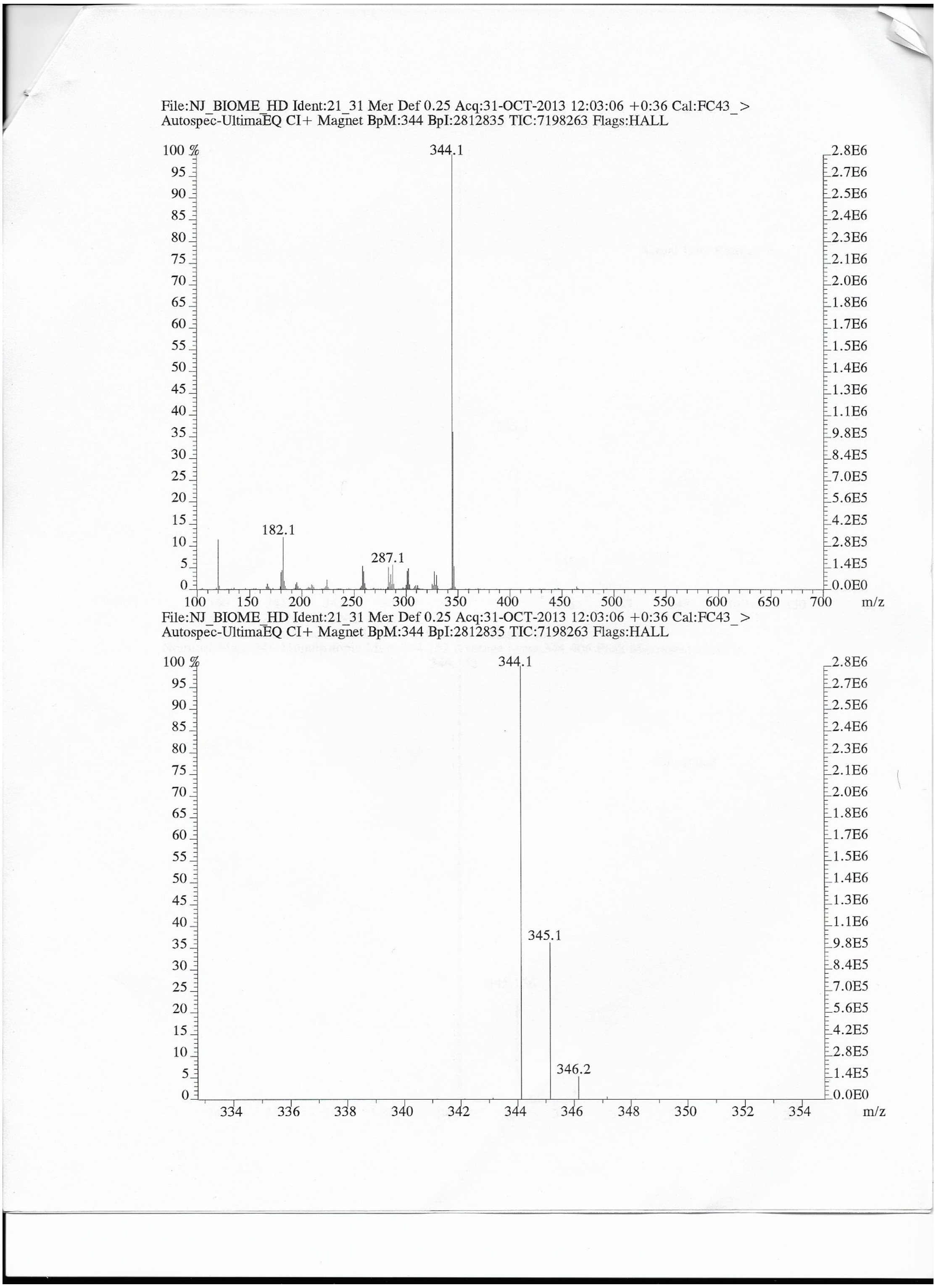

File:NJ_BIOME_HD Ident:21_31 Mer Def 0.25 Acq:31-OCT-2013 12:03:06 +0:36 Cal:FC43_>
Autospec-UltimaEQ CI+ Magnet BpM:344 BpI:2812835 TIC:7198263 Flags:HALL

File:NJ_BIOME_HD Ident:21_31 Mer Def 0.25 Acq:31-OCT-2013 12:03:06 +0:36 Cal:FC43_>
Autospec-UltimaEQ CI+ Magnet BpM:344 BpI:2812835 TIC:7198263 Flags:HALL

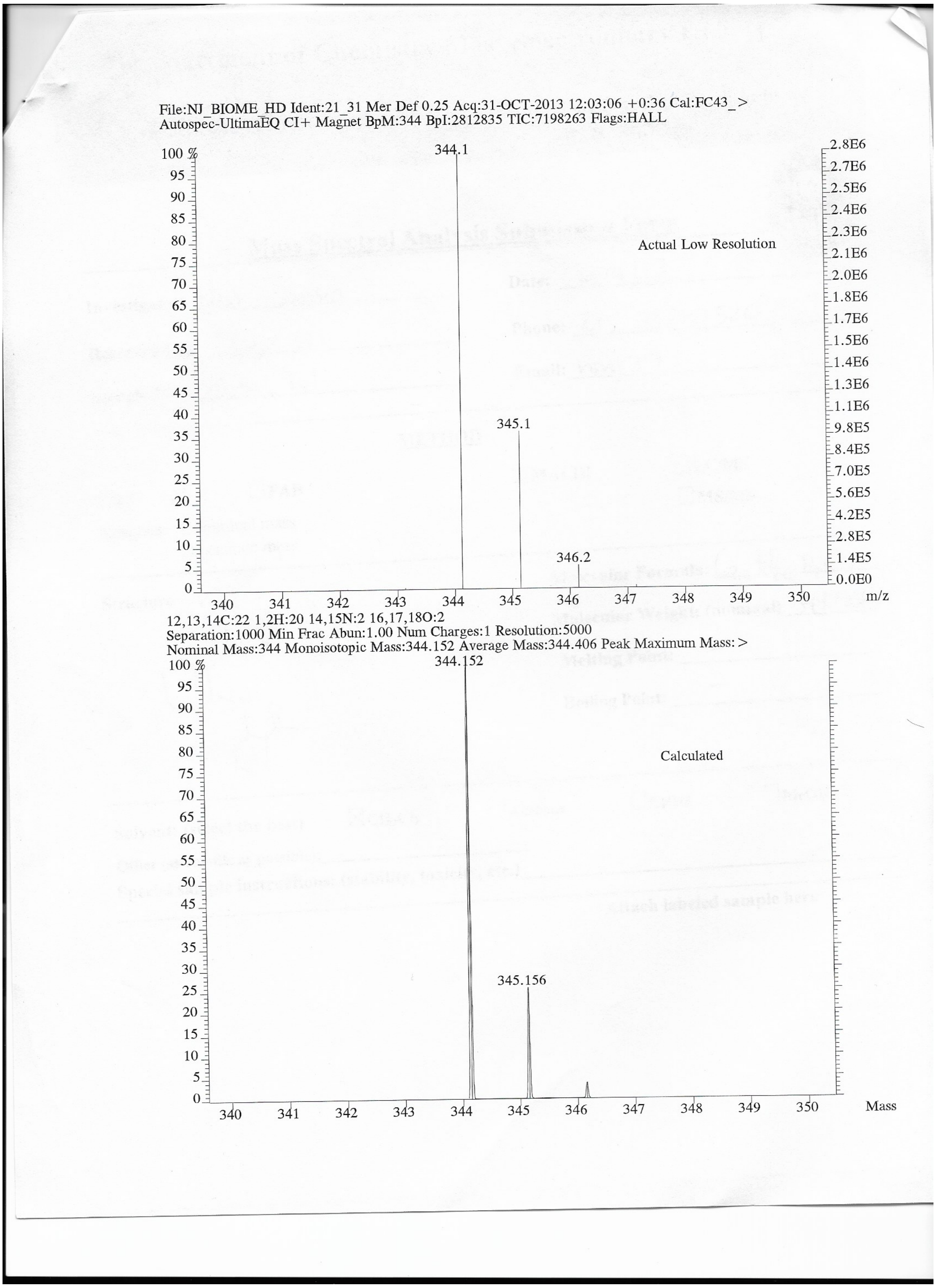

File:NJ_BIOME_HD Ident:21_31 Mer Def 0.25 Acq:31-OCT-2013 12:03:06 +0:36 Cal:FC43_>
Autospec-UltimaEQ CI+ Magnet BpM:344 BpI:2812835 TIC:7198263 Flags:HALL

12,13,14C:22 1,2H:20 14,15N:2 16,17,18O:2
Separation:1000 Min Frac Abun:1.00 Num Charges:1 Resolution:5000
Nominal Mass:344 Monoisotopic Mass:344.152 Average Mass:344.406 Peak Maximum Mass:>

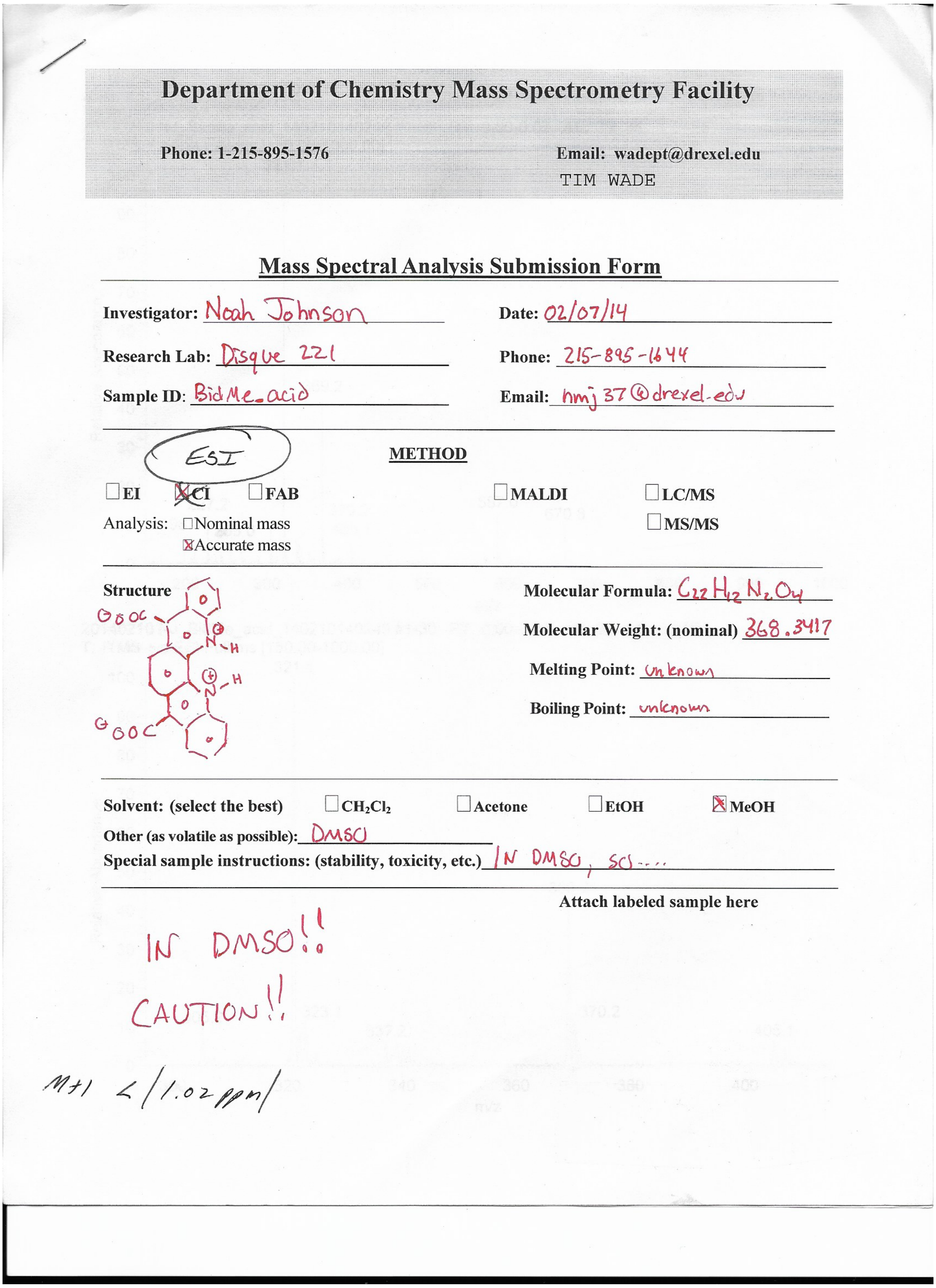

Department of Chemistry Mass Spectrometry Facility

Phone: 1-215-895-1576 **Email: wadept@drexel.edu**
TIM WADE

Mass Spectral Analysis Submission Form

Investigator: Noah Johnson **Date:** 02/07/14
Research Lab: Disque 221 **Phone:** 215-895-1644
Sample ID: BidMe_acid **Email:** hmj37@drexel.edu

METHOD

ESI

☐**EI** ☒**CI** ☐**FAB** ☐**MALDI** ☐**LC/MS**
☐**MS/MS**

Analysis: ☐Nominal mass
☒Accurate mass

Structure

⊖OOC
⊖OOC
⊕
N
H
⊕
N
H

Molecular Formula: $C_{22}H_{12}N_2O_4$
Molecular Weight: (nominal) 368.3417
Melting Point: unknown
Boiling Point: unknown

Solvent: (select the best) ☐**CH_2Cl_2** ☐**Acetone** ☐**EtOH** ☒**MeOH**
Other (as volatile as possible): DMSO
Special sample instructions: (stability, toxicity, etc.) IN DMSO, SCI....

Attach labeled sample here

IN DMSO!!

CAUTION!!

M+1 < |1.02 ppm|

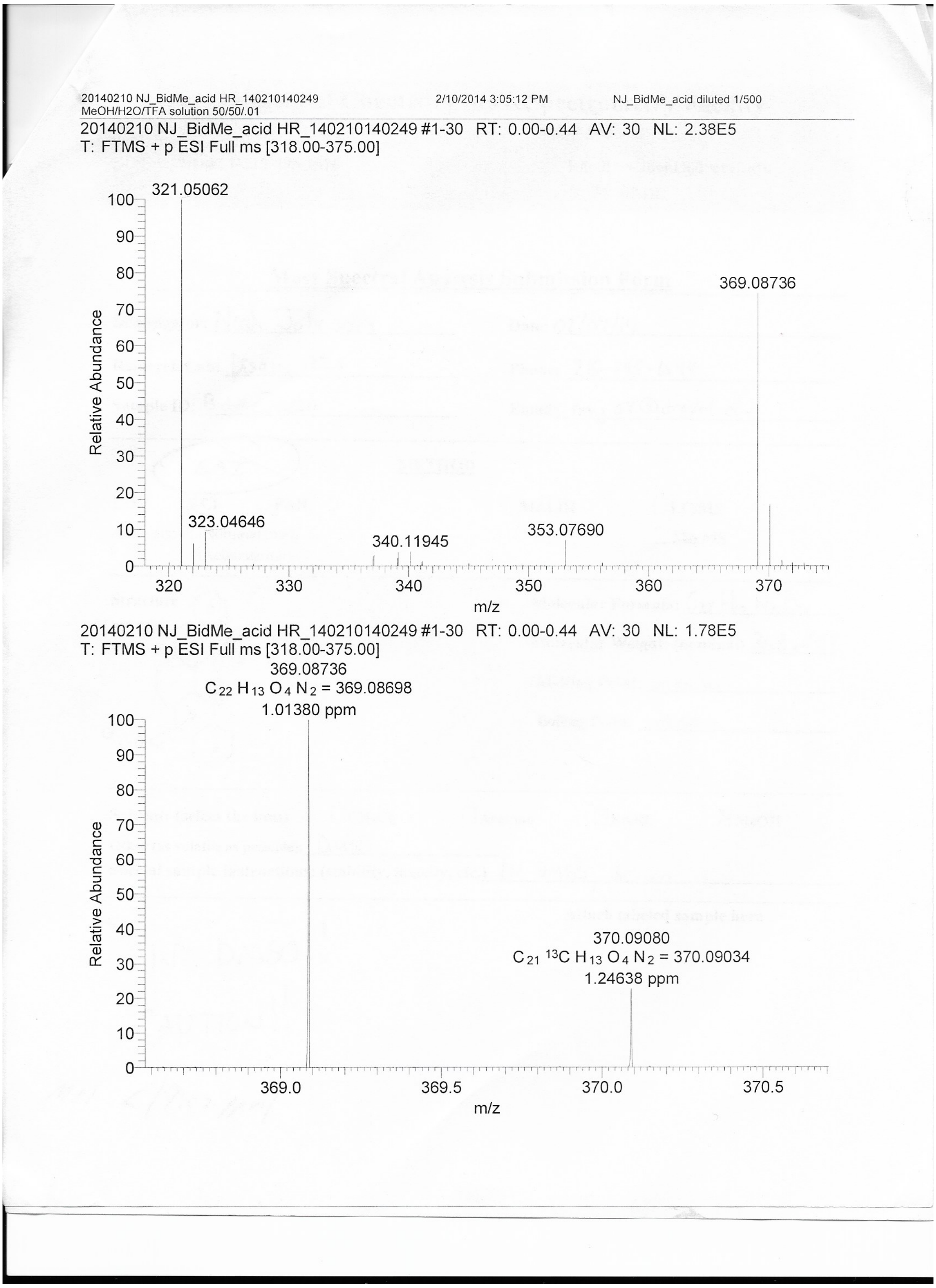

```
20140210 NJ_BidMe_acid HR_140210140249                2/10/2014 3:05:12 PM          NJ_BidMe_acid diluted 1/500
MeOH/H2O/TFA solution 50/50/.01
20140210 NJ_BidMe_acid HR_140210140249 #1-30   RT: 0.00-0.44   AV: 30   NL: 2.38E5
T: FTMS + p ESI Full ms [318.00-375.00]
```

```
20140210 NJ_BidMe_acid HR_140210140249 #1-30   RT: 0.00-0.44   AV: 30   NL: 1.78E5
T: FTMS + p ESI Full ms [318.00-375.00]
```

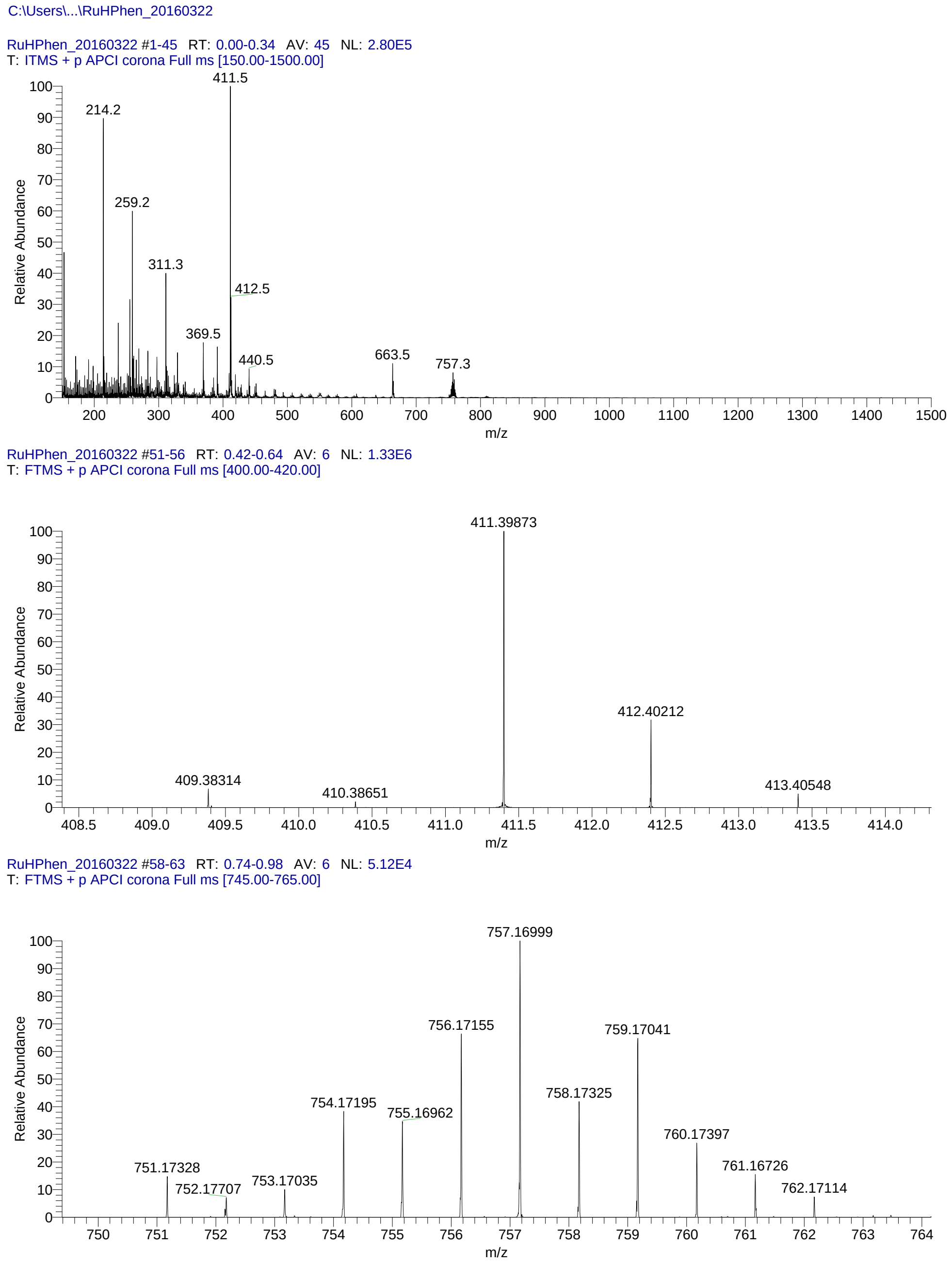
C:\Users\...\RuHPhen_20160322
RuHPhen_20160322 #1-45 RT: 0.00-0.34 AV: 45 NL: 2.80E5
T: ITMS + p APCI corona Full ms [150.00-1500.00]
Relative Abundance
411.5
214.2
259.2
311.3
412.5
369.5
440.5
663.5
757.3
m/z
RuHPhen_20160322 #51-56 RT: 0.42-0.64 AV: 6 NL: 1.33E6
T: FTMS + p APCI corona Full ms [400.00-420.00]
411.39873
412.40212
409.38314
410.38651
413.40548
RuHPhen_20160322 #58-63 RT: 0.74-0.98 AV: 6 NL: 5.12E4
T: FTMS + p APCI corona Full ms [745.00-765.00]
757.16999
756.17155
759.17041
758.17325
754.17195
755.16962
760.17397
751.17328
761.16726
752.17707
753.17035
762.17114

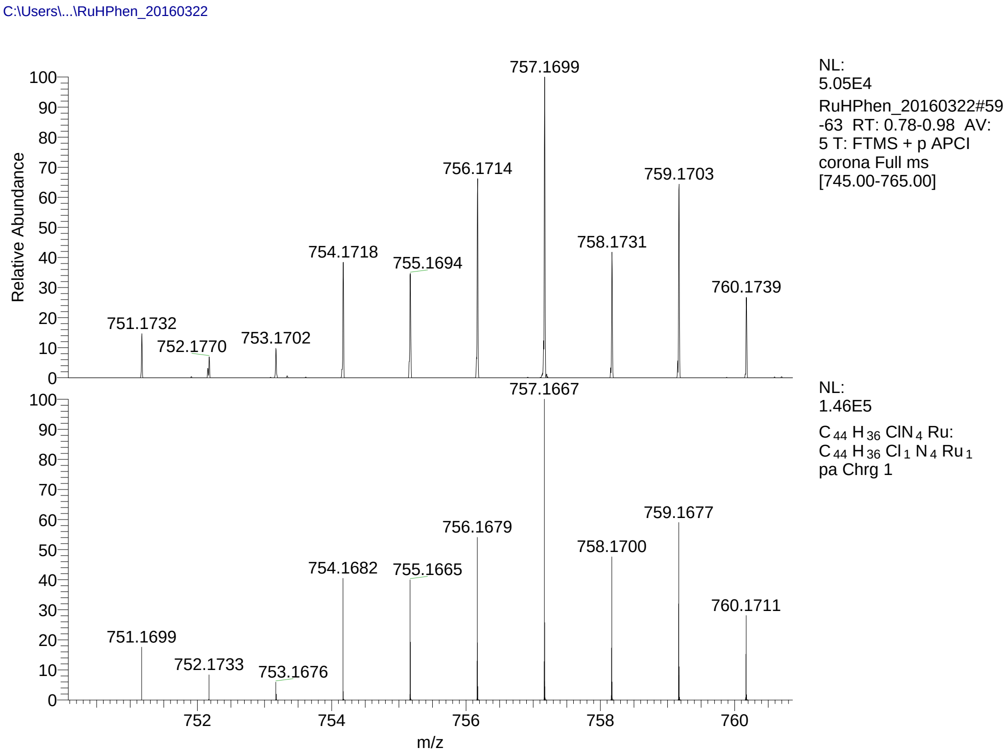
C:\Users\...\RuHPhen_20160322
Relative Abundance
100
90
80
70
60
50
40
30
20
10
0
757.1699
756.1714
759.1703
754.1718
755.1694
758.1731
760.1739
751.1732
752.1770
753.1702
NL:
5.05E4
RuHPhen_20160322#59
-63 RT: 0.78-0.98 AV:
5 T: FTMS + p APCI
corona Full ms
[745.00-765.00]
757.1667
759.1677
756.1679
758.1700
754.1682
755.1665
760.1711
751.1699
752.1733
753.1676
NL:
1.46E5
C 44 H 36 ClN 4 Ru:
C 44 H 36 Cl 1 N 4 Ru 1
pa Chrg 1
752
754
756
758
760
m/z

Vita

Noah Johnson was born in Saint Paul, Minnesota, on September 2nd, 1988. He attended Cornell University from the fall of 2006 to the spring of 2010, receiving multiple named Dean's Scholar awards, and obtaining a Bachelor's of Arts in the field of chemistry. During this time he did research for the Cornell University Department of Plant Breeding and Genetics, as well as performing research during the summer of 2005 at Lehigh University under Drs. Kai Landskron and Guido Pez. He began the Ph.D. program at Drexel in 2010 at Drexel University under Dr. Frank Ji. He was the recipient of both the Ruth and Eugene Rosenbaum Graduate Teaching Assistant Award, and the Drexel University Teaching Excellence Award. He was a co-founder of the new iteration of the Chemistry Graduate Student Association, where he served as both the vice-president and president. He is a member of both the American Association for the Advancement of Science and the American Chemical Society.

(This page is intentionally left blank)